AN OPTICAL FIBRE BASED POLARISATION MODULATION TECHNIQUE: DEVELOPMENT AND APPLICATIONS

By

R Chitaree

A Thesis
Submitted to City University for
the Degree of Doctor of Philosophy in
Electrical and Electronic Engineering

City University
Measurement and Instrumentation Centre
Department of Electrical, Electronic and Information Engineering
Northampton Square, London EC1V OHB
September 1994

to

my beloved country, *THAILAND*

TABLE OF CONTENTS

CHAPTER 1
INTRODUCTION

CHAPTER 2
PRELIMINARY STUDIES OF POLARISATION MODULATION TECHNIQUES

CHAPTER 3
A HIGH BIREFRINGENCE FIBRE POLARISATION MODULATION SCHEME: SYSTEM AND PERFORMANCE

CHAPTER 4

ELLIPSOMETRIC MEASUREMENTS USING A HIBI FIBRE POLARISATION MODULATION SCHEME

CHAPTER 5

FIBRE OPTIC ELLIPSOMETRY FOR THIN FILM MEASUREMENTS AND SENSOR APPLICATIONS

CHAPTER 6
CONCLUSION

LIST OF TABLES

LIST OF FIGURES

Acknowledgements

First and foremost, the author would like to acknowledge sincerely his supervisors: Dr K Weir, Dr A W Palmer and Prof K T V Grattan for their advice and guidance throughout this work. Particularly, Dr K Weir who has been very helpful and so kind as to provide valuable discussions, at any time and on every matter, from optical fibres to dinosaurs.

The author is also pleased to acknowledge support from the Engineering and Physical Science Research Council (EPSRC) for this work, and the support from the Thai Government by way of a studentship.

Also, the author would like to extend his appreciation to Mr R Valsler and other colleagues who create a pleasant and unforgettable atmosphere in the laboratory during the years of working with the fibre optics group, City University.

Special thanks have to be given to all Thai brothers and sisters (Dr Preecha and his wife, Pee Lek and Pee Moo [from City University] as well as Pee Dang and Nok [from Queen Mary College]) who have been with the author over this period of great joy.

And, finally, the author would like to show a very deep gratitude to his caring father, mother, brother and girlfriend for their encouragements and support throughout this important study.

Declaration

I grant powers of discretion to the University Librarian to allow this thesis to be copied in whole or in part without further reference to the author. This permission covers only singles copies made for study purposes, subject to normal conditions of acknowledgements.

ABSTRACT

This thesis undertakes an investigation of polarisation modulation techniques arriving from optical transmission in both free-space and optical fibres with the aim of determining relative performances for prospective applications. The system of optimal performance is then applied to make ellipsometric measurements.

Polarisation modulation techniques considered allow control of the state of polarisation through an interferometric method and modulation of the phase difference. Precise state and orientation of polarised light at any instant of time are obtainable. These qualities match the specific requirement of a range of optical instruments, such as polarimeters and ellipsometers.

The evolution and development of various polarisation modulation techniques are discussed in terms of important features such as the operating speed, the number of optical components required and methods of controlling the polarisation. After initial considerations, two configurations were chosen for more detailed experimental study. Their arrangement produces a rotating plane polarised output and are based on interferometric techniques. One configuration is characterised by free-space propagation (Michelson interferometer); whereas, the other uses highly birefringent (HiBi) fibre as the light propagation medium.

The theoretical and experimental performances of both these configurations are investigated. Full studies focusing on the output quality of the controlled light in terms of the degree of polarisation and ellipticity from the two arrangements were undertaken. These factors are used to determined which configuration offers better performance. Further extensive investigations, particularly on performance-related factors, for the chosen scheme (the optical fibre based system) are carried out to optimise the quality of the rotating plane polarised light emitted. Improvements through a range of the factors were undertaken and are clearly demonstrated.

The achievements resulting from the improvement of the rotating plane polarised light include a reduction in ellipticity (in the range of 10^{-2}), a much smaller effect due to the direction of rotation (a 1-2% asymmetry) and potentially high speed detection (up to 1 kHz). These achievements are considered to be appropriate enough to employ the improved optical fibre polarisation modulation technique to ellipsometric measurements.

The optical fibre modulation scheme is applied to the ellipsometric measurements of a simple system consisting of interfaces of two semi-infinite media. Various materials are investigated and experimental results are shown in terms of the ellipsometric parameters ψ and Δ which then allow an individual sample refractive index to be determined. The accuracy found in measuring the two ellipsometric parameters is within 2% of the parameter mean values. A broader application range is also demonstrated as the optical fibre polarisation modulated ellipsometer is used to characterise ambient-film-substrate samples differing in film thickness. The results gained are then compared with corresponding reference values, obtained from a commercial ellipsometers, in order to demonstrate the degree of sensitivity. The novel implementation of the technique as a thin film based sensor device is demonstrated by detecting the change of a thin film properties on exposure to external stimuli.

CHAPTER 1
INTRODUCTION

1-0 Introduction

Long before it was known that light is an electromagnetic wave, its wave nature had been demonstrated by interference and diffraction experiments. Furthermore, it had also been proven that light is a particular kind of wave, a transverse wave. With this description, there are a number of possible directions in which the wave may vibrate, all at right angles to the propagation direction of the wave.

A convenient way to describe this circumstance is to use an electromagnetic theory (Williamson and Cumming, 1983). This describes the light wave in terms of the periodic movement of the end point of the electric (and also magnetic) vector of an electromagnetic wave, with increasing time. In general, this traces out the shapes of an ellipse (as viewed when looking towards the source), which may, of course, reduce in special cases to a circle or a straight line. With one of such geometrical appearances (circular, linear or elliptical) of the vibration, light is described to be *polarised.*

In many respects, linear polarisation (when the electric vector is confined to vibrate in a single plane) is found to be the most attractive and advantageous for exploitation in many optical instruments, due to its simple mathematical form. This allows more convenient manipulation and simplified signal analysis when dealing with a particular optical application of interest.

Thus, light can be polarised in a number of different ways (circular, linear or elliptical) (Jenkins and White, 1957). As suggested, linearly polarised light may be conveniently used in instrumentation and the usual and simple method to produce it is to use an unpolarised light source and shine the output light through a polariser, or

exploit the optical phenomenon of the light reflected, at an appropriate angle of incidence from a dielectric surface, to produce such polarised light.

The analysis of linearly polarised light in measurement applications involves considering how the beam is transformed and how it may be depicted under different optical interactions, such as reflection, transmission or scattering, due to properties of an optical sample. When the beam encounters a variety of media such as a birefringent crystal, an oblique dielectric or a metallic surface, a change of the polarisation state is normally observed. This produces the basis of using linearly polarised light as a tool, or probe for evaluating some interesting properties of matter such as indices of refraction, absorption coefficients and thicknesses. A good illustration of such an implementation can be found in polarimetric instrumentation (Takasaki, 1961a). Such a device is generally used to characterise an optical medium by analysing any alteration of the incident linearly polarised beam when it is reflected, scattered or it propagates through the medium.

Some years ago, it was a cumbersome process to carry out the complete characterisations of an optical sample, for example in terms of refractive index and absorption coefficient, by employing only a light source, and a few polarising components. This is because, in the characterising process, many orientations of the polarised light incident on the sample are normally required and to accomplish these several adjustments of the components are required and a considerable measuring period is inevitable. This obviously limits the performance of the optical instrument using the method in many respects such as speed and then its range of practical applications.

However, this inconvenience may be overcome by adding a modulation unit to the instrument in order to control the orientation and state of the polarisation. Several approaches, such as using rotating elements, or electric, magnetic and mechanical phase shifters were proposed to achieve this. As a result, the modified systems became speedier and could cover a wider range of applications, for instance, the monitoring of an optical thin film growth, or the detection of a chemical reaction

between a chemical substance and an optical surface. Although the modulation concept has brought a number of potential configurations to polarisation-measuring systems, only some of them can be fully implemented in practice because the controllability of the polarisation state is not the only feature necessary for a fully-effective system. The system must satisfy some fundamental requirements such as its ability to produce a high quality modulated linear polarisation, with cost-effectiveness and ease of system arrangement. Therefore, it is both interesting and important to discuss and study some previously used configurations which could fulfil such fundamental requirements. It is also equally valuable to investigate, in detail, the polarisation modulation technique in relation to a useful practical application. At the present time, there is considerable interest in the application of the technique to ellipsometric systems. Any new proposed system will require many additional features (such as a higher speed of operation) compared with conventional ellipsometric instruments.

In this chapter, the evolution and development of the polarisation modulation will be presented chronologically. The descriptions include comprehensive reviews of polarisation modulation technique from its early stages to the present day. Also, the evolution and development of the practical utility of the polarisation modulation system to ellipsometric measurement are briefly reviewed. In addition, aims of the work and structure of the thesis based on this background, and development of the polarisation modulation technique are also presented.

1-1 The History of Polarisation State Control

Generally, linear polarisation state control can be classified into to two main types based on the medium of the light propagation. The first type is commonly known as the free-space scheme. It bears the name because the process of polarisation control takes place entirely in the free-space medium using bulk optical components. A general configuration for this type uses mostly conventional optical components such as mirrors and polarising elements, while the second type has emerged due to

recent advances in optical fibre technology. This second type termed here the fibre optic scheme, allows the modulation to be performed within an optical fibre by use of appropriate means, as will be described.

1-1-1 Free-Space Schemes

Firstly, some work that has contributed to free-space linear polarisation modulation is considered in light of its contribution to developments of the instrumentation. Several early arrangements of the modulation scheme, used for an application of characterising optical samples, simply employed appropriate manual adjustments of polarising elements introduced next to a light source (Conn & Eaton, 1954). Even though the configuration conveniently allowed the use of an unpolarised light source, the manual adjustments involved reduced the attraction of this method for instrumental applications. In later work, polarisation modulation was further developed by Takasaki (1961b) in order to eliminate the inconvenience and experimental delay caused by the manual adjustments. In his report, the concept of modulating the linearly polarised light was based on the longitudinal electro-optical effect, better known as the Pockels effect. The linearly polarised light propagated through a modulation unit composed of a crystal of ammonium dihydrogen phosphate (ADP) which acted as a retardation plate of variable retardation. An alternating voltage was applied across the ADP crystal in the direction of the beam propagation causing variations in the refractive indices of two orthogonal components perpendicular to the light propagation direction and defined by the crystal axes. As a result, a time-varying phase difference between the two components along the crystal axes was obtained, and in general, elliptically polarised light would emerged from the crystal. However, the introduction of a quarter-wave plate oriented appropriately could turn the elliptical to a linear state of polarisation (Fig. 1-1). This arrangement obviously provided a remedy for the early slower systems by offering the advantage of being completely automated and speedy in use.

P   Pockels cell   QWP
(linear)   (elliptical)   (two possible
                                                                             linear outputs)

                                                                  or ⟶

                                                                  light propagation
                                                                  direction

0°   45°   0°
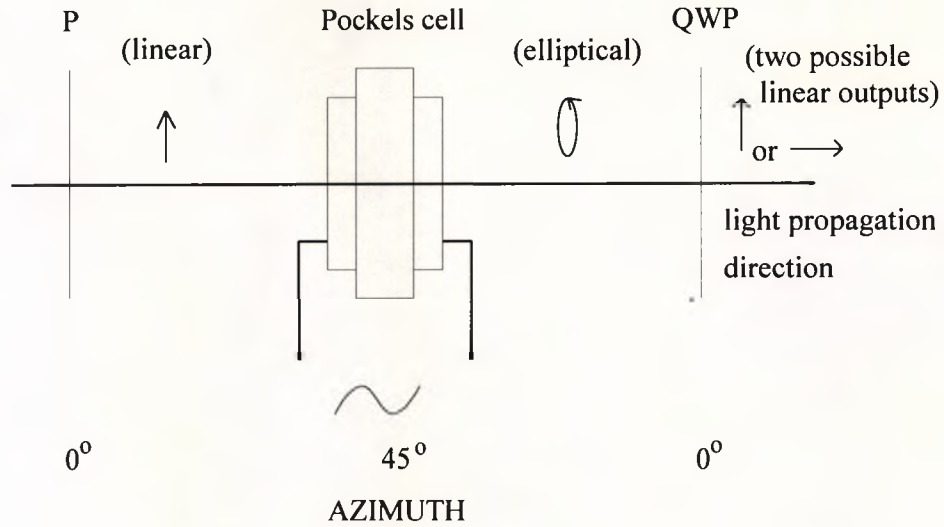
AZIMUTH

Figure 1-1 The polarisation azimuth controller. The element P is a linear polariser. The Pockels cell is an ADP crystal with electrodes on both surfaces, and QWP is a quarter-wave plate (after Takasaki, 1961b).

An alternative configuration to achieve polarisation modulation was proposed by Jasperson and Schnatterly (1969), accomplished by using high frequency (50 kHz) modulation of the optical properties of a stationary, normally isotropic block of fused quartz through which a linearly polarised beam passed. Specifically, a strain induced along the $\hat{j}$ axis of a fused quartz block caused the phase velocity of light polarised along the $\hat{i}$ and $\hat{j}$ axes to differ in a periodic manner, as shown schematically in Fig. 1-2, equivalently to the use of a variable retardation plate. If a linearly polarised light beam was incidentally polarised at an angle to those axes so as to have non-zero components along both axes, the transmitted beam would consequently have the state of its polarisation modulated. This method was demonstrated and successfully applied to ellipsometric measurements by these authors.

In the same year, Takasaki and Yoshino (1969) also proposed a new polarisation modulation technique based on a well-known interferometric arrangement, the Michelson interferometer, utilising an ADP crystal to vary the state of polarisation. Although there was no significant breakthrough at this stage, the idea

led to some remarkable developments in free-space polarisation modulation. At this point there was an increasing operating speed and non-mechanical, continuous polarisation control. In 1983, Hu described a new polarisation modulation scheme based on a modified Michelson interferometer known as a Twyman-Green interferometer, devised with the initial purpose of testing optical elements. This author proposed the combination of an interferometer with a mechanically rotating analyser to provide an alternative to control the linear polarisation. However, the work showed an obvious disadvantage in his system, in terms of the low operating speed due to the limitations of the mechanical rotation of components.
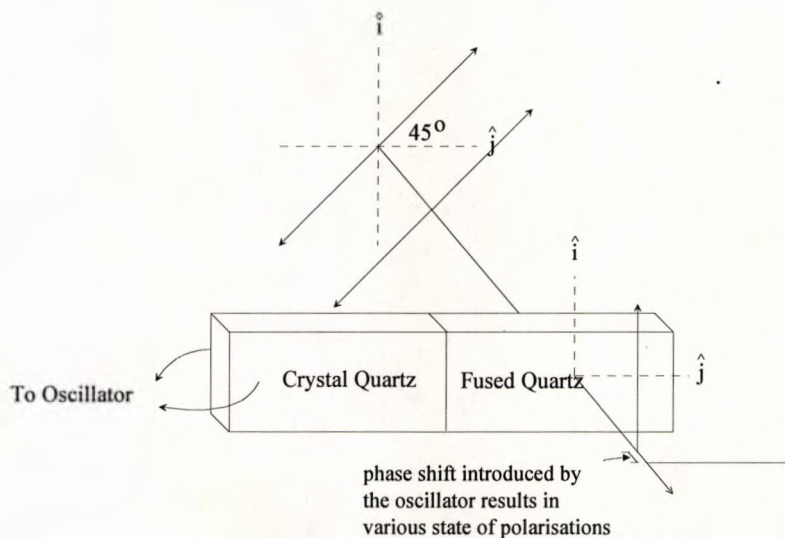
Figure 1-2 Polarisation Modulation (after Jasperson and Schnatterly, 1969).

Later, this inconvenience was overcome in a system proposed by Shamir and Klein (1986). They described a new method for the production of a linearly polarised light beam, in which the plane of polarisation rotates uniformly at high frequencies. The method was based on the superposition of two circularly polarised waves, of opposite sense that differed in frequency, introduced by a frequency shifter. The authors also claimed that the method was versatile and applicable using most laser sources. The system is outlined schematically in Fig. 1-3. The frequency shift was induced by an acousto-optic cell (AO) which split the laser beam into two, each of

different frequencies. One of which was frequency shifted by an amount equal to the frequency applied to the cell. The two mirrors (Ms) directed the beams into the beam splitter (BS) where they were combined. Each beam was circularly polarised in the required sense by a suitably aligned quarter-wave plate (QWP).
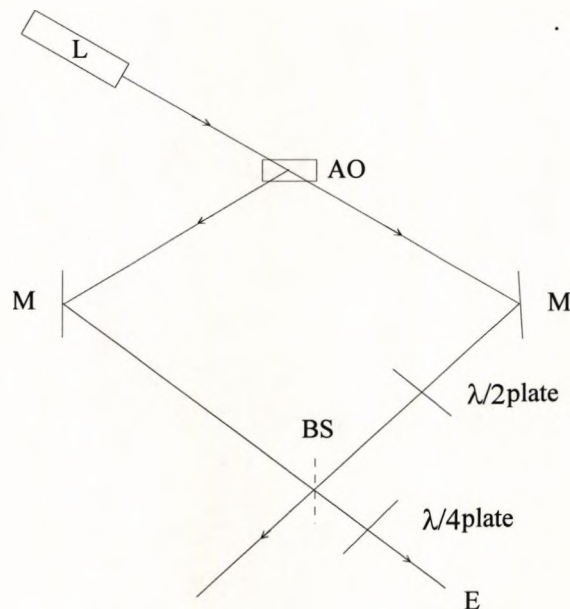
Figure 1-3 Diagram of the system for production of rotating plane polarised light beam (E); L, laser; AO, acousto-optic modulator; Ms, mirrors; BS, beam splitter, and corresponding wave plates (after Shamir and Klein, 1986).

More applications of the AO in polarisation modulation can be found in the work discussed by Tatam *et al* (1986) (Fig. 1-4). In this scheme, the optical arrangement used a Bragg cell to produce a relative frequency shift in one path of a Mach-Zehnder interferometer. Again the frequency of modulation of the polarisation azimuth is equal to the frequency shift imposed by the Bragg cell.

Unfortunately, even though the proposed optical polarisation state control scheme using a Bragg cell was non-mechanical and able to offer a high speed of operation, the frequency shifter itself was bulky and rather expensive. This difficulty could be overcome if the Bragg cell modulation were replaced by another suitable modulation method. One such modulation method will be described in the following paragraph.

A preferred method is proposed in this thesis that should provide an alternative to those earlier proposed systems, and has a much more compact arrangement. The configuration uses a polarisation Michelson interferometer (Fig. 1-5) with an incorporated polarising beam splitter (PBS). This approach is capable of generating a linear polarisation with rotating azimuth as a function of the linear displacement of one of the two mirrors. A polariser at the input is orientated at 45º to the plane of the PBS and the QWP introduced at the output of the interferometric system has its optical axes adjusted to be at 45º to the plane of the PBS. Modulation is achieved by the displacement of mirror M2.
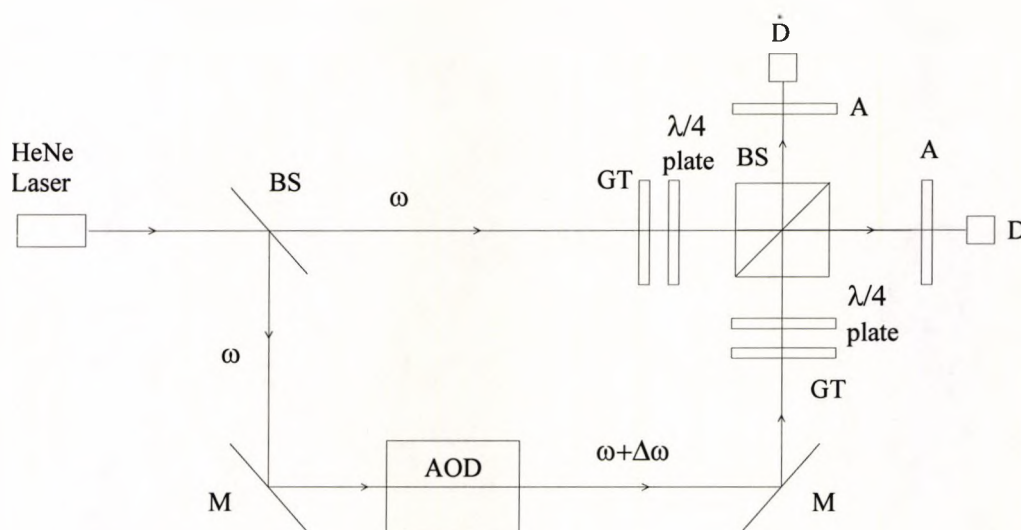
Figure 1-4 High speed polarisation azimuth rotation using a Bragg cell. AOD, acousto-optic device (Bragg Cell); GTs, Glan-Thompson polariser; BS, beam splitter; Ms, mirrors; As, analysers; Ds photodetectors; ω, frequency and Δω, frequency shift (after Tatam *et al*, 1986).

The latter configuration obviously provides some significant advantages over the previous arrangements, such as the ability to perform total-optical polarisation control and the use of a small number of optical components. The performance of this system will be discussed in detail later.

With the development of optical fibre technology, recently reaching a mature state the use of this technology has become very much evident in many modern optical instruments, including those with polarisation state control systems. The

following sub-section will review some experimental work that has been carried out on this topic by several researchers over the past years, emphasising major developments in the field.
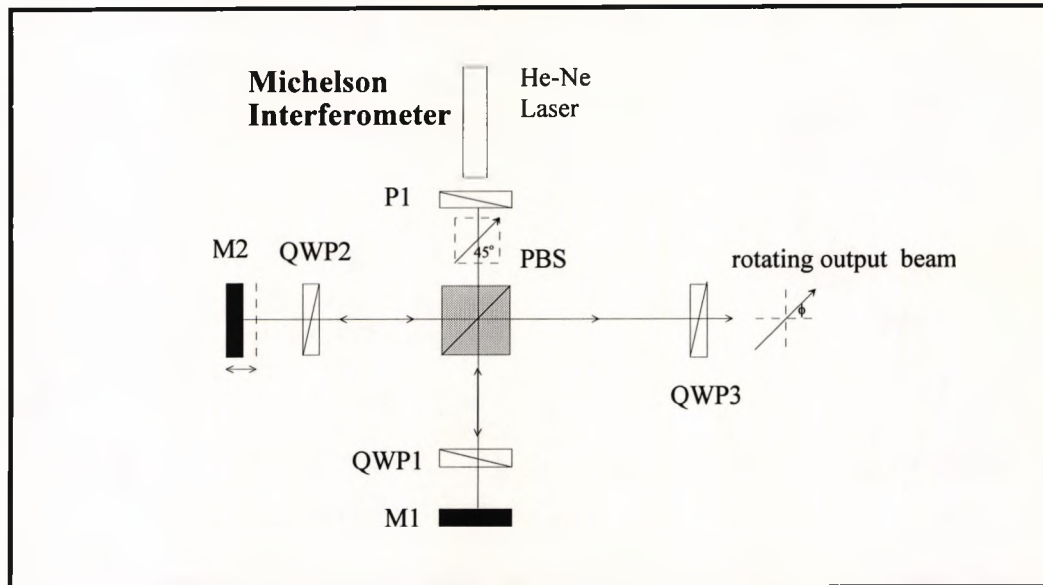
Figure 1-5 Illustration of a proposed free-space arrangement using a Michelson interferometer. Ps : Polarisers; QWPs : Quarter-Wave Plates; PBS : Polarising beam splitter; Ms : Mirrors.

1-1-2 Optical Fibre Schemes

Since the advent of optical fibres in the late 1960, many new approaches for single-mode optical fibre based polarisation control have been constructed and studied. Many of the fibre optic schemes were trying to stabilise or control the output polarisation states (as discussed later in this Section). Using optical fibres as the light medium has become popular because of their significant advantages over the free space medium. For instance, the confinement of light inside flexible fibres allows the output to be easily directed in any required direction and it also offers increased system tolerance to external influences such as vibration. These advantages cannot easily be obtained when performing an experiment in free space because the arrangement is subject to vibrations and easily mis-aligned by such a disturbance.

In ideal fibres with perfect rotational symmetry, any polarisation state injected into the fibre would propagate unchanged. In other words, the phase difference

between two orthogonal components (into which the polarisation state may be resolved) would remain constant. In practical fibres, imperfections, such as asymmetrical stress, non-circularity of the core, etc., cause a loss of the circular symmetry of the ideal fibre and affect the state of polarisation (SOP) by disturbing the phase difference between the two orthogonal components. This suggests that the components propagate with difference phase velocities and accordingly experience refractive indices. The phenomenon is known as *birefringence* in the fibre. Its origins has been studied in detailed (Rashleigh, 1983). In fact the exploitation of these perturbations are the key to producing a known polarisation state from a fibre. Many experimenters have proposed to control the state of polarisation (SOP) under some kind of fibre perturbation such as bending, twisting, or subjecting the fibre to transverse pressure, longitudinal magnetic or electric fields. By using one of these methods, asymmetric properties are introduced into the fibre and, as a result, an appropriate phase shift is imposed on the components of the polarised light inside it. In other words, at the point where the interaction takes place, a "waveplate condition" is simulated by that part of the fibre, giving rise to a change of the polarisation state. With an appropriate arrangement of the perturbed point and a proper value of the phase shift along the length of the fibre, a controllable polarisation state can be achieved.
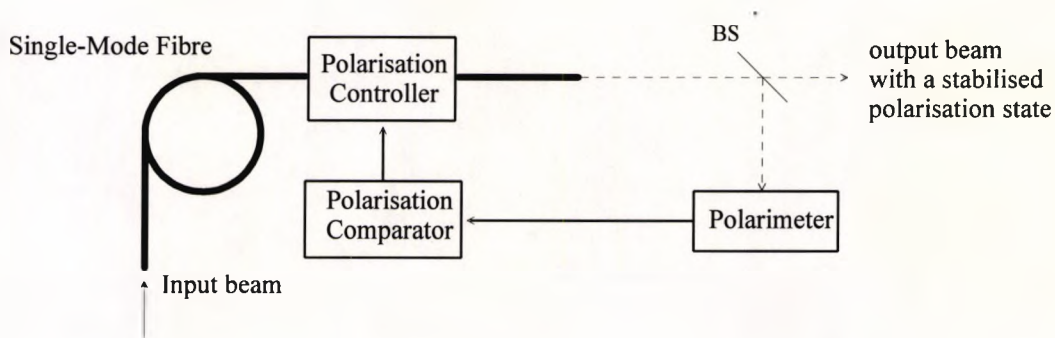
Figure 1-6 Principle of polarisation stabilisation at the output of a single mode fibre. BS, beam splitter (after Ulrich, 1979).

Probably the earliest work to investigate this was discussed by Ulrich (1979). The arrangement was composed of three major parts; a polarisation controller, a polarisation comparator and a polarimeter (Fig. 1-6). The polarisation controller made physical contact with a length of conventional single-mode fibre through electromagnetic fibre squeezers which introduced variable amount of stress-birefringence directly onto the fibre. The principle of this approach can be briefly described as follows. The polarisation state of the output may be monitored by the polarimeter, and the difference of the polarisation state with a desired polarisation state at the polarisation comparator is determined. The deviation obtained then provides a feedback signal electronically to the polarisation controller (fibre squeezers) to apply appropriate pressure to the fibre in order to turn the polarisation state at the output into the required polarisation state. Some disadvantages of this arrangement include elaborate electronic control circuits and the large number of optical components are involved.
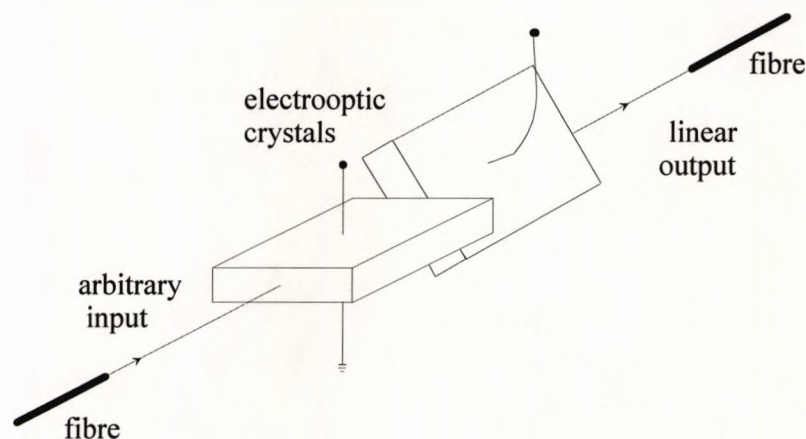
Figure 1-7 Setting of the two crystal modulators for polarisation state controller (after Kubota *et al*, 1980).

In 1980, Kubota *et al* proposed an alternative method to control the polarisation of the output light of the optical fibre following the work carried out by Ulrich. In this work, active control of the polarisation in the single-mode fibre was achieved by an electro-optical feedback system which was very compact and was also

free from any fatigue problems of optical fibre. The approach was able to generate a linear polarisation state with the desired azimuth direction by utilising two carefully aligned birefringent materials whose axes were inclined to each other (Fig. 1-7). There were many disadvantages of the arrangement that made it very unattractive. They included the requirement of applying a very high voltage (425 V) to the two birefringent materials to operate as waveplates. Also, since this type of modulation technique could not be integrated into the fibre, light had to be coupled out from one fibre to be modulated and then coupled back into the other fibre, with the result that there was potentially a high insertion loss.
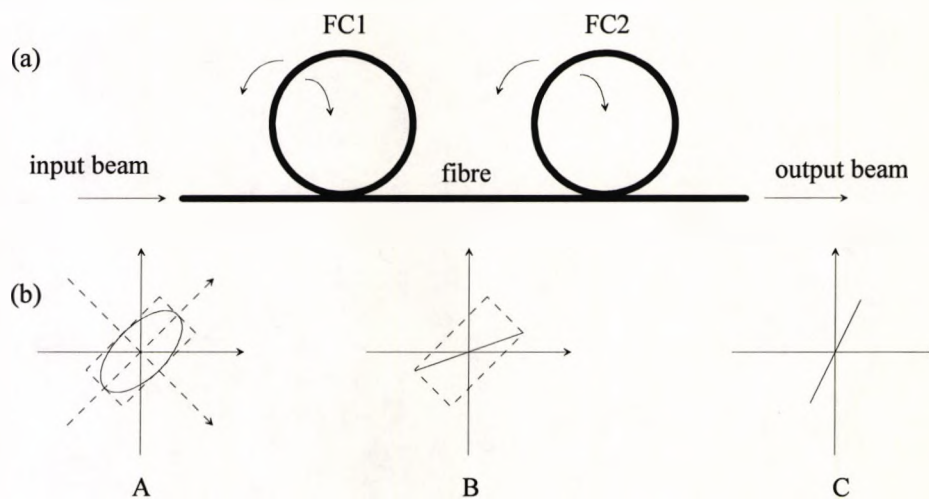
Figure 1-8 (a) Configuration of single-mode fibre fractional wave devices, indicating freedom of rotation of plane of each individual coil.

(b) Illustration of a polarisation state evolution along the fibre coils,

A. an elliptical polarised beam as input light,

B. a tilted linear polarisation transformed by a $\lambda/4$ wave-plate like fibre coil (FC1),

C. a linear polarisation with an arbitrary angle controlled by a $\lambda/2$ wave-plate like fibre coils (FC2) (after Lefevere, 1980).

Later that year, a new method for controlling the polarisation state was presented by Lefevere (1980). The principle was similar to the previous work just mentioned. It was again an attempt to create the required phase retardation conditions

in order to transform an arbitrary polarisation state into the desired output state of polarisation, such as a linear state. This new single-mode fibre optic device, which was completely equivalent to the waveplates of classical optics, employed a very simple configuration (Fig. 1-8). It used the stress birefringence induced by bending the fibre and by using several devices in combination, the required state of polarisation was then obtained. However, depending on the nature of the configuration, energy loss is likely to occur due to the small radius of the fibre bend created. Typically, the energy loss of the single mode fibre increases dramatically as the diameter of the fibre bending becomes smaller than 50 mm (Shibata *et al*, 1985).

A further study on linear polarisation state control was carried out by Okoshi *et al* (1985a), in whose work the new SOP control scheme used Faraday rotators as the SOP conversion elements to obtain controllable, including linear polarisation states. The instrument employed the well-known principle of the magneto-optic effect. It concerned the change in the refractive index of the material (single-mode fibre in this case) subjected to a steady magnetic field, and the change in orientation of the output plane polarised light was proportional to the magnetic field component parallel to the direction of the light propagation. Although the authors had managed to reduce the effect of external fibre birefringence induced due to the bending, the arrangement still had some disadvantages such as using many optical components and elaborate circuitry.
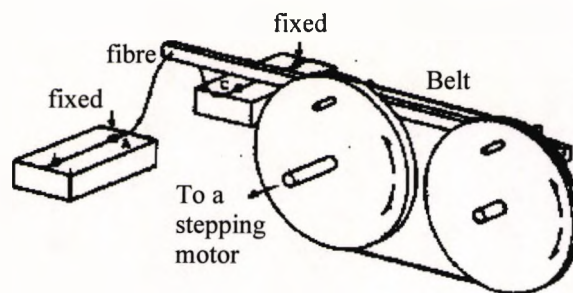
Figure 1-9 Rotatable fibre crank (RFC). Driving mechanism for 'translation' movement (after Okoshi *et al*, 1985b).

Following these studies, another all-fibre device for controlling the state of polarisation in a single-mode fibre was proposed by Okoshi *et al* (1985b). The most notable feature of this set-up was that it consisted of two fibre devices called rotatable fibre crank (RFC) elements, which were equivalent to rotatable quarter-wave and half-wave plates. Each of these elements is made by bending a short section in crank form (Fig. 1-9). This action then generated linear birefringence which causes a phase shift between two principal components; thus, a device equivalent to a $\lambda/2$ and $\lambda/4$-plate may be envisaged.

It had been implied by Jones (1941) that an arbitrary SOP could be achieved, including linear polarisation oriented in any desired direction, by using two rotatable phase plates ($\lambda/4$ and $\lambda/2$-plates), and hence, the principle was directly applied to the operation with the two RFC elements proposed. Nevertheless, the employment of mechanical components to operate the rotatable fibre cranks in this approach makes it less capable of high speed operation and physically quite bulky.

With the use of a similar principle of $\lambda/4$ and $\lambda/2$-plates in combination, Matsumoto and Kano (1986) proposed a scheme termed an "endlessly rotatable fraction-wave device for single-mode fibre optics". The device bore such a name because of its ability to create the induced stress birefringence by fibre bending without introducing twist into the fibre while being rotated. Hence, the device was free from unwanted birefringence potentially imposed by twisting. The construction of the endlessly rotatable fractional-wave devices, equivalent to quarter-wave and a half-wave plates in this case are quite complicated. Hence, the scheme does not offer a practical new way of polarisation state control.

In the meantime, efforts on sustaining a single linearly polarised state over long lengths in fibre optic were becoming more successful. This was an important development as it originally provided a thrust in the development of light communication systems, especially, for long distances. Consequently, a new kind of single-mode optical fibre known as polarisation-maintaining (or highly birefringent) fibre was developed (Noda *et al*, 1986). The new fibres are specially fabricated by

introducing a large asymmetric stress distribution, either by the use of the geometrical effect of the core, or the stress effect around the core. Such an induced asymmetry gives rise to a difference in the propagation constants of the two orthogonally polarised fibre modes. In this case, the fibre then supports two orthogonally polarised modes with differing phase velocities, that is the fibre is birefringent. This prevents these modes from exchanging energy as they propagate along the fibre. The fibres are therefore able to maintain a linear polarisation within an eigenmode.

With such a property, the fibre has then been considered a useful optical component and widely used in many optical fibre applications involving linear polarisation state control. An early application in polarisation control was exercised by Tatam *et al* in 1986. The scheme used highly birefringent single-mode optical fibre (HiBi fibre), in the configuration shown in Fig. 1-10.
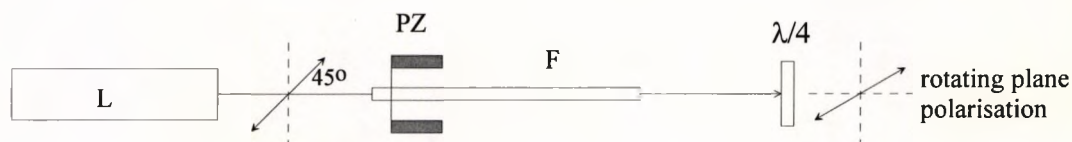
Figure 1-10 Polarisation state azimuth control using a highly birefringent monomode fibre. L, laser; PZ, piezoelectric translator; F, highly birefringent fibre; λ/4 waveplate (after Tatam *et al*, 1986).

This provided a better solution to polarisation stability than previous polarisation controllers, based on conventional single-mode optical fibres, since the SOP can be controlled without bending, twisting, or subjecting the fibre to transverse pressure, electric and magnetic fields. Instead, the novel configuration employs longitudinal stretching to modulate the birefringence of the fibre (Fig. 1-10). This is theoretically equivalent to the modulation of the phase between the two eigenmodes. In such an arrangement, the two main features were the use of a piezoelectric transducer to modulate the polarised light and a λ/4 orientated at 45° to the eigenaxes of the fibre to turn the output to the rotating plane polarised light. In the following year, Tatam *et al* (1987) again proposed another HiBi fibre polarisation modulation

arrangement. This time, the configuration was designed to be able to work as a full polarisation state controller which, of course, includes linear polarisation states. In this configuration, two sections of HiBi fibre were used. Each section of the fibre was again longitudinally stretched by piezoelectric transducers to generate the required polarisation state. The authors also showed experimentally that the plane polarisation state control previously reported was a special case of this new configuration. This was done by modulating the first fibre section while maintaining the second fibre section with a constant phase bias of $\pi/2$, i.e. this section therefore behaved as a quarter-wave plate. Nevertheless, it is worth noting that, in the proposed configuration, launching light from one fibre section to the other could reduce considerably the intensity of light. It could be possible to reduce this using a fusion splice. However, a more fundamental problem to overcome for the practical application of this scheme would be drift in the phase bias with temperature.

Recently Johnson and Pannell (1992) proposed another way to produce a HiBi fibre polarisation state controller. The technique employed the feedback-controlled delivery of non-eigenstates through the fibre (Fig. 1-11). In their work, the eigenstate directions are defined by the eigenaxes of the fibre. Ideally, if linear polarised light orientated at 45° to the eigenaxes of the fibre is launched into the fibre, a constant phase relationship between the two orthogonal plane polarisations, introduced by the fibre, may be expected at the output. Practically, the phase varies with the environmental temperature variation. To fix the phase value for a required state of polarisation, several experimental procedures have to be performed.

If the output signal is returned by a reflector alone, then the reflected orthogonal planes still align with the fibre eigenaxes when they re-enter and propagate back along the fibre, where they can be detected at the control unit. This eigenstate reflection gives rise to an undesired situation and a measurement problem. The situation results in an ambiguity in the output SOP because the double transit causes two possible phase values to correspond to the same SOP.
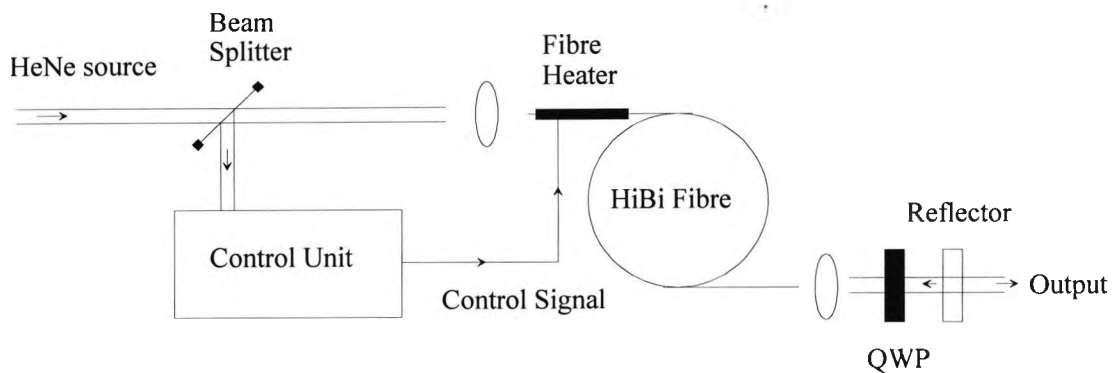
Figure 1-11 The polarisation state of light exiting a HiBi fibre is monitored after a double-pass through the fibre and a quarter-wave plate (QWP) orientated at an angle to the fibre axes. The control unit then performs the stabilisation of the output state (Adapted from Johnson and Pannell, 1992).

However, this can be avoided by rotating the planes of the output from the eigenstate directions, after the output leaves the fibre. According to the authors' report, the output propagated through a quarter-wave plate orientated at an angle of 22.5° relative to the eigenaxes of the fibre before being reflected. The reflected beam passes through the QWP again and no longer enters the fibre in the eigenstates from which it emerges. Under this condition, the ambiguity is eliminated, and as a result, the required SOP of the output beam can be correctly locked on by the control unit. In this way, if there is any perturbation, such as randomly occurring handling stresses or temperature variations in the fibre, the control unit will try to offset the effect by applying suitable heating to the fibre to compensate.

It can be concluded, in this section, that the above descriptions indicate that the considerable level of effort made over recent years has resulted in many different schemes for polarisation state control based on free space and fibre propagation. However, these techniques have not been extensively applied; hence, a further investigation into the performance of individual schemes with a view to application in measuring systems is required, and this constitutes a substantial part of this thesis. The

study will objectively determine the most effective linear polarisation state modulation mechanism for application in polarimetric type measurements.

After having reviewed and considered many of the optical fibre configurations proposed by a number of researchers in the past years, it is considered that the HiBi fibre configurations proposed by Tatam *et al* appear to be the most attractive prospect for optical fibre based polarisation control. This is because the configurations obviously offer a more compact set-up, the use of fewer optical components, easier alignment and potentially high operating speed. To study such a scheme, it would be adequate and more convenient at this stage to deal with a configuration using a hybrid of HiBi fibre and a quarter-wave plate. In addition, using the quarter-wave plate should provide an easier way to examine the effects of mis-alignment.

1-2 Ellipsometry

The analysis of the system performance will not be completely satisfactory unless it is made in relation to the proposed application. In fact, the linear polarisation modulation system has been investigated quantitatively for a range of interesting optical measurements for years. Examples include measurement of optical activity (Tatam *et al*, 1986), electric current via Faraday rotation (Tatam *et al*, 1988) and, especially, ellipsometry (Yoshino and Kurosawa, 1984). However, the last scheme reveals a number of disadvantages, such as a slow measuring speed and difficulties in the alignment.

Ellipsometry is one of the most powerful techniques for the non-destructive and non-invasive evaluation of optical parameters such as the thickness of thin films, birefringence, optical activity, and the complex refractive index of optical materials. Considerable research and development on the subject has been carried out over several decades, and as a result, a variety of the ellipsometric configurations are evident, many of which are now commercially available. Many reasons govern the way an ellipsometer should be designed. For instance, an ellipsometric system specially used for real-time measurements of a thin film growth on a substrate

obviously requires fully-automatic functions such as a high speed data acquisition to cope with such a rapid variation in the process. This is conveniently achieved by employing a polarisation modulated ellipsometer (Moritani *et al*, 1983).

To have a better understanding of the operation and use of instrument, the following sub-section will describe the development of some major configurations proposed in the past years.

1-2-1 The Historical Aspect of Ellipsometric Systems

The progress of system development will be partly based on the availability and state of development of the optical components and electrical instruments available at the time when the study took place. It is clear that the early ellipsometric arrangement was very simple, as proposed by Archer (1962). The instrument was technically known as a null ellipsometer, as is shown in Fig. 1-12.
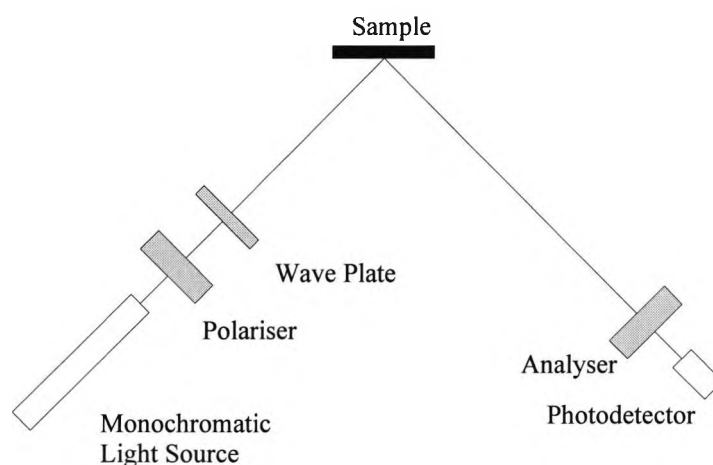
Figure 1-12 Schematic representation of a null ellipsometer (after Archer, 1962).

It employed Glan-Thompson polarising prisms, a mica waveplate and a mercury arc light source. The basic procedure of the ellipsometric configuration was based on finding a set of azimuth angles of all polarising components involved, such that the light flux (after interaction with a sample under investigation) falling on a photodetector was extinguished. The outcome would provide characteristic data relating to the sample which could be manipulated further to determine other optical parameters, such as the sample index of refraction. Since the adjustments of optical

components had to be performed manually, its range of application became, accordingly, limited only to slow process applications. However, these instruments have been available commercially for many years and are well-understood (Azzam and Bashara, 1977). The null ellipsometer is also regarded as the most accurate of all the ellipsometric configurations (Jellison and Modine, 1990).

In 1969, Jasperson and Schnatterly proposed an improved method for ellipsometric measurements based on a new polarisation modulation technique. The authors pointed out that the newly-automatic technique was required to replace the nulling system which was slow when making measurements, an interval of several minutes was required at every datum point, during which time several manual adjustments were performed to extract the desired information. This was undesirable since, in some cases such as metallic surface study, surface contamination could occur rapidly, even in a good vacuum chamber. In contrast, the new technique made possible the measurement of rapid changes in the optical response as well as facilitating the observation of long term effects. The technique shows a good example of the use of the technique of polarisation modulation in an ellipsometric system.
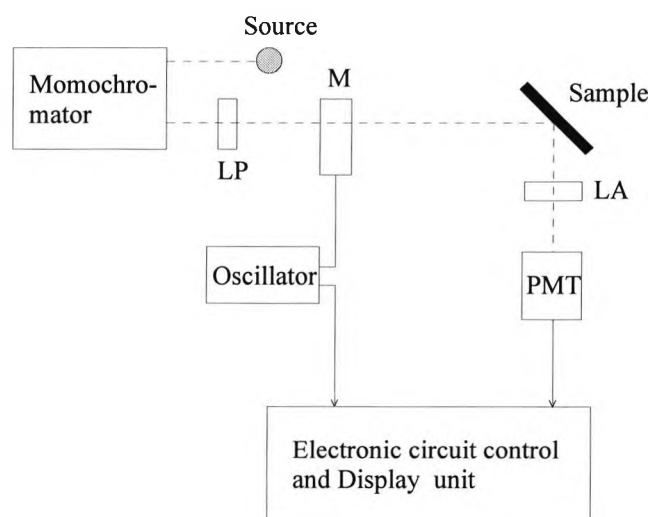
Figure 1-13 Schematic diagram of the ellipsometric system. LP and LA are linear polarisers, M is the polarisation modulator, and PMT is the photomultiplier tube (after Jasperson and Schnatterly, 1969).

The modified ellipsometry, shown in block form in Fig. 1-13, is based on a photoelastic modulator, M, operating at a frequency of 50 kHz (as described previously in Sec. 1-1-1). Property changes in M such as density variation along the medium can affect the polarisation state of the incident light. In addition, the detection circuit shown in the figure provided the electronic recovery of the designed signal.

A few years later, Aspnes and Studa (1975) introduced an alternative configuration for an automatic ellipsometer. The instrument was designated as a rotating analyser ellipsometer (RAE), where the incident light was plane polarised and the reflected light passed through another polariser (the analyser). The analyser was rotated mechanically at frequencies from 20 to 100 Hz. In this case, the role of the rotating analyser as a polarisation state detector was clear. Because of the extensive works on RAE designs, the calibration and operation of the RAE type of device have become well-understood, are commercially available and have become more or less an industry standard (Collin, 1990). In fact, the use of a rotating polariser in the ellipsometer or RPE is also possible as recently was presented by Kim *et al* (1990).

A primary conclusion at this stage is that the use of a polarisation modulation system is a clear choice in real-time monitoring applications in which high speed is a priority, such as in studies of fast changes at surfaces. The system is preferable to the rotating element system as the latter is limited due to the mechanical control involved.

The following examples of ellipsometric systems based on polarisation modulation techniques indicates more and more attention has been directed to this particular type of technique.

Shamir and Klein (1986) proposed an ellipsometric system using rotating plane-polarised light which was a product of the linear polarisation modulation controller mentioned earlier in Sec. 1-1-1 (Fig. 1-3). The approach described was free from mechanically moving parts; therefore, it was applicable to fast time-varying processes.

Singher *et al* (1990) presented a new arrangement for ellipsometry. The authors claimed an advantage of their new proposed set-up over previous ellipsometric configuration in terms of there being fewer complications in generating the rotating plane polarised light. The set-up employed a commercially available stabilised Zeeman laser (SZL) which interestingly produced a beam with similar characteristics to the controllable linear polarisation system.

The SZL emits a single beam consisting of two opposite circularly polarised components that differ in frequency. This obviously is equivalent to the principle of linear polarisation control in a polarising interferometric configuration (Sec. 1-1-1).

A real interferometric ellipsometry was proposed by Lin *et al* in 1990. The authors combined a Mach-Zehnder interferometer and signal processing to form an interferometric ellipsometer for measuring the optical properties of metal surfaces.

Finally, as mentioned at the beginning of this section, the influence on ellipsometric design of the availability of particular instruments at the time of the study is clear from the first fibre optic-based ellipsometric system reported. This was due to the advent of polarisation-maintaining fibres in the 1980s and such ellipsometry equipped with HiBi fibre was proposed by Yoshino and Kurosawa (1984) (Fig. 1-14).
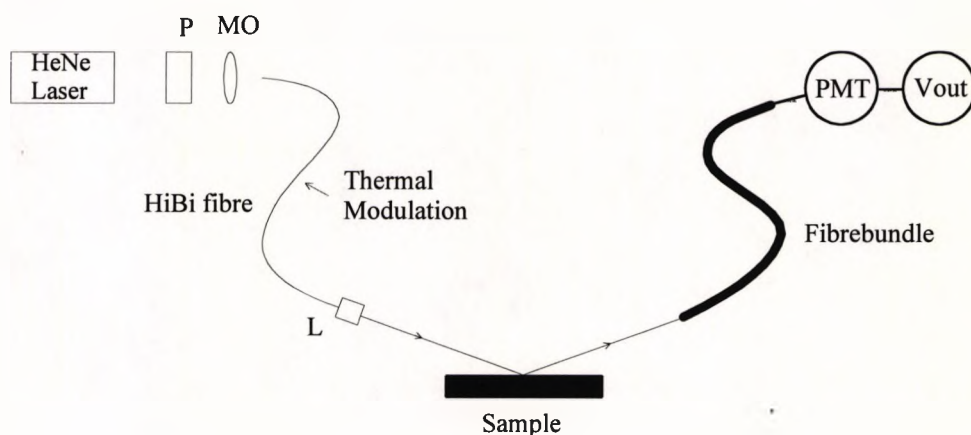
Figure 1-14 All-fibre ellipsometer: P, polariser; MO, microscope objective; L, selfoc lens; PMT, photomultiplier (after Yoshino and Kurosawa, 1984).

The instrument used a polarisation-maintaining single-mode fibre as the polarisation modulator. The authors pointed out that their configuration provided a flexible and compact alternative for the currently available bulky ellipsometric system. In addition, they reported that their all-fibre ellipsometer could be used to determine the optical constants of materials and act as a surface state sensor. However, there was still a disadvantage for the use of this optical fibre configuration. This was the difficulty of pre-aligning the orientation of the eigenaxes of the fibre relative to the plane of incidence of a sample. A remedy for this problem will be discussed in Chapter 2 under the general description of novel polarisation modulation systems given there.

It can be concluded at this point that although ellipsometric measurements, particularly those incorporating linear polarisation modulation techniques, have come a long way, some developments and refinements are still needed for better performance. The changes may include redesigning the configuration to make the alignment more convenient and thus reduce the cost of the complete instrument. These demands can possibly be met by utilising the polarisation modulation techniques proposed here. Such speculation obviously inspires further study into the application of the polarisation modulation techniques to the ellipsometric system which forms the basis of this thesis.

1-3 Aims of the Work

The information given so far has provided a background to the work reported in this thesis and has provided several objectives of research in this field. The following presents the primary aims of the work presented here.

(i) Two distinctive configurations: free-space and optical fibre, are of interest. Hence, both arrangements will be set up, studied and their performances examined in detail.

(ii) These two configurations will be compared in order to decide which provides higher quality of the rotating plane polarised light, better performance and hence is most appropriate for further application.

(iii) Once the selection, based on general basic performance characteristics such as the quality of the polarisation generated, is made, specific improvements will be made in order to enhance the performance of the chosen system. Hence, every possible aspect concerning the performance of the chosen scheme, such as optical components and modulation methods used, have to be closely analysed. This investigation will result in optimising the system performance.

Features	Commercial ellipsometers*	Specifications for proposed systems
1) period of measurement	1-10 s	10^{-3} s
2) accuracy of ellipsometric parameters (ψ and Δ)	ψ: 0.002°-0.015° Δ: 0.004°-0.08°	ψ: 0.01° Δ: 0.01°
3) extinction ratio	10^{-8}-10^{-6}	10^{-4}
4) mount precision	0.01°	0.1°
5) mechanical movement	main feature	none
6) Software and D/A converter resolution	specially written for specific ellipsometers and no mention of the resolution used	turbo-PASCAL based programme and 8-bit resolution converter

Table 1-1 shows features commonly found in commercial ellipsometers against the proposed instrument featured expected to achieve.

*Data represents typical values achievable using either the ELX-1 Precision Ellipsometer (LOT-Oriel Ltd., UK) or Variable Angle Spectroscope Ellipsometer (JA Woollam Co., USA)

The polarisation modulation technique is to be developed as an instrument for ellipsometric measurements. These are extensively used in many industrial areas such as material characterisations and sensing applications. It is important at this stage to set out the specifications required of the proposed system. These requirements are given in Table 1-1 together with the corresponding data for commercial ellipsometers. For this initial study the development of high measurement speed is seen as the important factor.

(iv) It is equally important to demonstrate how well the improved scheme can perform with respect to a particular application. Simple experiments on material characterisation by ways of ellipsometry are to be performed. Chosen optical samples under investigation at this primary stage should have a simple structure, such as interfaces of two semi-infinite isotropic media. This will offer a suitable means to evaluate the system potential for this particular type of application, such as a characterisation of a substrate for a purpose of a thin film deposition.

(v) Once the results obtained from the first stage of application are achieved, the system will be implemented in a further, more detailed study, to characterise an ambient-thin film-substrate system. In addition, the application of the ellipsometric system to thin film-based sensors will be investigated at this stage to investigate the potential for such a sensor system to be widely used.

1-4 Structure of the Thesis

Clearly, the above aims have a direct influence on the way the research is to be performed and, hence, the structure of this thesis. The subsequent description gives the outline of the thesis.

In the next Chapter a discussion of the theoretical and experimental details of both free-space and optical fibre polarisation modulation techniques is made. For the

theoretical aspect, one set of popular mathematical representations, Jones vectors, are used to describe and analyse the systems. Then, in the associated practical investigation, the other commonly used mathematical description of polarisation, Stokes vectors, which are related to observable parameters, are employed. At the end of the Chapter, a discussion on the performance comparison between the two configurations is then presented.

Extensive considerations on the characteristic of the chosen scheme then follows (Chapter 3). Important aspects relating to the system performance, such as optical components and modulation methods, are thoroughly investigated. Examinations of potential error factors associated with the operation of the scheme are carried out, and some significant improvements are also demonstrated as a result of this extensive analysis.

In Chapter 4, the principles of optical reflection resulting from Fresnel's laws of reflection are reviewed as this knowledge is a basis of the technique of reflection ellipsometry to be studied. A description of the arrangement of the reflection ellipsometer incorporating the chosen polarisation modulation technique is given. Then, ellipsometric parameters of various semi-infinite media taken by the ellipsometer are presented. The optical media used include non-, low- and highly-absorbing materials. The results from the investigation can be used to give a direct indication of the sensitivity of the system. The performance of the ellipsometer is examined in both short and long term operations, and a discussion of the results in terms of ellipsometric parameters of relevant materials is also presented.

To show the wider range of applications, the polarisation-modulated ellipsometer has been used to characterise a chemical thin films with different thicknesses. This is described in Chapter 5. The details of the thin film and the method of film/substrate preparation are briefly described, and experimental results are again presented in terms of ellipsometric parameters determined. It is to be noted that, to the best of the author's knowledge, these results, characterising the thin films are the first-ever obtaining using an optical fibre based ellipsometer. To verify the accuracy of the

ellipsometric system, comparisons are also made between reference and experimental results of the thin film/substrate for each sample. In addition, the potential of the ellipsometric system for applications in thin film sensor systems, where some optical property of the film may respond to the presence of an environmental effect (e.g. temperature and humidity), are indicated and discussed.

A final conclusion, summarising the evaluation of the ellipsometric system along with suggestions of further improvements and work are discussed in the last Chapter. Relevant published work is referenced throughout.

In Appendix A, details of the data acquisition and step-by-step procedures for automated polarisation state analyses employed throughout the thesis are presented. Appendix B shows a detail of how to determine a complex index of refraction of a planar interface between two semi-infinite media provided that necessary optical information is known. The theoretical analysis of an ambient-film-substrate system is given in Appendix C. This indicates how to obtain ellipsometric parameters theoretically, if enough information is known. This is followed by Appendix D, a list of work published during the period of the study. Finally, a list of references used in this thesis is presented.

1-5 Conclusions

In this introductory Chapter, two categories of linear polarisation modulation schemes have been reviewed: free-space and optical fibre. The system considerations were presented in terms of their evolution and development from early configurations to present ones. Discussions on the individual systems were given to evaluate the prospect for practical application. In addition, one of the most interesting application of the polarisation modulation technique, ellipsometry, was also discussed. The quantity of work carried in this area has suggested the implementation of polarisation modulation techniques to ellipsometric systems was worthy of being investigated. Finally, aims of the study and structure of the thesis were also presented.

In the next Chapter, general descriptions of the two polarisation modulation schemes will be discussed both theoretically and experimentally.

CHAPTER 2
PRELIMINARY STUDIES OF POLARISATION
MODULATION TECHNIQUES

2-0 Introduction

The ability to create an optical beam of a controllable or modulated azimuth of linear polarisation is an important requirement in a range of optical instruments. This feature of the beam allows speedy and continuous optical measurements to be performed as well as simple signal processing to be undertaken. Many optical instruments such as ellipsometers and polarimeters make use of the changes in the state of polarisation occurring as a result of reflection, scattering or transmission by an optical medium. Monitoring this change then allows optical parameters of the medium, like the index of refraction or the birefringence, to be determined.

The ellipsometer, as it is normally envisaged, traditionally involves precise engineering to control accurately the position and orientation of the optical components. It requires defined mechanical adjustments to enable the measurement process to characterise completely the material under study. In this work, the use of polarisation modulation techniques to overcome these obstacles is proposed and discussed in details.

A rotating plane polarised beam is very attractive product from a polarisation modulation system. The beam provides a convenient way to deal with optical applications, such as ellipsometry (discussed later in Chapter 4), in which orientation-relating measurements are prime requirements.

The basis for generating the rotating plane polarised beam is based on the principle that two orthogonal (left and right) circular polarised beams recombine to

29

produce a linear state (Fig. 2-1), whose azimuth is dependent on the phase difference between the two circular states (Jackson *et al*, 1986).

| Left-circular light | Right-circular light | Linear light |
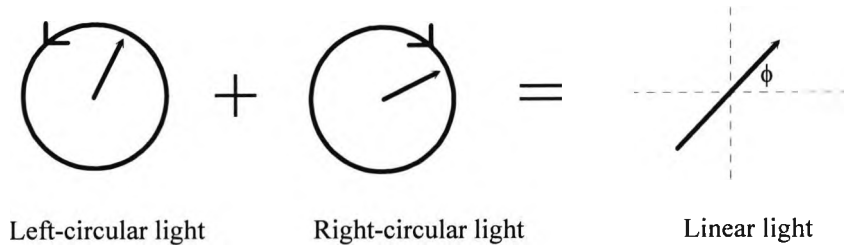
Figure 2-1 Schematic of the combination of two opposite circular polarised beams to form a linear polarised state.

The difference between the two polarisation modulation approaches in either free-space or in an optical fibre, lies in the technique used to achieve modulation of the relative phase difference between the circularly polarised beams, and hence the polarisation azimuth of the output state.
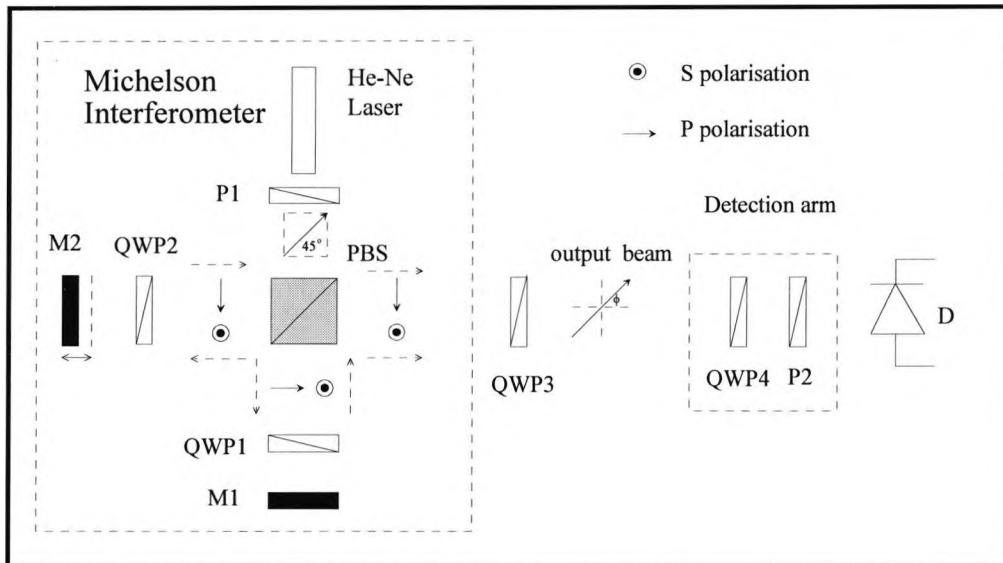
Figure 2-2 Illustration of the Free-Space arrangement, with a detection arm representing a polarisation-characterising system.
Ps : Polarisers, QWPs : Quarter-Wave Plates, PBS : Polarising beam splitter, Ms : Mirrors and D : Photodetector.

The two arrangements for producing beams to meet this requirement are based on interferometric techniques. One configuration is characterised by free-space propagation (Michelson interferometer) as illustrated in Fig. 2-2. This configuration

employs a technique of phase modulation through an optical path change of the mirror M2, while, the other configuration uses highly birefringent (HiBi) fibre as the light propagation medium (Fig. 2-3) in which the modulation of the phase difference between the two circular polarisations is performed by modulating the HiBi fibre birefringence.
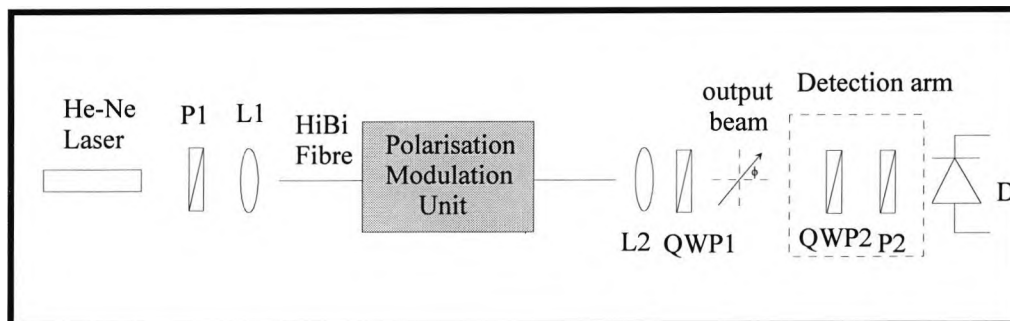
Figure 2-3 Illustration of the HiBi fibre arrangement, with a detection arm representing
                  a polarisation-characterising system.
                  Ps : Polarisers, QWP : Quarter-Wave Plate, Ls : Objective Lenses
                  D : Photodetector.

To describe the mechanism and performance of these methods, an in-depth analysis of each individual arrangement has been carried out and an experimental comparison between the two schemes was also performed.

2-1 General Descriptions

The general concept for an idealised optical arrangement used to produced a linearly polarised output state of controllable azimuth can be described as follows. Linearly polarised light is divided to produce two equal orthogonal polarised beams. Both beams then transmits along different optical paths, varying with time within the polarisation modulation unit. At the output stage, both beams are transformed into left and right circularly polarised states (via a quarter-wave plate (QWP) adjusted to an appropriate orientation) which, when recombined, results in a linear state. By introducing such a variable optical path difference or phase difference between the beams, the azimuth of the linearly polarised output can then be controlled.

It is worth noting that the introduction of the QWP at the output provides a solution for the alignment difficulty encountered in the configuration proposed by Yoshino and Kurosawa (1984) (Sec. 1-2-1). The problem is solved as using the output, rotating plane polarisation, from the system removes some of the restriction of optical alignments.

2-2 General Performance

The process described above can be represented mathematically using the matrix approach developed by Jones (1941). This simplifies the system analysis because each optical component involved in the arrangement under investigation has its own matrix notation which allows for simple manipulation, following conventional matrix algebra.

By following the general descriptions given above, the electric vector of the output beam, $\vec{E}_{output}$, written in terms of Jones matrix notations is given by,

$$\vec{E}_{output} = Q_\theta M \vec{E}_{input} \qquad\qquad (2\text{-}1)$$

where $\vec{E}_{input}$ is the Jones matrix representing the electric field vector of the input light beam, M represents the modulator matrix which can be a series of optical components involved in the particular polarisation modulation system, and Q_θ is a Jones matrix for a quarter-wave plate with its optical axes at an angle θ to the plane of the system.

The series of optical components required to perform the modulation depends on the optical configuration used in the system. However, no matter what configuration is employed, i.e. either the free-space or optical fibre as illustrated in Figs. 2-2 and 2-3, respectively, the output beam - the controllable linear polarised state - will be the same. This fact will be verified and investigated both theoretically and experimentally. The mathematical agreement achieved between the two arrangements will be shown by using the Jones matrix approach, and experimentally by measuring the output polarisation characteristics.

2-2-1 Free-Space Arrangement

2-2-1-1 Experimental Configuration

A Michelson type interferometer, as shown in Fig. 2-2 which allows the two orthogonal components of circularly polarised light to interfere. A HeNe laser ($\lambda = 632.8$ nm) is used as a light source in the arrangement. The laser tube is rotated to make the polarised output be orientated approximately at 45° to the plane of the interferometer. A polarising prism (with an extinction ratio of 10^{-4}) with its transmission axis orientated at 45° to the plane of the interferometer is introduced to improve the quality of the polarised beam. The linearly polarised beam produced is then incident on a polarising beam splitter (PBS) with and an extinction ratio of 10^{-3}, which divides the light into two beams with orthogonal planes of polarisation. The *p* component (parallel to the plane of the interferometer) of the incident beam is transmitted by the PBS to one arm, where a quarter-wave plate (QWP1) with its azimuth at 45° to the interferometer plane is situated. The QWP1 transforms the outgoing beam into a circularly polarised beam (e.g. right handed) which is then reflected back by a mirror M1 (the reflected beam is then seen to be left handed). Again, the QWP1 transforms the reflected beam back to being linearly polarised but in a direction perpendicular to the plane of the interferometer. This is then reflected by the PBS to the output of the system. This circumstance is equivalent to the rotation of the azimuth of the linear polarisation through 90° relative to the interferometric plane. Similarly, the *s* component (perpendicular to the plane of the interferometry) of the incident beam is reflected by the PBS to the other arm, passed through another quarter-wave plate (QWP2) oriented at 45° to the interferometer plane, reflected by a modulated mirror M2, converted into parallel linearly polarised light by the second passage through QWP2 and then transmitted by the PBS to the output end of the interferometer. The modulating system used consisted of mounting one of the mirrors (M2) on a piezo-electric transducer, driven by specially designed ramp signal circuitry to generate the required optical path shift.

At the output of the interferometer, the two linearly polarised beams are converted by a third quarter-wave plate, QWP3 (with its fast axis oriented at 45° to the plane of the interferometer), into right and left circularly polarised light, respectively. Then these two beams recombine and give rise to a linear state. The translation of one of the two mirrors of the interferometer (mirror M2) introduces a time-varying phase difference, or retardance ϕ between the orthogonal p and s linear polarisations and produces at the output a linear state whose azimuth is controlled by ϕ. It should be noted that all quarter-wave plates used in this arrangement and the next have retardation tolerance of $\lambda/50$ (typical retardation tolerance value for mica quarter-wave plates).

The alignment of QWP3 must be undertaken with great care because the precision of the operation, especially in terms of an orientational alignment, can affect the quality of the output. The alignment can be done by allowing an output, of two orthogonally polarised light beams, from the system (without the QWP3) to propagate through a polarising prism orientated parallel to one of the two polarisation states defined by the plane of interferometer. Ideally, the output detected by a photodetector should be a DC signal. However, when QWP3 is inserted at the output of the polarisation modulation system, generally fringes become visible due to interference between the light beams. The QWP3, therefore, has to be adjusted until the DC signal is regained and then this component can be rotated to the required orientation, i.e. at 45°, relative to the orientation of the plane of interferometer.

It has to be emphasised that this polarising Michelson interferometer offers the potential of producing a good quality rotating plane polarisation over other alternative Michelson arrangements. For example, although a Michelson arrangement with replacements of PBS by an ordinary beam splitter, QWP1&2 with eight-wave plates and no QWP3 can generate the same light product (the rotating plane polarisation) the quality of the polarisation may be different. This is because the polarising element such as the PBS polarisation-divides an incident light (from polariser P1), orientated at 45° to the plane of the interferometer, into two completely separate orthogonal

components and then recombines the two polarised lights before they enter the QWP3. Under this circumstance, the linearity of the lights obtained from the PBS is defined by the extinction ratios of the PBS alone. This then results in a high quality of the rotating plane polarised light if, subsequently, a good quality QWP3 is used. Conversely, using an ordinary beam splitter, the polarisation at the output is highly dependent on the performance of the beam splitter and λ/8 plates. Thus higher tolerances on all of the optical components are required.

At this stage, it is worth pointing out that the quality of the PBS and QWP3 used are, indeed, critical to achieve acceptable characteristics of the rotating plane polarised light for further ellipsometric applications.

2-2-1-2 Theoretical Analysis

To get an insight into the process, a theoretical analysis is performed. Let the phase change introduced by the static and dynamic arms to the two beams be ϕ_a and ϕ_b , respectively. The electric vector of the input light from the HeNe laser may be given by,

$$\vec{E}_{input} = \frac{E_o}{\sqrt{2}} \begin{bmatrix} 1 \\ 1 \end{bmatrix} e^{i\omega_o t} \qquad (2-2)$$

where E_o is the amplitude of the beam, ω_o is the angular frequency and t is time.

According to the general expression given by Eq. (2-1), the output beam can be found in this specific case as,

$$\vec{E}^{(1)}_{output} = Q_\theta (M)(\vec{E}_{input})$$

$$= Q_\theta \left(Q_{+45^o} C Q_{-45^o} K_a P_p + Q_{-45^o} C Q_{+45^o} K_b P_s \right) \left(\frac{E_o}{\sqrt{2}} e^{i\omega_o t} \begin{bmatrix} 1 \\ 1 \end{bmatrix} \right) \qquad (2-3).$$

where M, again, a modulator matrix, P_p and P_s are the Jones matrix for the p and s polarisations, respectively, transmitted by the PBS, K_a and K_b are the propagation matrices in the static and dynamic arms, respectively, $Q_{\pm 45^o}$ are the Jones matrices for the quarter-wave plates oriented with their optical axes at ±45° to the interferometric plane and C is the phase retardation introduced by the mirrors M1 and M2. Explicitly:

$$P_p = \begin{bmatrix} 1 & 0 \\ 0 & 0 \end{bmatrix}, P_s = \begin{bmatrix} 0 & 0 \\ 0 & 1 \end{bmatrix}, K_{a,b} = \begin{bmatrix} e^{i\phi_{a,b}} & 0 \\ 0 & e^{i\phi_{a,b}} \end{bmatrix}, Q_{\pm 45^\circ} = \frac{1}{\sqrt{2}} \begin{bmatrix} 1 & \pm i \\ \pm i & 1 \end{bmatrix}, C = \begin{bmatrix} 1 & 0 \\ 0 & e^{i\pi} \end{bmatrix}$$

(2-4).

The group on the left-hand side inside the first brackets (Eq. (2-3)) refers to the effect of the series of optical transformations in the static arm (with mirror M1) and the second group represents the series of optical transformations encountered by the reflected beam from the PBS in the dynamic arm (with mirror M2).

Firstly, considering the transformation of the *p* polarisation incident beam, the process can be described as,

$$\vec{E}_a = \left(Q_{+45} C Q_{-45} K_a P_p \right) \left(\vec{E}_{input} \right)$$

(2-5)

By substituting Eq. (2-4) into Eq. (2-5), the electric field in the static arm becomes,

$$\vec{E}_a = \begin{bmatrix} 1 & +i \\ +i & 1 \end{bmatrix} \begin{bmatrix} 1 & 0 \\ 0 & e^{i\pi} \end{bmatrix} \begin{bmatrix} 1 & -i \\ -i & 1 \end{bmatrix} \begin{bmatrix} e^{i\phi_a} & 0 \\ 0 & e^{i\phi_a} \end{bmatrix} \begin{bmatrix} 1 & 0 \\ 0 & 0 \end{bmatrix} \begin{bmatrix} 1 \\ 1 \end{bmatrix} \frac{E_o}{2\sqrt{2}} e^{i\omega_o t}$$

(2-6)

The product is found to be,

$$\vec{E}_a = \begin{bmatrix} 0 \\ 1 \end{bmatrix} \frac{E_o}{\sqrt{2}} e^{i\left(\omega_o t + \phi_a + \frac{\pi}{2}\right)}$$

(2-7).

Similarly, the above procedure can be applied to the transformation of the *s* polarisation beam in the dynamic arm. The process can be described in terms of the Jones notations as,

$$\vec{E}_b = \left(Q_{-45^\circ} C Q_{+45^\circ} K_b P_s \right) \left(\vec{E}_{input} \right)$$

(2-8).

The description of the transformation procedures for this arm is similar to those for the previous one but the beam transmitted by the PBS to the output end is *p* polarised.

The resultant electric field is given by,

$$\vec{E}_b = \begin{bmatrix} 1 \\ 0 \end{bmatrix} \frac{E_o}{\sqrt{2}} e^{i\left(\omega_o t + \phi_b + \frac{\pi}{2}\right)}$$

(2-9).

At the output of the interferometer before the third quarter-wave plate, QWP3, the outgoing beams from the interferometer are composed of two linearly polarised beams with orthogonal polarisations, $\vec{E}_a$ & $\vec{E}_b$. The combination can be expressed in the following form,

$$\bar{E}_c = \left\{ \begin{bmatrix} 0 \\ 1 \end{bmatrix} + \begin{bmatrix} 1 \\ 0 \end{bmatrix} e^{i\phi^{(1)}} \right\} \frac{E_o}{\sqrt{2}} e^{i\left(\omega_o t + \phi_a + \frac{\pi}{2}\right)} \tag{2-10}$$

where $\phi^{(1)}(=\phi_b - \phi_a)$ is the phase difference between the two polarised beams.

As stated in Eq. (2-1), the two linearly polarised beam are transformed by the quarter-wave plate QWP3 to left and right circularly polarised beams which then recombine to give a linear state,

$$\begin{aligned}
\vec{E}^{(1)}_{output} &= Q_{+45^\circ} \vec{E}_c \\
&= \begin{bmatrix} 1 & i \\ i & 1 \end{bmatrix} \left\{ \begin{bmatrix} 0 \\ 1 \end{bmatrix} + \begin{bmatrix} 1 \\ 0 \end{bmatrix} e^{i\phi^{(1)}} \right\} \frac{E_o}{2} e^{i\left(\omega_o t + \phi_a + \frac{\pi}{2}\right)} \\
&= \left\{ \begin{bmatrix} 1 \\ -i \end{bmatrix} e^{i\frac{\pi}{2}} + \begin{bmatrix} 1 \\ i \end{bmatrix} e^{i\phi^{(1)}} \right\} \frac{E_o}{2} e^{i\left(\omega_o t + \phi_a + \frac{\pi}{2}\right)}
\end{aligned}$$

$$(2\text{-}11).$$

It should be noted that the left term inside the braces explicitly shows a left circularly polarised light and the right term clearly indicates a right circularly polarised one. This output electric field can be rewritten as,

$$\vec{E}^{(1)}_{output} = \begin{bmatrix} \left(1 + e^{i\left(\phi^{(1)} - \frac{\pi}{2}\right)}\right) \\ \dfrac{\left(1 - e^{i\left(\phi^{(1)} - \frac{\pi}{2}\right)}\right)}{i} \end{bmatrix} \frac{E_o}{2} e^{i\left(\omega_o t + \phi_a + \pi\right)} \tag{2-12}.$$

Factorizing each element from the Eq. (2-12) by a common factor of $e^{-i\left(\frac{1}{2}\right)\left(\phi^{(1)} - \frac{\pi}{2}\right)}$, the equation becomes,

$$\vec{E}^{(1)}_{output} = \begin{bmatrix} \dfrac{\left(e^{i\left(\frac{1}{2}\right)\left(\phi^{(1)}-\frac{\pi}{2}\right)} + e^{-i\left(\frac{1}{2}\right)\left(\phi^{(1)}-\frac{\pi}{2}\right)} \right)}{2} \\[2em] -\dfrac{\left(e^{i\left(\frac{1}{2}\right)\left(\phi^{(1)}-\frac{\pi}{2}\right)} - e^{-i\left(\frac{1}{2}\right)\left(\phi^{(1)}-\frac{\pi}{2}\right)} \right)}{2i} \end{bmatrix} E_o e^{i\left(\omega_o t+\phi_a+\frac{3\pi}{4}+\frac{\phi^{(1)}}{2}\right)}$$

(2-13).

Using the following identity (Selby, 1968),

$$\cos\Omega = \frac{e^{i\Omega}+e^{-i\Omega}}{2},$$ (2-14a),

$$\sin\Omega = \frac{e^{i\Omega}-e^{-i\Omega}}{2i}$$ (2-14b),

where Ω is defined as an angular argument, the output electric field in Eq. (2-13) can be rewritten as,

$$\vec{E}^{(1)}_{output} = \begin{bmatrix} \cos\left\{\frac{1}{2}\left(\phi^{(1)}-\frac{\pi}{2}\right)\right\} \\[1em] -\sin\left\{\frac{1}{2}\left(\phi^{(1)}-\frac{\pi}{2}\right)\right\} \end{bmatrix} E_o e^{i\left(\omega_o t+\phi_a+\frac{3\pi}{4}+\frac{\phi^{(1)}}{2}\right)}$$

(2-15),

which is a linear state whose azimuth varies according to $\phi^{(1)}$.

In this system (Fig. 2-2) the relative phase between the beams is continuously varied by modulating one of mirrors in the interferometric system. The amplitude of the driving signal is set such that the phase difference between the beams is varied to generate the required variation in orientation of the electric vector of the output.

2-2-2 Optical Fibre Arrangement

2-2-2-1 Experimental Configuration

As an alternative, the necessary phase modulation can be achieved through the use of single mode fibre optic components. This has the obvious advantage over the previous arrangement that there is no requirement for many bulk optical components and their careful alignment.

The principle of this alternative scheme is based on the modulation of the birefringence of HiBi fibre (Fig. 2-3). The optical fibre polarisation modulation arrangement can again be described in terms of the effect on the polarised light beam emitted from a HeNe laser (λ=632.8 nm). The light from the laser was polarised at 45º

to the eigenaxes of the fibre and launched into it by means of a x10 objective lens, causing the two eigenmodes of the HiBi fibre to be equally populated. The birefringence of the fibre may then be modulated in some appropriate way as will be described later. The output from the fibre was then collimated using another x10 objective lens and passed through a quarter-wave plate (with a retardation tolerance of $\lambda/50$) with its optical axis at 45º to the axes of the fibre, transforming the output from each eigenmode into circularly polarised light of opposite handedness which then are combined together to give a linear state.

2-2-2-2 Theoretical Analysis

It is useful to gain an understanding of the mechanism of this configuration through a simple analysis using Jones vector notation. Suppose that the input light from the HeNe laser is again given by Eq. (2-2)

$$\vec{E}_{input} = \frac{E_o}{\sqrt{2}} \begin{bmatrix} 1 \\ 1 \end{bmatrix} e^{i\omega_o t}$$

The beam transmits through a series of optical components: a length of modulated HiBi fibre and a quarter-wave plate oriented at 45º to the eigenaxes of the fibre. Then, according to Eq. (2-1) and following the above details, the output vector can be found to be

$$\vec{E}_{output}^{(2)} = Q_{+45^\circ}(M)(\vec{E}_{input})$$

$$= \begin{bmatrix} 1 & i \\ i & 1 \end{bmatrix} \begin{bmatrix} e^{i(\phi_f)} & o \\ o & e^{i(\phi_s)} \end{bmatrix} \begin{bmatrix} 1 \\ 1 \end{bmatrix} \frac{E_o}{2} e^{i\omega_o t}$$

$$= \begin{bmatrix} \dfrac{(e^{i(\phi^{(2)}-\frac{\pi}{2})}+1)}{2} \\ -\dfrac{(e^{i(\phi^{(2)}-\frac{\pi}{2})}-1)}{2i} \end{bmatrix} E_o e^{i(\omega_o t+\phi_s)} \quad , \text{ where } \phi^{(2)} = \phi_f - \phi_s$$

(2-16),

where M represents the properties of a linear birefringent fibre described in terms of a pseudo-Jones matrix (Tatam *et al*, 1986), and ϕ_f and ϕ_s are the phase retardances corresponding to the fast and slow eigenmodes respectively.

Again, factorizing each element in Eq. (2-16) by a common factor of $e^{-i\left(\frac{1}{2}\right)\left(\phi^{(2)}-\frac{\pi}{2}\right)}$, and using identities, Eqs. (2-14a) and (2-14b), the electric field output may be rewritten as,

$$\vec{E}_{output}^{(2)} = \begin{bmatrix} \cos\left\{\frac{1}{2}\left(\phi^{(2)}-\frac{\pi}{2}\right)\right\} \\ -\sin\left\{\frac{1}{2}\left(\phi^{(2)}-\frac{\pi}{2}\right)\right\} \end{bmatrix} E_o e^{i\left(\omega_o t + \phi_s + \frac{\pi}{4} + \frac{\phi^{(2)}}{2}\right)}$$
(2-17),

which is again a linear state with the azimuth controlled by $\phi^{(2)}$, as before. The relative modal retardance $\phi^{(2)}$ can be modulated by several techniques such as heating, longitudinal stretching and cylindrical piezoelectric stretching, thus yielding the azimuth rotation. A detailed investigation of modulation techniques is given later in this work (Sec. 3-4-2).

As can be clearly seen, both configurations provide essentially the same result (Eqs. 2-15 and 2-17), which is a controllable linear polarisation state. It is worth noting at this point a few of the properties of the output. If the emerging polarised beam is detected immediately by a photodetector, a photocurrent that is proportional to the light intensity will be obtained. Summing the squares of the amplitudes of the two orthogonal components from Eqs. (2-15) or (2-17), the intensity of the output may be given by,

$$I_{output} = \left(\vec{E}_{output}^{(i)}\right).\left(\vec{E}_{output}^{(i)}\right)^* \qquad i = 1 \text{ or } 2$$
$$= I_o$$
(2-18)

where $I_o = E_o^2$ = a constant.

Thus a DC signal is obtained from the photodetector. In addition, if an analyser is introduced before the photodetector, the transmitted electric field will becomes

$$\vec{E}_{analyser} = A_{\theta}\vec{E}^{(i)}_{output}$$

$$= \begin{bmatrix} \cos^2\theta & \cos\theta\sin\theta \\ \cos\theta\sin\theta & \sin^2\theta \end{bmatrix} \begin{bmatrix} \cos\left\{\frac{1}{2}\left(\phi^{(i)}-\frac{\pi}{2}\right)\right\} \\ -\sin\left\{\frac{1}{2}\left(\phi^{(i)}-\frac{\pi}{2}\right)\right\} \end{bmatrix} E_o e^{i\varepsilon}$$

$$= \begin{bmatrix} \cos^2\theta\cos\left\{\frac{1}{2}\left(\phi^{(i)}-\frac{\pi}{2}\right)\right\} - \cos\theta\sin\theta\sin\left\{\frac{1}{2}\left(\phi^{(i)}-\frac{\pi}{2}\right)\right\} \\ \cos\theta\sin\theta\cos\left\{\frac{1}{2}\left(\phi^{(i)}-\frac{\pi}{2}\right)\right\} - \sin^2\theta\sin\left\{\frac{1}{2}\left(\phi^{(i)}-\frac{\pi}{2}\right)\right\} \end{bmatrix} E_o e^{i\varepsilon}$$

(2-19),

where A_{θ} represents the Jones matrix for an analyser at an arbitrary orientation, θ, and the phase $\varepsilon = \omega_o t + \phi_a + \frac{3\pi}{4} + \frac{\phi^{(1)}}{2}$ in case of the free space arrangement and $\varepsilon = \omega_o t + \phi_s + \frac{\pi}{4} + \frac{\phi^{(2)}}{2}$ when using fibre optics.

Consequently, the intensity detected after the analyser may be given by,

$$I_{analyser} = \left(\vec{E}_{analyser}\right).\left(\vec{E}_{analyser}\right)^*$$

$$= \frac{I_o}{2}\left(1 + \cos 2\left\{\theta + \frac{1}{2}\left(\phi^{(i)}-\frac{\pi}{2}\right)\right\}\right) \qquad i = 1 \text{ or } 2$$

(2-20)

This shows that the output signal is a sinusoidal function of the orientation of the analyser, θ, and the modulation phase, $\phi^{(i)}$, regardless of which configuration is chosen. Moreover, as the analyser rotates, the amplitude of the output signal remains stable while its phase changes. This is important in the alignment procedure of the polarisation modulation system and its subsequent applications.

In all, this theoretical analyses would appear to suggest that both arrangements have similar capability to offer the required, controllable linear polarisation. Nevertheless, the conclusion does not ensure that both arrangements will work practically with the same performance and operational characteristics. These experimental aspects of the two schemes are examined in the next section.

2-3 Comparison of Experimental Performance

The ability to create a controllable or modulated state of polarisation is not the only requirement for an effective optical measurement. Equally important for such instruments is their sensitivity and their ability to make an accurate measurement. Here, the sensitivity of the polarisation modulation system is dependent on the quality

of the state of polarisation (SOP) of the recombining beams produced by the chosen system. If the two recombining optical beams have orthogonal circular SOPs then a plane polarised beam with 100% degree of polarisation (DOP) will result. The DOP is defined most generally as (Hecht and Zajac, 1974),

$$DOP = \frac{I_p}{I_p + I_u} \times 100\% \qquad (2\text{-}21)$$

in which I_p and I_u are the constituent intensities of polarised and unpolarised light.

However, even if a 100% DOP is detected for the beam under study this does not mean the required state of polarisation is provided since other states of polarisation such as completely circular and elliptical polarisation may also give the same DOP. In order to tell the difference between these states when encountering such a case, the quantity known as ellipticity is needed. The ellipticity is generally defined as the ratio of the semi-minor to semi-major axes of an elliptical pattern (Schurcliff, 1962). Clearly, in the case of a completely plane polarised beam, the ellipticity is zero and for completely circular polarised beam the ellipticity is unity. This criterion can also be used for checking how the quality of the detected beam compares to that of one which is completely linear one. As a result, with a rotating plane polarised light beam under study, it is reasonable to carry out an experimental performance comparison based on the investigation of the DOP and the ellipticity of an output beam produced by each of the two arrangements in a point in time.

For the free-space configuration, the performance of the Michelson interferometer, previously described in Sec. 2-2-1, was examined and in the second arrangement a replacement of the interferometer was made with a length (10 m) of HiBi fibre (York HB-600). A cylindrical piezo-electric transducer (PZT) was used as the optical fibre modulation method by winding the length of the fibre around it, with the PZT then driven sinusoidally to stretch the fibre and modulate the birefringence. The rest of the procedures are similar in detail to that described earlier, under the general performance (Sec. 2-2-1).

To characterise any state of polarisation, three independent quantities are necessary to form a complete description, e.g. the amplitudes of an electric field along two principally orthogonal axes and the phase difference between the two axes. However, these parameters cannot be measured instantly. The first limitation is as the beam of light propagates through space, transversely to the direction of propagation, the light electric vector traces out some figure depending on the SOP (either a line, circle or ellipse) in a time interval of the order of 10^{-15}s. This period of time is clearly too short to allow any available detecting system to follow the changing electric vector. Secondly, the circumstance becomes even more impracticable in the case of unpolarised light whose SOP is continually changing since the amplitude and phases of the electromagnetic waves vary irregularly in time.

However, these limitations can be surmounted by considering only the average values of the electromagnetic field, i.e. the representation of polarised and unpolarised light in terms of observables. The remedy to this situation was proposed by G G Stokes, as far back as the year 1852, who introduced alternative and practical ways for characterising the state of polarisation using four parameters (S_0, S_1, S_2, S_3) all of which have the same physical dimension of intensity; each corresponds not to an instantaneous intensity but to a time averaged intensity, i.e. the average being taken over a period long enough to permit practical measurement. Such polarisation parameters are now known as the "Stokes parameters". Apart from the normal purpose of describing the SOP of a beam, the parameters can be used to determine its DOP as well.

The four parameters can be defined from many theoretical bases such as the operational approach (Schurcliff, 1962) and electromagnetic theory (Hecht, 1970). As the operational definition provides a practical solution to the characterisation of a polarised beam, the following performance comparison will be based entirely on this description.

The operational approach can be formulated using directly measurable quantities as indicated by Born and Wolf (1989). The quantities may be determined

from simple experiments. If $I(\theta,\xi)$ denotes the intensity of the light beam polarised in the x direction making an angle, θ, with a fixed laboratory Cartesian co-ordinate system, when the orthogonally composite component, is subjected to retardation, ξ, with respect to the x component. Then the Stokes parameters are given by

$$S_0 = I(0^o,0) + I(90^o,0) \qquad\qquad (2\text{-}22\text{a}),$$

$$S_1 = I(0^o,0) - I(90^o,0) \qquad\qquad (2\text{-}22\text{b}),$$

$$S_2 = I(45^o,0) - I(135^o,0) \qquad\qquad (2\text{-}22\text{c}),$$

$$S_3 = I(45^o,\frac{\pi}{2}) - (135^o,\frac{\pi}{2}) \qquad\qquad (2\text{-}22\text{d}).$$

The parameter S_0 evidently represents the total intensity. The parameters S_1 is equal to the excess in intensity of the light transmitted by a polariser which accepts linearly polarised light in the azimuth $\theta = 0^o$, over the light transmitted by a polariser which accepts linear polarisation in the azimuth $\theta = 90^o$ to the chosen reference direction. For the parameter, S_2, there is a similar interpretation with respect to the azimuth $\theta = 45^o$ and $\theta = 135^o$. Finally, the parameter S_3 is equal to the excess in intensity of light transmitted by a device which accepts right-handed circular polarisation of light over that transmitted by a device which accepts left-handed circular polarisation. It should be noted that the circular polarisation filter device can be formed by letting a beam under study impinge first on a quarter-wave retarder first, and then an analyser with the appropriate orientation (Hecht, 1970).

Thus in summary, the quantity S_0 is simply the total intensity while S_1, S_2 and S_3 specify the state of polarisation and they are indeed directly observable.

The four parameters are obtained by measuring the intensity transmitted by various orientations and combinations of an analyser and a quarter-wave plate (Fig. 2-4). The required combination is then included in the system under investigation. Figs. 2-2 and 2-3 show the output-analysing part added to the specific configurations.
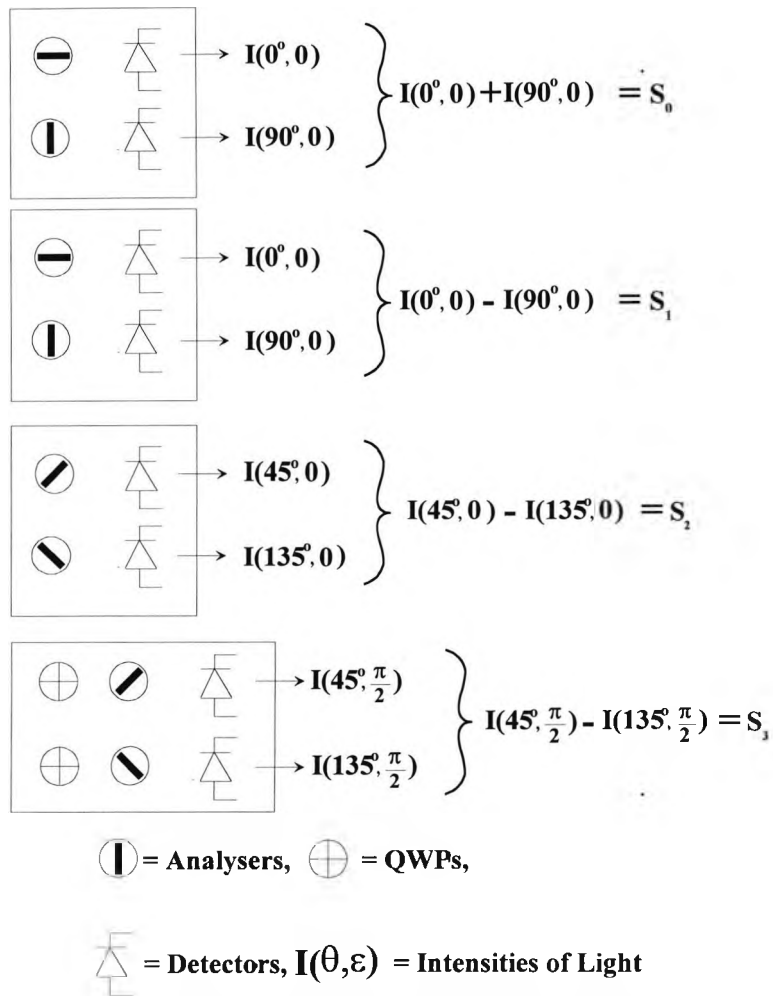
Figure 2-4 Illustration of various combinations of an analyser and
quarter-wave plate for measuring Stokes parameters.

Two particular quantities, the DOP and the ellipticity, obtained from each arrangement were to be compared, since these quantities can readily provide details on the quality of the two outputs. As already mentioned, the values of these quantities for the case of perfect linearly polarised light are 100% for the DOP and zero for the ellipticity. Clearly, the closer the measured values of the DOP and ellipticity from each arrangement are to these desired optimum values, the better the performance of the particular arrangement. The values of the DOP and ellipticity are easily obtainable from the Stokes parameters.

The two specific quantities required for the performance comparison between the two arrangements, written in terms of the Stokes parameters, can be expressed as (Born & Wolf, 1989)

1) the degree of polarisation, DOP,

$$DOP = \frac{\sqrt{S_1^2 + S_2^2 + S_3^2}}{S_0} \times 100\%$$

(2-23),

and

2) ellipticity, e,

$$e = \tan\left(\frac{1}{2}\left\{\sin^{-1}\left[\frac{S_3}{\sqrt{S_1^2 + S_2^2 + S_3^2}}\right]\right\}\right)$$

(2-24).

Intensities	Free-Space arrangement Intensities (arb. units)	HiBi fibre arrangement Intensities (arb. units)
$I(0^o,0)$	0.40±0.05	0.010±0.005
$I(90^o,0)$	3.90±0.05	0.720±0.005
$I(45^o,0)$	2.35±0.02	0.370±0.004
$I(135^o,0)$	2.10±0.04	0.370±0.04
$I(45^o,\frac{\pi}{2})$	2.25±0.03	0.334±0.006
$I(135^o,\frac{\pi}{2})$	2.35±0.03	0.442±0.003

Table 2-1 Summary of measured intensities of the output beam at various orientations of polarising prism and QWP from the Free-Space and HiBi fibre configurations.

To evaluate the Stokes parameters, the intensities of the output beam, at various orientations and combinations of optical components involved, have to be measured. Table 2-1 summarises the experimental results from the investigation of a number of output beams. These results correspond to the output polarisation orientated at 90º to the defined reference.

The four Stokes parameters can be determined through Eqs. (2-22a) to (2-22d) by substituting for the intensities, the measured values from Table 2-1. The calculated values obtained are shown in Table 2-2.

From the definitions given for the Stokes parameters, the four parameters have the same dimension of intensity. In particular, the scale for the parameters depends totally on a corresponding total intensity of the beam represented by S_0.

Stokes parameters	Free-Space arrangement Intensities (arb. units)	HiBi fibre arrangement Intensities (arb. units)
S_0	4.30±0.07	0.73±0.007
S_1	-3.50±0.07	-0.72±0.007
S_2	0.25±0.04	0.00±0.04
S_3	-0.10±0.04	-0.108±0.006

Table 2-2 Summary of the calculations of the Stokes parameters from their operational definitions.

This can be seen from Table 2-2, whereby the two configurations generated different ranges of the Stokes parameters. The HiBi fibre arrangement has a much lower total intensity $S_0 = \left(I\left(0^o,0\right) + I\left(90^0,0\right) \right)$ than does the Free-space. This arises as the HiBi fibre arrangement contains a length of optical fibre as the light propagation medium tends to have stricter launching conditions (such as matching the input beam size to the acceptance angle of the fibre) and lower efficiency. As such, an intensity reduction will result.

The values of the DOP and e for each arrangement are then calculated and shown in Table 2-3.

As shown in the table, in case of the free-space arrangement, the DOP was measured to be 81%. With this value of DOP, it is unlikely that a satisfactory result would be achieved if this partially polarised beam is introduced into a polarimetric measuring system, and so this cannot be used.

Quantities of interest	Free-Space arrangement	HiBi fibre arrangement
Degree of polarisation	$\approx 81\%$	$\approx 99\%$
Ellipticity	$\approx 10^{-2}$	$\approx 10^{-2}$

Table 2-3 Summary of the calculated two characteristics describing the polarisation of the output beams from two arrangements.
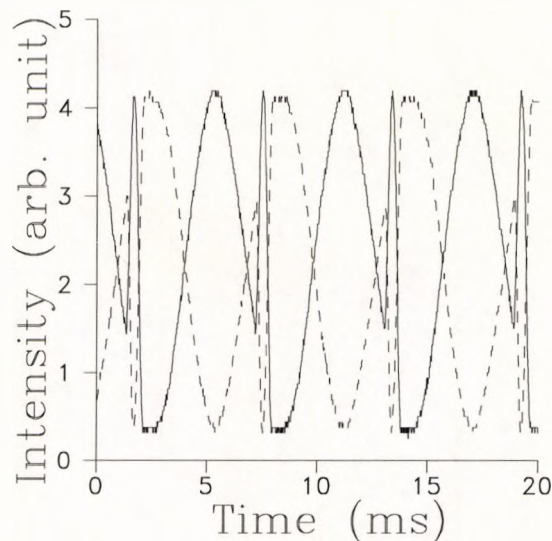
Figure 2-5 Intensities transmitted through analyser at 0° (dashed line) and 90° (solid line) for the free-space arrangement.

Fig. 2-5, illustrating the detected output intensities from the free-space arrangement, was obtained when an analyser in the detection arm was orientated at 0° (dashed line) and 90° (solid line) to the chosen reference direction. Each curve shows a non-zero minimum intensity which implies a large unpolarised component in the relevant output beam under investigation. The ellipticity was also calculated using Eq. (2-24) and the value was found to be of the order of 10^{-2}.

Fig. 2-6 describes the intensities transmitted through an analyser orientated at 0° (dashed line) and 90° (solid line) in the detection arm for the HiBi fibre polarisation modulation arrangement. As can be seen from the figure, the minimum intensity of the polarised light approaches zero, which clearly means that the

unpolarised light fraction is dramatically reduced in this situation over the previous case (Fig. 2-5). From the experimental result obtained, the DOP was about 99% which is much more acceptable for the practical use of such a system. The ellipticity of the light beam was calculated and the result was also found to be in the order of 10^{-2}.
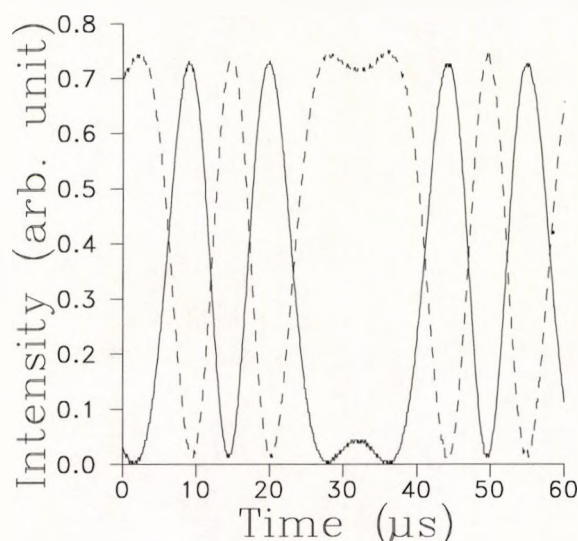
Figure 2-6 Intensities transmitted through analyser at 0° (dashed line) and 90° (solid line) for the HiBi fibre arrangement.

It should be noted that the DOPs obtained from both arrangements are significantly different, whereas, the ellipticities are somewhat similar. These results require a more detailed description of what makes the two systems behave differently.

An explanation that could account for the difference in the DOP obtained from the two arrangements can be reasonably drawn from a consideration of the practical arrangement. The result suggests that the free-space arrangement allows the introduction of an increased quantity of unpolarised light over that with the optical fibre. This occurrence may be justified when the basic structure of each arrangement is analysed.

First of all, when considering the free-space arrangement, the apparatus is composed of a number of discrete optical components such as PBSs and QWPs whose

alignments and qualities, in practice, are such as to be prone to induce more or less unrelated electric fields which can contribute to the depolarisation of transmitted beam.

Having checked the specifications of the PBSs and QWPs (supplied by Melles Groit (1992)), a further explanation is possible. In case of the PBS, it has a low extinction ratio of 10^{-4} and any irregularities in the splitting ratio would also contribute to the effect. Likewise, mica, a common material used to manufacture QWPs and used in these arrangements often has regions of inhomogeneity and a retardation tolerance of $\lambda/50$. This implies that any procedure in the polarisation modulation technique, which has QWPs involved (such as the process of transforming two circular polarised lights into a linear) may not give rise to the required SOP of the output and may reduce the DOP. In addition, the multiple reflections occurring between surfaces of the optical components as aligned in Fig. 2-2 can also contribute to the depolarising effect.

In the other case, the arrangement of the optical fibre system is rather different from that in the free-space since in the former case many less bulky optical components are replaced with a single length of optical fibre. Optical fibre production is a very specialised process. Many years of development have gone in to the manufacturing of low loss single mode fibre optic for long haul communications systems. As a result, regions of homogeneity and inclusions are negligible, and this is also true for the HiBi fibre used here.

The measured DOP obviously shows that the technique using fibre suffers less depolarisation than the previous one.

Since the unpolarised light is operationally defined (Schurcliff, 1962) as a beam that, operated on by optical devices like polarisers and retarders, is divided the beam into two completely polarised subbeams, these subbeams have equal power (in a time interval long enough to permit the power to be measured). Thus, it can be detected in such a way as to provide an input to each intensity involved in the calculation of the Stokes parameters.

If the total intensity of the unpolarised light is given by $2I_u$, the modified Stokes parameters become,

$$S_0' = \left\{I(0^o,0) + I_u\right\} + \left\{I(90^o,0) + I_u\right\}$$ (2-25a),

$$S_1' = \left\{I(0^o,0) + I_u\right\} - \left\{I(90^o,0) + I_u\right\}$$ (2-25b),

$$S_2' = \left\{I(45^o,0) + I_u\right\} - \left\{I(135^o,0) + I_u\right\}$$ (2-25c),

$$S_3' = \left\{I(45^o,\tfrac{\pi}{2}) + I_u\right\} - \left\{I(135^o,\tfrac{\pi}{2}) + I_u\right\}$$ (2-25d).

The above combination treatments for particular Stokes parameters, S_1', S_2' and S_3', are thus independent of I_u, and the parameters then can be considered to be the same as S_1, S_2 and S_3.

By using Eq. (2-23), the DOP can be found to be a function of the unpolarised factor,

$$DOP' = \frac{\sqrt{S_1^2 + S_2^2 + S_3^2}}{S_0'} \times 100\%$$ (2-26).

This clearly explains why a large amount of the unpolarised intensity, as found in the free-space configuration, deteriorates very much the DOP of the output beam.

The similarity of the ellipticities observed from the two arrangements may also be explained by the same analysis. If the Stokes parameters in the ellipticity expression in Eq. (2-24) are substituted by the modified parameters (Eqs. (2-25a) to (2-25d)), the expression remains unchanged since the unpolarised light terms cancel out completely. Therefore, the value of the ellipticity obtained from each arrangement is not affected by the existence of the unpolarised constituent. Although it suggests that both configurations can generate the required polarisation factor, the output beam quality determined by the DOP still shows the obvious difference in the depolarising effect of the free-space and optical fibre techniques.

2-4 Conclusions

The operation of the two polarisation modulation techniques has been studied and quantified. Both techniques produce a low ellipticity rotating linear polarisation

state. However, the degree of polarisation obtained was much higher in the fibre case than in the free-space instance. Thus, for use in polarimetric measurement systems, the optical fibre modulation scheme would appear to be the better choice, in terms of simplicity and ease of alignment, as well as achieving adequate DOP.

To obtain an even higher performance including a higher DOP from the optical fibre arrangement, more extensive studies and development on the system were carried out. The investigation will be presented in terms of performance-related aspects, such as the properties of the HiBi fibre, the modulation methods and the optical components involved, in the next Chapter.

CHAPTER 3

A HIGH BIREFRINGENCE FIBRE POLARISATION MODULATION SCHEME: SYSTEM AND PERFORMANCE

3-0 Introduction

The previous Chapter has described two approaches to achieve the required linear polarisation modulation for use in the ellipsometer measurements to be described. The employment of free-space bulk optical components and optical fibre has been studied and investigated in detail, to determine their experimental performance in terms of the degree of polarisation (DOP) and ellipticity achievable. The results have demonstrated that a higher quality output, more applicable to polarimetric measurement systems, was achieved by using the fibre optic scheme.

Nevertheless, further improvement to the quality of the rotating polarised light, which is the essence of the technique, is still required for the application in mind. This is because, from the previous Chapter, the degree of polarisation of the output is found to be related to the structure of the configuration itself. This suggests a problem to be tackled in order for the system to achieve the performance target set up in Sec. 1-3 This Chapter describes an extensive quantitative investigation into the performance of such a fibre-based system, detailing and experimentally verifying some important performance-related aspects, (namely, the properties of the high birefringence (HiBi) fibre, the modulation method and optical components involved) which could influence the quality of the rotating polarised light.

Before analysing the main factors involved, it is necessary to derive a theoretical basis to the behaviour of the optical fibre approach used in order to gain a fundamental insight of the processes taking place in the generation of the desired rotation.

53

3-1 Theoretical Analysis

The optical fibre polarisation modulation technique used to generate a linear state whose azimuth is dependent on the phase difference between two combining circular states can be illustrated conveniently using the familiar Jones vector notation, as described in Sec. 2-2-2.

In this configuration, the light emitted from a HeNe laser passes through a series of optical components: a length of modulated HiBi fibre and a quarter-wave plate oriented at 45° to the eigenaxes of the fibre. Thus the output electric vector is given by

$$\vec{E}_{output} = \begin{bmatrix} \cos\left\{\frac{1}{2}\left(\phi(t) - \frac{\pi}{2}\right)\right\} \\ -\sin\left\{\frac{1}{2}\left(\phi(t) - \frac{\pi}{2}\right)\right\} \end{bmatrix} E_0 e^{i\zeta(t)} \qquad (3\text{-}1),$$

where
$$\phi(t) = (k_y - k_x)(L + L(t)) \qquad (3\text{-}2),$$

and
$$\zeta(t) = \omega_o t + \frac{\pi}{4} + \frac{1}{2}(k_x + k_y)(L + L(t)) \qquad (3\text{-}3),$$

L is the length of the HiBi fibre, $L(t)$ is the fibre length extension due to the modulation unit (the modulation length) and k_x and k_y are propagation constants for each eigenmode defined as $k_x = n_x \dfrac{2\pi}{\lambda_o}, k_y = n_y \dfrac{2\pi}{\lambda_o}$, respectively (Longhurst, 1973).

Clearly, there is a temperature and strain effect which will be reflected in k_x and k_y, but for the purposes of the operation of the instrument, k_x and k_y are assumed constant and all possible modulation effects are considered to be included implicitly in $L(t)$. In the actual instrument, the referencing technique used means that details of the specific origin of the modulation are not required.

Eq. (3-1) represents a linear polarised wave in which the orientation of the polarisation has been rotated through an angle, $\frac{1}{2}\left(\phi(t) - \frac{\pi}{2}\right)$, the azimuth angle. This rotation is proportional to the modulation of the HiBi fibre, as given in Eq. (3-2).

3-2 Systematic Details

In this section, descriptions of the optical fibre system arrangement, the rotating plane polarisation generation, and methods of data evaluation are discussed.

3-2-1 System Arrangement

The initial polarisation modulation scheme employed was produced by winding a length (10 m) of HiBi fibre (York HB-600) around a cylindrical piezo-electric transducer (PZT) as shown schematically in Fig. 3-1. The PZT used is ceramic with a length of 76.2 mm, outer diameter of 76.2 mm and wall thickness of 5.08 mm (supplied by Morgan Matroc). The resonant frequency of the PZT is 14 kHz.
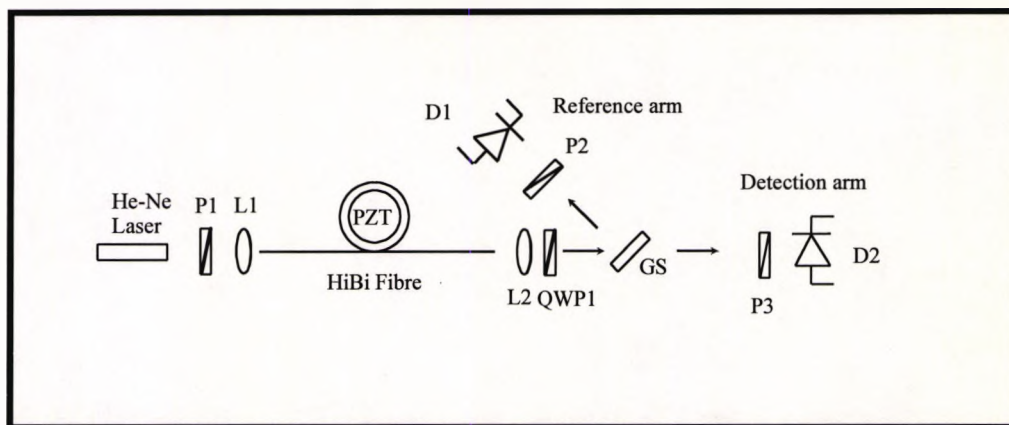
Figure 3-1 Illustration of a HiBi fibre polarisation modulation arrangement.
Ps, Polarising Prisms; Ls, Lenses; QWP, Quarter-Wave Plate;
GS, Glass Slide; Ds, Detectors.

This was driven sinusoidally to stretch the fibre and modulate its birefringence characteristics. As a result, a beam with a rotating linear state of polarisation was obtained.

A reference signal was provided by reflecting a small fraction of the beam via a glass slide (at an incidence angle of 3°) through a polarising prism onto a photodetector and the main beam was then analysed via a polariser (orientated at 45° to that in the reference arm) and a photodiode. The detected and reference signals were transferred to a computer for analysis. It should be noted that the reference signal

allows for the ability to determine particular polarisation states exiting the modulation unit.

3-3 System Performance Study

As already mentioned, the essence of the polarisation system designed is the production of good quality rotating plane polarised light as an output beam. Therefore, a close look at the beam characteristics would reveal what deficiencies need be addressed to improve the beam quality.

3-3-1 Detailed Analysis of the Output Signal

Fig. 3-2 shows a typical output signal obtained from the polarisation modulation scheme when the output from the fibre is transmitted directly through a polariser (angled at 45° relative to the orientation of the polariser in the reference) and then to the photodetector (Fig. 3-1). Signal intensities with known polarisation orientations relative to the reference signal thus can be evaluated, utilising the signal processing method briefly summarised in Fig. 3-3 and fully described in Appendix A.
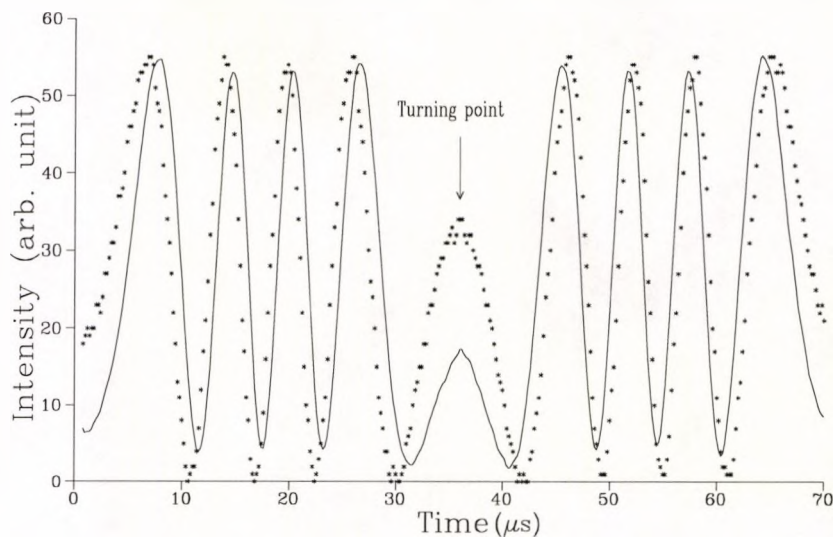
Figure 3-2 Illustration of typical fringes taken from the polarisation modulation unit. (Solid line : Detected signal, Dotted line : Reference signal)

```
┌─────────────────────────────────────┐
│            import data               │
│   (reference and detected signals)   │
└─────────────────────────────────────┘
                  ↓
┌─────────────────────────────────────┐
│        smooth the reference curve    │
└─────────────────────────────────────┘
                  ↓
┌───────────────────────────────────────────────────┐
│  check for a peak (trough) in the reference curve, where the orientation of
│  the output polarisation is parallel (perpendicular) to the reference polariser
└───────────────────────────────────────────────────┘
                  ↓
┌───────────────────────────────────────────────────┐
│  determine time corresponding to the peak (trough) position in the reference
│  signal [interpolation applied if necessary]
└───────────────────────────────────────────────────┘
                  ↓
┌───────────────────────────────────────────────────┐
│  match the time found with the corresponding detected intensity parallel Ip (perpendicular, Is) to
│  the reference polariser [interpolation applied if necessary]
└───────────────────────────────────────────────────┘
                  ↓
┌───────────────────────────────────────────────────┐
│  in the case of having an interest in another intensity in between Ip and Is such as I45
│  the time half way between a peak and a consecutive trough corresponding to 45 degrees
│  orientation would match I45 in the detected signal
└───────────────────────────────────────────────────┘
                  ↓
┌───────────────────────────────────────────────────┐
│  further calculation procedures, i.e. ellipsometric parameters, index
│  of refraction and etc.,applied using Ip, Is & I45
└───────────────────────────────────────────────────┘
                  ↓
              ◇ end of data? ◇
          Yes ↓          No →
            Stop
```

No

No

Figure 3-3 Flow chart showing a summary of the procedures for processing the signals to determine parallel (I_p) and perpendicular (I_s) intensities. Other calculations are then performed using this data. (more details in Appendix A)

Since the polarised light emitted from the polarisation modulation unit is modulated by driving the PZT sinusoidally, when the PZT is expanded electrically, the linear output state rotates in one direction (say clockwise), and then in the other direction (counterclockwise) when the PZT is relaxed. Thus, as can be seen (Fig. 3-2),

the group of fringes to the left of the turning point is a mirror image of the fringes on the right of the turning point (where the direction of the rotation changes).

Initial considerations suggest that both orientations of the rotating polarised light should result in the same type of output. However, by using the procedures described in Appendix A to determine both intensities parallel (I_p) and perpendicular (I_s) to the direction defined by the polarising prism in the reference arm, it was found that the average of the ratio I_s / I_p of the fringes situated on one side of a turning point differed significantly from the average ratio found on the other side.

This raised the question of a differing performance depending on the direction of rotation. This inconsistency in the ratio could give rise to unreliable measurements, once the system has been implemented in practical applications.

An initial suggestion for the source of the inconsistency was based on a property of the PZT itself as all piezoelectric ceramics exhibit hysteresis (Jaffe *et al*, 1971). This arises from the difference in the strain that occurs when a particular voltage is approached from a lower voltage and then from a higher voltage (as occurred due to the application of a sinusoidal signal in this case).

However, this view was dismissed experimentally because the referencing scheme employed provided the orientation of the polarisation state, independent of the drive signal, and consequently, the hysteresis of the PZT cannot contribute to this effect. A closer analysis was made by monitoring the output of the polarisation modulation as shown in Fig. 3-4, taken from the "straight-through" optical set-up (with no polariser (P3) in detection arm) where the output from polarisation modulation system is incident directly on the photodetector (Fig. 3-1). The figure reveals that the signal 'a' is partly composed of high frequency components, in contrast to the expected output DC signal. The signal 'b' is the reference signal. The form of the output signal can be understood once a careful and extended analysis has been made, as discussed below.
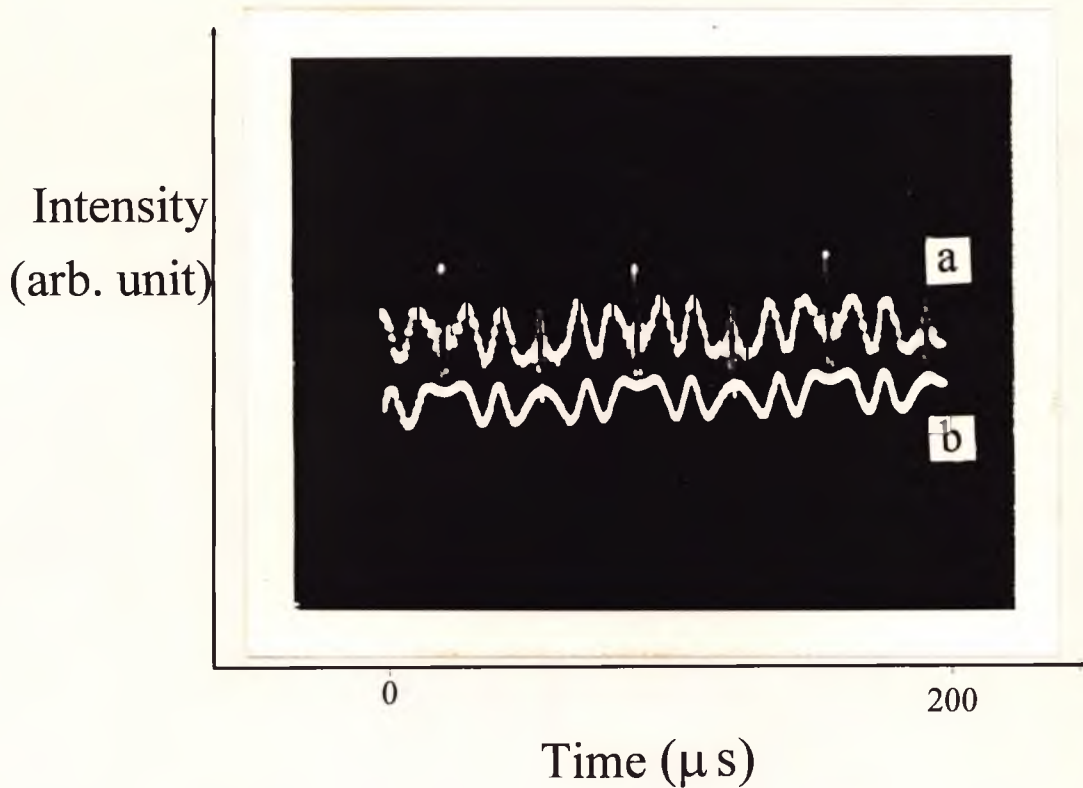
Figure 3-4 Illustration of signals obtained from a "straight through" set-up. Signal 'a' was directly detected from the output of the set-up and signal 'b' was taken after the output beam reflected at a glass slide and propagated through a polarising prism.

3-3-2 Extended Analysis

The signal from a detector placed immediately after the quarter-wave plate (QWP1) at the output end of the polarisation modulation unit can be derived by using Jones matrices. For convenience, the two orthogonal modes may be designated as x and y; thus, the electric field of the wave which propagates along the mode, x, of the fibre is given by,

$$\bar{E}_x = \begin{bmatrix} ae^{i(\omega_o t - k_x(L+L(t))+\varepsilon_x)} \\ 0 \end{bmatrix} \qquad (3\text{-}4),$$

59

where a = amplitude of the wave, k_x = propagation constant in mode x, L = an initial length of the fibre, $L(t)$ = the fibre length extension due to the modulator unit and ε_x = the initial phase in the mode x.

Similarly, the wave propagating along the mode, y, may be written as,

$$\vec{E}_y = \begin{bmatrix} 0 \\ be^{i\left(\omega_o t - k_y\left(L+L(t)\right)+\varepsilon_y\right)} \end{bmatrix} \qquad (3\text{-}5),$$

where b = amplitude of the wave, k_y = propagation constant in mode y, and ε_y = the initial phase in the mode, y.

When the light passes through the QWP1 oriented at 45° to the eigenmodes of the fibre, the light from each mode is transformed into a circular polarised light with different handedness. The wave in mode x becomes right circular polarised light given by,

$$\vec{E}_x^{(1)} = ae^{i\left(\omega_o t - k_x\left(L+L(t)\right)+\varepsilon_x\right)} \begin{bmatrix} 1 \\ i \end{bmatrix} \qquad (3\text{-}6),$$

while the wave in mode y is transformed to be left circular polarised light given by,

$$\vec{E}_y^{(1)} = be^{i\left(\omega_o t - k_y\left(L+L(t)\right)+\varepsilon_y+\frac{\pi}{2}\right)} \begin{bmatrix} 1 \\ -i \end{bmatrix} \qquad (3\text{-}7).$$

The total intensity, I, at this stage may be found to be the sum of the intensities of the right and left circularly polarised beams, $I_x^{(1)}$ and $I_y^{(1)}$ respectively, i.e.

$$I = I_x^{(1)} + I_y^{(1)} = \left(\vec{E}_x^{(1)}\right)\cdot\left(\vec{E}_x^{(1)}\right)^* + \left(\vec{E}_y^{(1)}\right)\cdot\left(\vec{E}_y^{(1)}\right)^*$$
$$\propto a^2 + b^2 \qquad (3\text{-}8).$$

Therefore, it may be concluded that no matter how much the amplitudes of the circular polarised beams may differ, the output signal should be a DC signal.

However, in practice the electric field in each eigenmode is not only composed of the main light flux but it also involves light reflected backwards and forwards along the fibre.

As a result of the reflection, the reflected light, which is emitted from the fibre after being reflected by both end faces of the fibre is given in terms of the component of $\vec{E}_x^{(2)}$ by

$$\vec{E}_x^{(2)} = \eta^2 a e^{i\left(\omega_o t - 3k_x(L+L(t))+\varepsilon_x\right)} \begin{bmatrix} 1 \\ i \end{bmatrix} \qquad (3\text{-}9),$$

where η is the reflection coefficient at the fibre ends (assumed identical) and $3k_x(L+L(t))$ is the phase of the reflected beam for mode x.

Therefore, the intensity exiting this eigenmode is found to be

$$
\begin{aligned}
I_x^{(1)+(2)} &= \left(\vec{E}_x^{(1)+(2)}\right) \cdot \left(\vec{E}_x^{(1)+(2)}\right)^* \\
&= 2\left(a^2 + \eta^4 a^2 + \eta^2 a^2 \cos\left(2k_x\left(L+L(t)\right)\right)\right)
\end{aligned}
\qquad (3\text{-}10).
$$

The argument of the cosine term is given by $\Delta_x = 2k_x\left(L+L(t)\right)$ which can be rewritten in terms of the phase difference between the light exciting the two eigenmodes $\Delta_m = \dfrac{2\pi}{\lambda_o} B\left(L+L(t)\right)$ as,

$$\Delta_x = \left(\frac{2n_x \Delta_m}{B}\right) \qquad (3\text{-}11),$$

where $B(= n_x - n_y)$ is the linear birefringence of the fibre (Kaminow, 1981).

Similarly for the y mode, the reflected electric field, $\vec{E}_y^{(2)}$, can be written as

$$\vec{E}_y^{(2)} = \eta'^2 b e^{i\left(\omega_o t - 3k_y(L+L(t))+\varepsilon_y+\frac{\pi}{2}\right)} \begin{bmatrix} 1 \\ -i \end{bmatrix} \qquad (3\text{-}12),$$

where η' is a reflection coefficient at the fibre ends and $3k_y(L+L(t))$ is the phase of the reflected beam for mode y. Thus, the total intensity in mode y is found to be

$$I_y^{(1)+(2)} = 2\left(b^2 + \eta'^4 b^2 + \eta'^2 b^2 \cos\left(2k_y\left(L+L(t)\right)\right)\right) \qquad (3\text{-}13),$$

where $2k_y(L+L(t))$ is equal to the phase difference between the two beams exciting eigenmode y and can be written in terms of the phase shift between the two eigenmodes as

$$\Delta_y = \left(\frac{2n_y\Delta_m}{B}\right) \tag{3-14}.$$

In addition, if the reflected beam and the main light flux of both eigenmodes are detected simultaneously, (as they will be in a practical situation) the detected intensity I_{total} is given by

$$I_{total} = \left(\vec{E}_x^{(1)} + \vec{E}_x^{(2)}\right)\left(\vec{E}_x^{(1)} + \vec{E}_x^{(2)}\right)^* + \left(\vec{E}_y^{(1)} + \vec{E}_y^{(2)}\right)\left(\vec{E}_y^{(1)} + \vec{E}_y^{(2)}\right)^*$$
$$= 2\left\{a^2 + b^2 + \eta^4 a^2 + \eta'^2 b^2 + \eta^2 a^2 \cos(2k_x(L+L(t))) + \eta'^2 b^2 \cos(2k_y(L+L(t)))\right\} \tag{3-15}.$$

If it is assumed that $a = b$ and $\eta = \eta'$, the last two cosine terms in Eq. (3-15) can be written as,

$$\cos(2k_x(L+L(t))) + \cos(2k_y(L+L(t))) = 2\cos\left[(k_x - k_y)(L+L(t))\right]\cos\left[(k_x + k_y)(L+L(t))\right] \tag{3-16}.$$

This indicates, theoretically, the presence of a beat effect with a modulated amplitude of $\cos\left[(k_x - k_y)(L+L(t))\right]$.

The first factor of Eq. (3-16) is low frequency, and the second, high frequency, as can be seen in the following analysis. An analysis of the modulated amplitude factor may be made by writing it as a function of the phase shift between the two eigenmodes, Δ_m, to give,

$$\left(k_x - k_y\right)(L+L(t)) = \frac{\Delta_x - \Delta_y}{2}$$
$$= \frac{n_x\Delta_m}{B} - \frac{n_y\Delta_m}{B}$$
$$= \Delta_m \tag{3-17}.$$

Eq. (3-17) indicates how the envelope of the beat is similar to the modulation phase between the two eigenmodes. The situation can be clearly observed from Fig. 3-5 which shows the output obtained (again from the arrangement of Fig. 3-1) where the modulation rate is greatly reduced (a low frequency linear ramp was used, giving rise to a polarisation rotation frequency of $\approx$ 1 Hz). This illustrates (a) the reference signal and (b) the signal from the "straight through" arrangement (without a polarising prism). In this case, the detector was not frequency limited as the signal frequencies generated were within the detector 3 dB bandwidth (100 kHz).
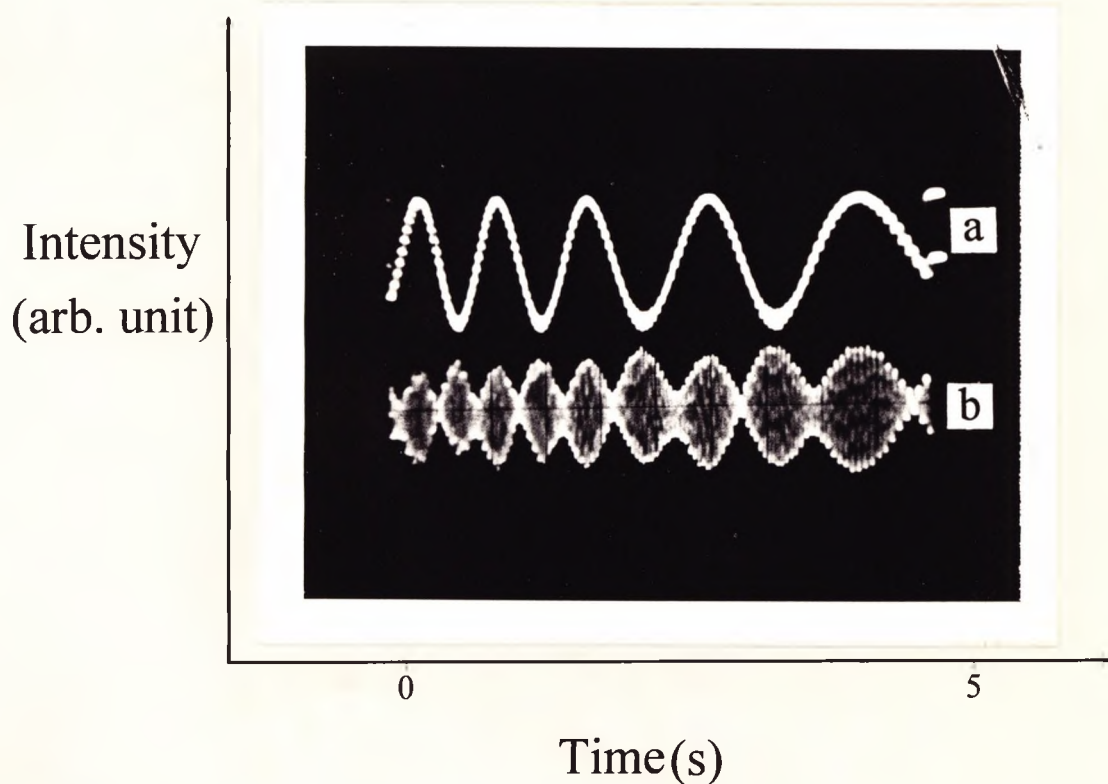
Figure 3-5 Illustration of the reference signal (a) and the beat pattern (b) due to the interference between the main light flux and a fraction of reflected beam. The situation was monitored from the straight through arrangement where modulation rate is low ($\approx$ 1 Hz).

Additionally, the characteristics of the components inside the envelope may be investigated. Again, rewriting all the factors in terms of the phase shift between the

two eigenmodes (Δ_m), the phase of the high frequency cosine factor (from Eq. (3-16)) may be given by

$$\left(k_x + k_y\right)\left(L + L(t)\right) = \frac{n_x \Delta_m}{B} + \frac{n_y \Delta_m}{B}$$

$$= \frac{\Delta_m}{B}\left(n_x + n_y\right)$$

(3-18).

As can be seen, this indicates the rapid phase change when compared to the modulation phase between the two eigenmodes as a typical value of B for HiBi fibre is in the order of 10^{-4} (Varnham, 1984). A useful comparison of Figs. 3-4 and 3-5 can be made, by considering the difference between the two modulation conditions in both frequency and form. In Fig. 3-4, the modulation was via the cylindrical PZT operating at a sinusoidal frequency of 14 kHz. In this case, $L(t)$ in Eq. (3-16) varies sinusoidally. Then Eq. (3-16) may be expanded as a Fourier series (whose terms are harmonics of the modulation frequency) involving Bessel functions (Connor, 1973). This gives rise to a complicated equation with an extended frequency spectrum. The actual detailed form of the power spectrum in such a situation depends on both the amplitude of modulation and the initial phase of the factor in Eq. (3-16). The situation was extensively modelled using a simple Fast Fourier Transform computer algorithm. Removing the high frequency components (above the cut off frequency of the detector circuit; i.e. 100 kHz [3 dB frequency bandwidth]) before performing the inverse Fourier transform was used to mimic the low pass filtering effect of the detector. This confirmed the low frequency content of Eq. (3-16) and the resultant, reconstructed time signal was similar in form to the reference signal. The exact form of this reconstructed signal is sensitive to initial conditions of phase and modulation amplitude. This is in agreement with the signal shown in Fig. 3-4 (a) which (for the particular initial phase and amplitude encountered experimentally) is observed to be similar to the reference signal, Fig. 3-4 (b). In Fig. 3-5, thermal expansion corresponding to a linear ramp was used (resulting in a frequency of ≈ 1 Hz for the

polarisation rotation) and a simple, sinusoidal, low frequency envelope can be seen (Fig. 3-5 (b)).
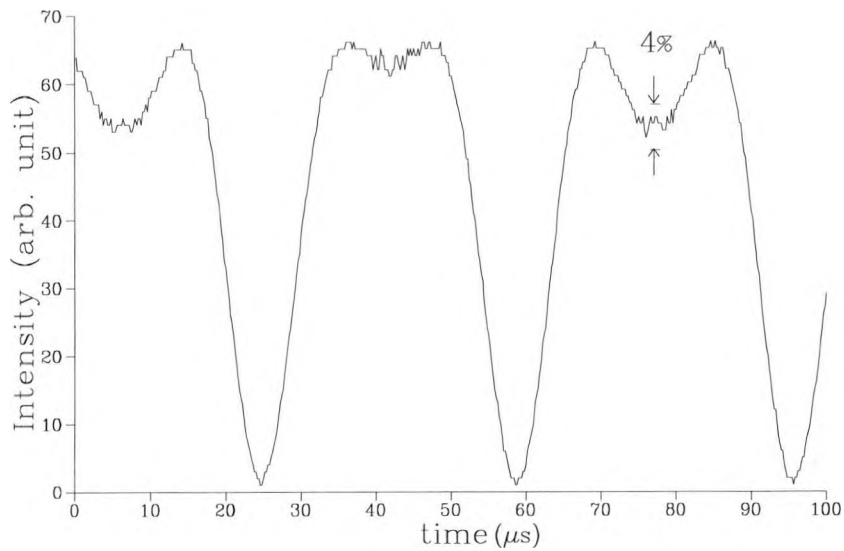
(a)
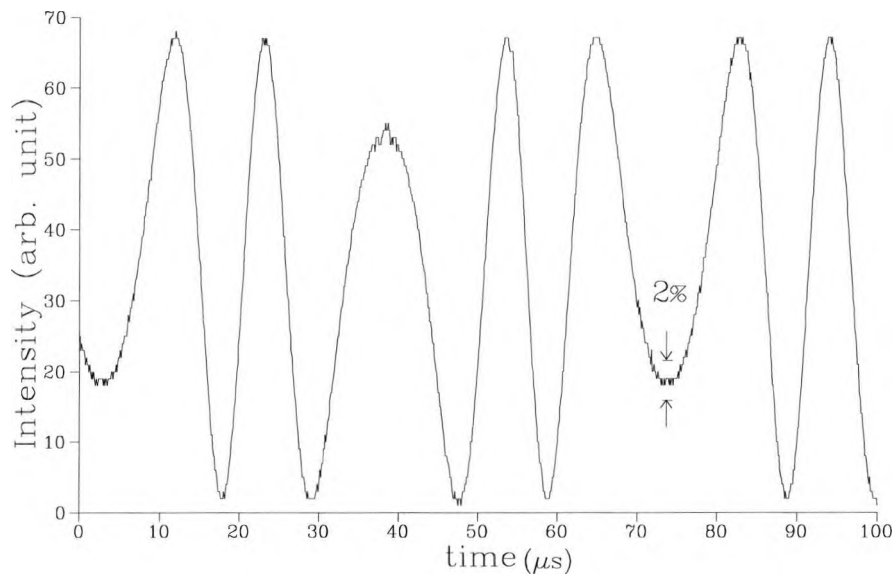
(b)

Figure 3-6 Illustration of the high frequency components reduction,

(a) shows the signal with significant high frequency components
taken before applying index matching gel and,
(b) shows the signal with decreased amplitudes taken immediately
after the application.
(The ratio of the high frequency component intensity to the maximum
intensity is represented in terms of percentage.)

Clearly, these higher order reflections should be minimised to ensure optimum performance because as well as giving rise to variations in intensity, changes in the output polarisation may occur. When high speed modulation is required, a sinusoidal modulation signal will normally be applied, as this is more easily applied at high frequencies, resulting in a signal with a complex frequency spectrum. Therefore, it is not an option merely to filter electronically these high frequencies, as was already shown in the high frequency modulation by the PZT.

This analysis suggests that the beat effect can be reduced by cutting down the intensity of the reflected light. This conclusion was initially tested experimentally by applying index matching gel to the output end of the fibre in order to reduce the amplitude of the reflected light imposed on the main light flux. Figs. 3-6 (a) and (b) show the high frequency components as elements of the output signals taken from the arrangement as shown in Fig. 3-1 and with an analyser at an arbitrary orientation placed in front of a photodetector, respectively.

Fig. 3-6 (a) shows that the high frequency components is found to be approximately 4% of the maximum value; whereas, in Fig. 3-6 (b), taken after applying the index matching gel to the output end face of the fibre, a reduction of the high frequency components to about 2% is observed. From Fig. 3-6 (a), it can be seen that the possibility of errors in resulting data readings is very high. Therefore, a reduction of these amplitudes obviously helps in reducing measurement errors when applying this system to an actual measurement situation. However, the use of an index matching gel does not represent a practical, permanent solution to the problem.

3-4 System Enhancement

3-4-1 The Properties of the HiBi Fibre

In order to improve the output from the polarisation modulation technique, for a better performance when implemented, it is desirable that the amplitude of the reflected light which contributes to the amplitude of the beat frequency should be reduced as much as possible. Techniques to cut down the reflections at the end faces

of the fibre included index matching gel (as discussed), anti-reflection (AR) coating of the fibre end face, the use of an immersion cell and a tilted end face to deviate the reflected light (Ulrich and Rashleigh, 1980).

The tilted end face of fibre was the most simple and thus a suitable approach to try in the laboratory, by polishing the end face at an angle other than 90º to the fibre axis. By tilting the end face of the fibre, the reflected light flux is separated from the main light flux. To achieve a low reflection factor, the tilted angle of the end face was required to be greater than 5.8º (Ulrich and Rashleigh, 1980), and this was achieved by hand polishing.

For the preparation of the flat tilted fibre end, the plastic coating of the fibre was stripped at the end of the fibre. This end was then glued into a capillary tube. The tube held the fibre during the process of polishing, and served, later, to mount the fibre in the fibre chuck. In this experiment, a tilt angle of 6º was chosen. During polishing, the capillary is mounted in a specially prepared jig that determines the tilt angle. The fibre is polished, by hand, using diamond and aluminium oxide films. With about 100 strokes for 5 different roughness of the films (i.e. 30, 12, 9, 3, and 1 μm) an acceptable surface finish is obtained. Finally, the fibre end was thoroughly cleaned. The same procedures were carried out for the other end face of the fibre.

The advantage of polishing both end faces is not only to reduce the internal reflection from them but also to prevent power fluctuations due to light coupling back into the laser light source.

The optical quality of the end face was checked by inspection and by coupling light from a HeNe laser (λ = 632.8 nm) into the fibre, then observing the far-field output from the polished end. A uniform circular spot of light was observed, representing an acceptable surface finish. The far-field beam profiles, the beat pattern and the ratio of the amplitude of the high frequency components to the maximum intensity output were compared for plane and angle polished end face preparation. The light from a HeNe laser was polarised at 45º to the eigenaxes of the fibre and coupled

into a length (10 m) of the HiBi fibre by way of a x10 objective lens: thus, both eigenmodes of the fibre were excited equally.

The purpose of this investigation is to check the presence of the high frequency components which are proportional to the modulation rate (Eq. (3-18)). It is worth pointing out that if a very high frequency modulation is used, the high frequency components generated (Sec. 3-3-2) could go beyond the photodetector bandwidth, which normally acts as a low pass filter. Thus, it would be difficult to determine whether or not the proposed improvement works as expected. The problem, however, can be overcome by using a low frequency modulation such as heating. Under such a low frequency circumstance, the detectable high frequency components would be observed and monitored.

The light was modulated by heating a small part of the fibre with a hot air blower. The output beam was divided into two parts to provide reference and "straight-through" signals, as shown in Fig. 3-1. The results of this experiment were compared with those using the HiBi fibre with plane cut end faces, and they are summarised in Table 3-1.

Preparation Fibre methods	Beat effect	Amplitude Ratio*	Degree Of Polarisation (DOP)
1. Plane cut end faces	Observed	$\approx 6\%$	$> 99\%$
2. Polished angled end faces	Observed	$\approx 2\%$	$> 99\%$

Table 3-1 This shows quantities measured, characterising the quality of the output beam from the different fibre configurations.

*Note: the ratio is calculated from the amplitude of the high frequency signals to the maximum output signal.

(a)

(b)
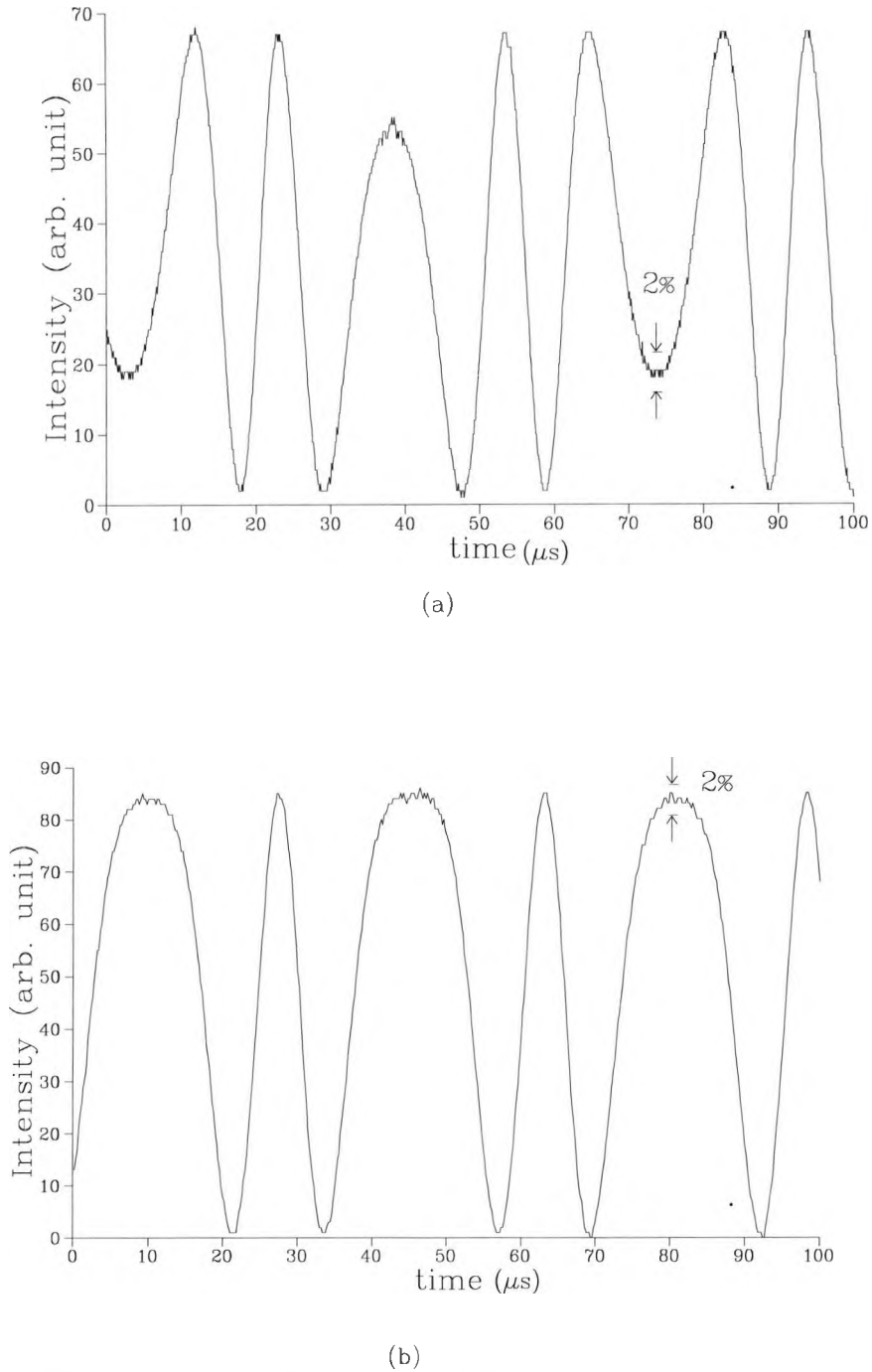
Figure 3-7 Illustration showing the agreement when

(a) the output end face of a HiBi fibre was coated by an index matching gel and when

(b) the end face of the fibre was polished at an angle of 6 deg.

(The ratio of the high frequency component intensity to the maximum intensity is represented in terms of a percentage.)

From the Table 3-1, this clearly indicates that the performance of the HiBi fibre system can be improved considerably by polishing the end faces of the fibre.

Furthermore, the reduction of the amplitude of the reflection observed with the polishing method, is in agreement with that obtained by applying index matching gel to the end face of the unpolished fibre.

Figs. 3-7 (a) and (b) show the agreement between the two methods as, in both cases, the output signals show the smaller contribution to the beat amplitude (the high frequency components highlighted).

This suggests that further improvement could be achieved in the contribution of the reflected constituent to the output beam by increasing the tilt angle of the fibre end faces.

An angle of 12° tilt was chosen in order to ensure the observation of any change that would be apparent. The preparation procedures for this test were almost the same as those previously except for the tilt angle used for the polishing jig. Once the polishing was finished, the polished ends were checked to guarantee that a uniform circular output beam was obtained.

The result was as expected. The amplitude ratio measured from the tilted end faces of 12° was approximately 1% compared to a ratio of 2% when using tilted end faces at 6° (Table 3-1). Nevertheless, the potential to increase of the angle is not indefinite because, apart from greater problems in the preparation process in which the intensity of the transmitted beam is reduced, a very large tilt angle could also upset the state of polarisation of the output beam. In all, the 12° polished end face exhibited a better performance than the 6° polished one.

3-4-2 Alternative Methods of Modulation

Since the 6° polished end faces were simpler to prepare and good enough to be implemented for the analysis of alternative methods of modulation, the subsequent study then adopted this approach. However, in subsequent applications (discussed in Chapters 4 and 5) in which a better quality output is required, the 12° polished end faces were used.

The polarisation modulation method using a length of fibre wrapped around a cylindrical PZT subjects the fibre to stress-induced birefringence from bending which

will couple light between the two polarisation modes of the fibre unless the axis of the cylindrical PZT is parallel to the fibre birefringence. However, in practice, the orientation between the fibre axes and those of the cylindrical PZT cannot easily be controlled. This then leads to the coupling of optical energy from one particular mode to the other. The effect can be observed as inconsistent power levels in each eigenmode, as the fibre is perturbed by various directions of forces relative to the fibre birefringence. To examine this, the distribution of intensities measured at the detection arm when a polariser is orientated at a chosen angle of 45° (to the direction of the polariser in the reference arm) were studied (Fig. 3-1).

In particular, the intensities parallel I_p, perpendicular I_s, and at half orientation between these two, I_{45}, relative to a reference direction defined by a polarising prism in a reference arm, were investigated. At these particular polarisation orientations, data obtained provide a convenient and simple way to check the system performance. For instance, if the system operates perfectly, the output with its azimuth parallel to the reference direction, I_p, will be identical to that with its azimuth perpendicular to the reference direction, I_s. In other words, the ratio I_s over I_p becomes unity (Sec. 3-3-1).

In an effort to reduce the coupling of power between the two eigenmodes, alternative ways of modulating the light were investigated. The intrinsic birefringence in the York Bow-Tie HiBi fibre used is caused by the difference in thermal expansion between the cladding and the stress-applying regions inside the fibre as it cools (Chiang *et al*, 1990). If the fibre is stretched with uniform axial strain, the stress-applying regions and the cladding of the fibre are strained differently in a longitudinal direction. As a result, this process introduces a strain-induced birefringence. The stretching of the HiBi fibre will increase the value of the intrinsic birefringence, but will not affect its direction. That means the problem of the energy coupling should be, if not completely removed, greatly reduced. Since the birefringence of the fibre changes as the fibre is strained, the stretching of the fibre can be used to modulate the phase between the two orthogonal polarised light beams. In the case of thermal

modulation (induced by heating a short length of the fibre), this method also does not affect the direction of the intrinsic birefringence because there is no external force that can cause the redirection of the birefringence. It should be expected that this method of polarisation modulation would be as effective as stretching the fibre.

To investigate this, a comparison of the performance of the system using each modulation method was made on the distribution of measured intensities I_p, I_s and I_{45}. The mean value and standard deviation were calculated for each side of a turning point (i.e. clockwise and counterclockwise, were considered separately) when the arrangement was "straight through", as shown in Fig. 3-1.

Modulation methods (polished end faces fibre)	Clockwise rotation	Counterclockwise rotation
a cylindrical PZT	$\overline{X}_{I_s} = 35.281$, $\sigma_{I_s} = 2.256$ $\overline{X}_{I_p} = 37.521$, $\sigma_{I_p} = 2.702$ $\overline{X}_{I_{45}} = 69.000$, $\sigma_{I_{45}} = 0.819$	$\overline{X}_{I_s} = 38.767$, $\sigma_{I_s} = 0.783$ $\overline{X}_{I_p} = 33.115$, $\sigma_{I_p} = 0.534$ $\overline{X}_{I_{45}} = 71.227$, $\sigma_{I_{45}} = 0.388$
heating	$\overline{X}_{I_s} = 32.627$, $\sigma_{I_s} = 0.878$ $\overline{X}_{I_p} = 33.344$, $\sigma_{I_p} = 1.194$ $\overline{X}_{I_{45}} = 64.496$, $\sigma_{I_{45}} = 0.487$	$\overline{X}_{I_s} = 32.568$, $\sigma_{I_s} = 0.343$ $\overline{X}_{I_p} = 33.094$, $\sigma_{I_p} = 0.304$ $\overline{X}_{I_{45}} = 65.400$, $\sigma_{I_{45}} = 0.489$
stretching	$\overline{X}_{I_s} = 26.508$, $\sigma_{I_s} = 1.177$ $\overline{X}_{I_p} = 28.634$, $\sigma_{I_p} = 0.437$ $\overline{X}_{I_{45}} = 62.900$, $\sigma_{I_{45}} = 0.238$	$\overline{X}_{I_s} = 28.122$, $\sigma_{I_s} = 0.875$ $\overline{X}_{I_p} = 28.771$, $\sigma_{I_p} = 0.317$ $\overline{X}_{I_{45}} = 61.667$, $\sigma_{I_{45}} = 0.200$

Table 3-2 The standard deviation (σ) of the intensities I_s, I_p and I_{45} around their mean values ($\overline{X}$).

The experimental set-up for the uniform stretching with polished angled end faces is similar to that for the thermal polarisation modulation, as described previously except, of course, for the modulation unit. For the uniform stretching set-up, a section of 20 cm from a 1 m length of HiBi fibre was held under longitudinal strain with one

end mounted at a fixed point and the other end attached firmly to a shaker which serves as a sinusoidal modulator, operating at a frequency of 30 Hz. Since the intrinsic birefringence of the HiBi fibre changes with the longitudinal strain, this means that the phase difference between the two orthogonal components also changes (Tatam *et al*, 1987). Under appropriate conditions, a 2π phase shift can be achieved, and Table 3-2 shows the distribution (standard deviation, σ) of interest around their mean values $(\overline{X})$.

As can be seen from Table 3-2, the scattering of the measured values (either from clockwise or counterclockwise orientation) around their means from the two methods of heating and longitudinal stretching are similar to each other, as expected, and have a smaller spread than the results obtained from the stretching by a cylindrical PZT. Further, the average of the ratio I_s / I_p of one group (say the clockwise rotation) of fringes situated on one side of a turning point was compared to the average of the ratio found in the group on the other side of the turning point (the counterclockwise rotation). The results are shown in Table 3-3, which indicates that the problem of grouping is greatly reduced when using heating or stretching as the means of modulation.

Modulation methods (polished end faces fibre)	Clockwise rotation	Counterclockwise rotation
a cylindrical PZT	0.940	1.170
heating	0.978	0.984
stretching	0.925	0.977

Table 3-3 The comparison of the average of the ratio I_s / I_p of the fringes situated on each side of a turning point.

In summary, the results obtained from the thermal and longitudinal stretching modulation scheme showed not only less scattering of I_p, I_s and I_{45} around their mean

values but also the reduction of the gap between groupings. Thus, it can be concluded that by changing the method of modulation, the power coupling can be reduced and, as a result, the measured intensities tend to concentrate around their mean values.

It is envisaged that the longitudinal stretching would be more practical in a measurement system due to the higher bandwidth that is available.

3-4-3 Optical Component Considerations

So far, the optical fibre polarisation modulation technique has been investigated in two major aspects; namely, the properties of the fibre and the modulation method, and improvement in performance were achieved over the optical fibre set-up initially studied.

Using the optical arrangement shown in Fig. 3-1; it is clear that the performance of the system is also critically dependent on the quality of the quarter-wave plate (QWP1) used. The first cause for concern is how closely the phase retardance of the plate corresponds to $\pi/2$ and the second is the precision of the orientational adjustment of the QWP optical axes to the eigenaxes of the fibre.

3-4-3-1 Imperfection on the Quarter-Wave Plate

The most appropriate way of showing the resultant effect on the output beam is to employ Jones vector notation. Previously, the manipulations of the rotating plane polarised beam were calculated relative to the optical fibre co-ordinate system. This time, for simplicity, the calculation will be performed relative to the input beam co-ordinate system (Fig. 3-8).
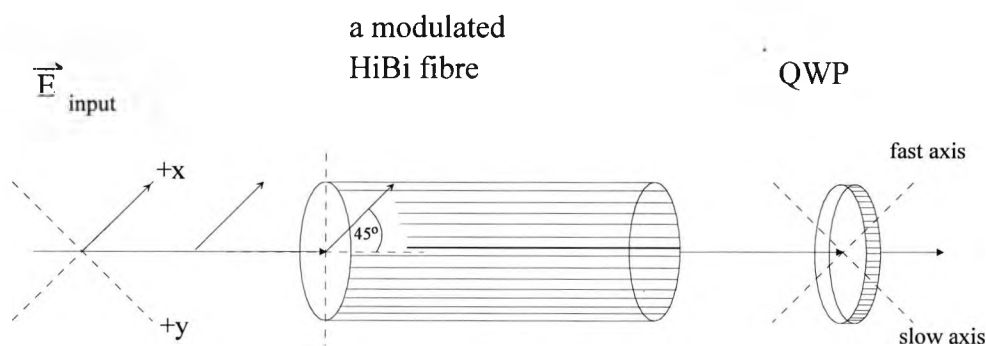
Figure 3-8 Illustration of an input beam , a modulated HiBi fibre and a QWP co-ordinate system.

Therefore, the electric field input, $\vec{E}_{input}$ may be given by

$$\vec{E}_{input} = \begin{bmatrix} 1 \\ 0 \end{bmatrix}$$
(3-19)

The Jones vector notation of an imperfect quarter-wave plate, Q', with its optical axis parallel to the input beam co-ordinate system may be written as

$$Q' = \begin{bmatrix} e^{i\gamma} & 0 \\ 0 & i \end{bmatrix}$$
(3-20),

where γ represents the retardance error.

In addition, according to the co-ordinate rotation procedure (Nussbaum and Phillips, 1976), the pseudo-Jones matrix for the properties of a linear highly birefringent fibre has to be rewritten in a new form relative to the input beam co-ordinate system.

Generally, this process can be accomplished by using the rotation matrices, $R_\theta^\pm$ which are given by

$$R_\theta^\pm = \begin{bmatrix} \cos\theta & \pm\sin\theta \\ \mp\sin\theta & \cos\theta \end{bmatrix}$$
(3-21).

where $\pm$ indicate rotational directions of the input beam co-ordinate system relative to the fibre co-ordinate system, e.g. a positive rotation matrix, R_θ^+ is defined from the +x plane toward the +y plane. θ represents an angular difference between the two co-ordinate systems.

In this particular case $\theta = 45°$ to the principal axis of the input beam co-ordinate system; thus, the matrices can be simplified to

$$R_\theta^\pm = \begin{bmatrix} 1 & \pm 1 \\ \mp 1 & 1 \end{bmatrix}$$
(3-22).

Then the modified modulator matrix, M', relative to the input beam co-ordinate system may be written as

$$R_{45^o}^- M' R_{45^o}^+ = \begin{bmatrix} 1 & -1 \\ +1 & 1 \end{bmatrix} \begin{bmatrix} e^{i\phi_a} & 0 \\ 0 & e^{i\phi_b} \end{bmatrix} \begin{bmatrix} 1 & +1 \\ -1 & 1 \end{bmatrix}$$

$$= \begin{bmatrix} e^{i\phi_a} + e^{i\phi_b} & e^{i\phi_a} - e^{i\phi_b} \\ e^{i\phi_a} - e^{i\phi_b} & e^{i\phi_a} + e^{i\phi_b} \end{bmatrix}$$

(3-23).

Now, if the input beam is launched into this modulated HiBi fibre, the beam emerging at the output end is given by

$$M'\vec{E}_{input} = \begin{bmatrix} e^{i\phi_a} + e^{i\phi_b} \\ e^{i\phi_a} - e^{i\phi_b} \end{bmatrix}$$

$$= \begin{bmatrix} \cos\left(\dfrac{\phi}{2}\right) \\ \sin\left(\dfrac{\phi}{2}\right)e^{i\frac{\pi}{2}} \end{bmatrix}$$

(3-24),

where $\phi (= \phi_a - \phi_b)$ is the modulation phase.

At this stage Eq. (3-24) illustrates the evolution of the state of polarisation (SOP) of the output beam before propagating through the waveplate. It indicates that the beam, with a varying amplitude and a constant phase difference of $\pi/2$, can give rise to different SOP. Specifically, if $\phi = 0$ or π radians, the output beam becomes linear, if ϕ is modulated to be $\pi/2$, the output then becomes circular and in general the output is elliptical.

It is obvious that if this modulated beam propagates through a perfect QWP, a rotating linear state will be obtained. However, the case of general interest occurs when transversing through an imperfect QWP. By following the process described in Eq. (2-1), the output electric field, $\vec{E}_{output}$, may be given by

$$\vec{E}_{output} = Q'M'\vec{E}_{input}$$

(3-25).

Substituting Eqs. (3-20) and (3-24) into Eq. (3-25), gives

$$\vec{E}_{output} = \begin{bmatrix} \cos\left(\dfrac{\phi}{2}\right)e^{i\gamma} \\ \sin\left(\dfrac{\phi}{2}\right)e^{i\pi} \end{bmatrix}$$

(3-26).

This shows a state of rotating azimuth is produced, but it will no longer be linear because of the existence of the retardance error, γ. It can be shown that, in fact, a state with varying azimuth and ellipticity is generated.

To verify this, first of all it is necessary to derive an expression for the ellipticity of this beam as a function of the retardance error, γ, and phase ϕ.

Generally, the ellipticity, e, of an ellipse written in terms of Jones vector

notation as $\begin{bmatrix} A_x e^{i\varsigma_x} \\ A_y e^{i\varsigma_y} \end{bmatrix}$ is give by (Schurcliff, 1962)

$$ellipticity(e) = \tan\left[\tfrac{1}{2}\sin^{-1}\left\{(\sin 2A)|\sin \varsigma|\right\}\right]\qquad (3\text{-}27),$$

where A and ς are defined as equal to $\left|\tan^{-1}\left(\dfrac{A_y}{A_x}\right)\right|$ and $\left(\varsigma_y - \varsigma_x\right)$, respectively.

With some simple manipulation, the expression for the ellipticity of the output beam (Eq. (3-26)) is found to be

$$ellipticity = \tan\left[\tfrac{1}{2}\sin^{-1}\left\{(\sin \phi)|\sin(\gamma)|\right\}\right]\qquad (3\text{-}28).$$

An illustration of this equation is shown in Fig. 3-9. It reveals a modulation phase-varying ellipticity. The effect shown, as a thin line, was calculated when the retardance error is $\pi/25$, a typical value for a standard mica QWP used in practice.

Interestingly, the calculated ellipticity found is comparable to the measured value obtained in the previous experimental investigation (Sec. 2-3). In addition, the calculation also predicts that if a higher quality QWP such as that made of quartz ($\gamma = \pi/250$) is used, the amplitude of the ellipticity will be significantly reduced as a result (thick line). It should be noted that the maximum ellipticity is obtained when the modulation phase is $\pi/2$, corresponding to a circular state emerging from the fibre (Eq. (3-24)).

A point worth considering here is that the problem was analysed, based on the assumption of a well-aligned linear input, i.e. the vector of the input polarisation state is seen to be perfectly parallel to the chosen co-ordinate system (referring to Fig. 3-8). If not, the misalignment which occurs can cause an unwanted orthogonal component,

whose magnitude totally depends on the angle of misalignment. This effect can be described as follows.
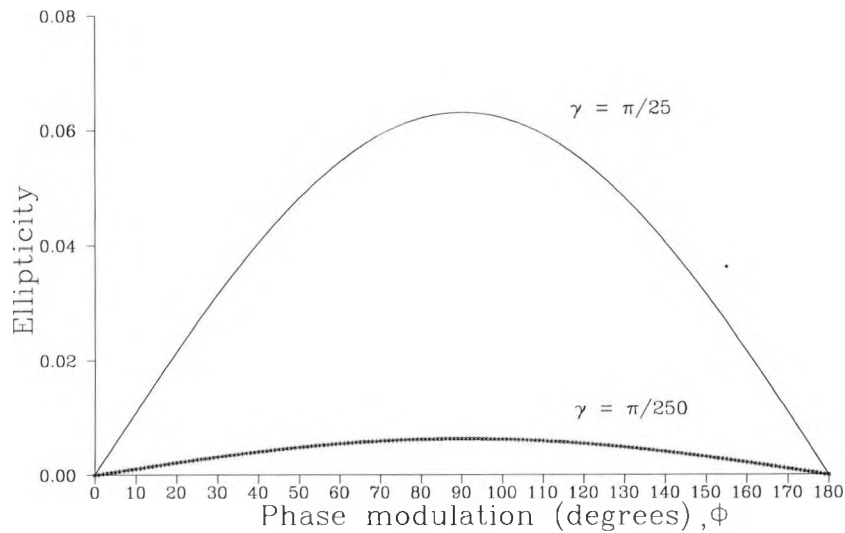
Figure 3-9 Illustration of an ellipticity evolution occurring when the optical fibre polarisation modulation system uses an imperfect QWP. The thin line represents the effect obtained from using a mica QWP; whereas, the thick line is obtained when using a quartz QWP.

If the input beam is misaligned by a small angle, $d\varphi$, relative to the axis of a given co-ordinate, the beam then may be given by

$$\vec{E}'_{input} = R^+_{d\varphi} \vec{E}_{input}$$
$$= \begin{bmatrix} \cos d\varphi \\ -\sin d\varphi \end{bmatrix}$$

(3-29).

Eq. (3-29) shows that the amplitude of the unwanted component ($-\sin d\varphi$) is, of course, a function of the misaligned angle, $d\varphi$. In practice, the degree of alignment precision was found to be 0.5º, where the positive angle is measured from the +x plane toward the +y plane. So, substituting this numerical value into Eq. (3-29), the amplitude of the unwanted component was calculated to be approximately 1.0 % of the main constituent.

By following the procedures described earlier (Eqs. (3-24), (3-25) and (3-28)), the new phase-varying ellipticities with $\gamma = \pi / 25$ (thin line) and $\gamma = \pi / 250$ (thick line) were determined and are shown in Fig. 3-10.
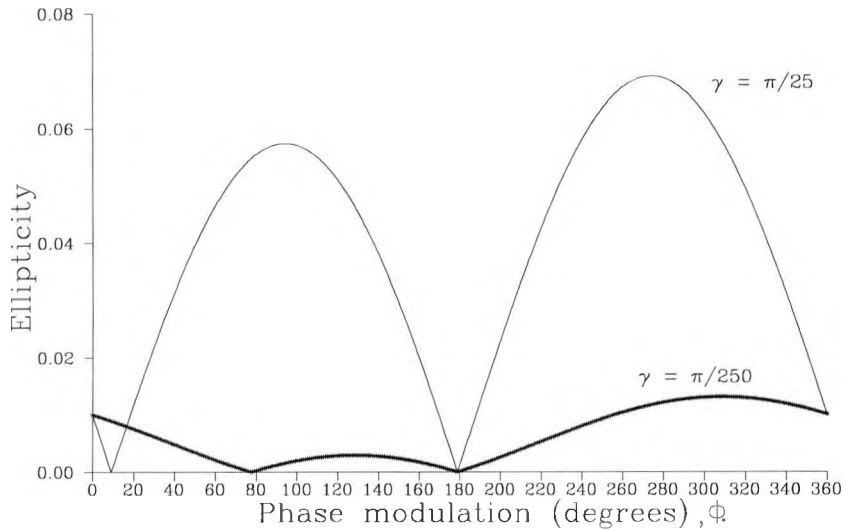
Figure 3-10 Illustration of an ellipticity evolution when the input beam is misaligned by 0.5° from a reference direction and the QWP used is imperfect. The thin line represents the effect of using a mica QWP; the thick line is obtained when using a quartz QWP.

From the graph, the unusual curvature of the ellipticity is dependent on a particular modulation phase and the magnitude of the ellipticity can be clearly seen when the retardance error is significant ($\gamma = \pi / 25$). In such a way, the error from the input misalignment can contribute to the total system error. However, this unusual trend of ellipticity becomes less pronounced when the retardance error, γ, is reduced to $\pi / 250$ (thick line). This suggests that by using a high quality QWP the error from the input misalignment can be tolerated.

It should be noted that curves shown in Fig. 3-10 are evidently out of phase. This is dissimilar to Fig. 3-9. This situation may be clarified by considering a series of misalignment angles, $d\varphi$, of the input beam. Fig. 3-11 illustrates the ellipticity evolution with various $d\varphi$ (i.e. $d\varphi$ = 0.0° [stars], 0.05° [squares], 0.1° [thin line] and 0.5° [thick line]) with $\gamma = \pi / 250$. The figure reveals that the ellipticity curves change

in phase as $d\varphi$ changes. It can be expected that this phenomenon can also be applied when $\gamma = \pi / 25$. However, with different retardance errors, the ellipticity evolution when $d\varphi = 0.5^\circ$ (as shown in Fig. 3-10) can be found.
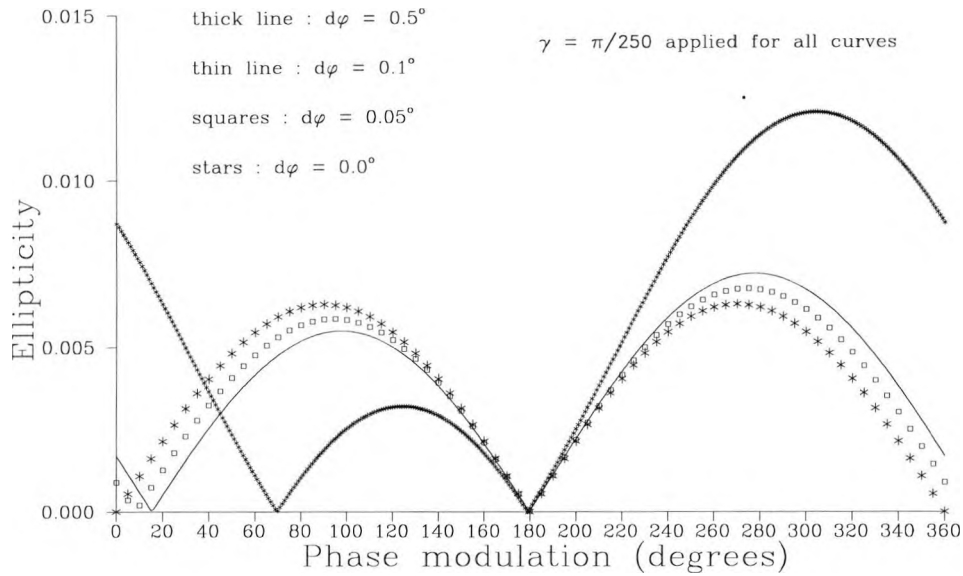
Figure 3-11 Illustration of an ellipticity evolution when the input beam is misaligned by 0.0° (stars), 0.05° (squares), 0.1° (thin line) and 0.5° (thick line) from a reference direction and the QWP is imperfect. The retardance error, γ, of the QWP is taken to be $\pi/250$.

In fact, any inaccuracy introduced by a QWP is not only from its imperfection but possibly also from its misalignment. These circumstance will be studied in detail in the next section.

3-4-3-2 Misalignment of the Quarter-Wave Plate

It is equally important to analyse the orientational adjustment of the QWP eigenaxes as its material imperfections. The effect of such a misalignment may be assessed by replacing Q' in the previous analysis (Eq. (3-20)) by

$$Q'' = \begin{bmatrix} \frac{1}{\sqrt{2}}(1+i) & \frac{1}{\sqrt{2}}i2\xi \\ \frac{1}{\sqrt{2}}i2\xi & \frac{1}{\sqrt{2}}(1-i) \end{bmatrix} \tag{3-30},$$

where ξ is the orientational misalignment measured relative to the input beam co-ordinate system and Q'' represents a matrix of a QWP with misalignment but no retardance error.

Thus, the output beam then becomes

$$\bar{E}_{output} = Q''M'\bar{E}_{input}$$

$$\propto \begin{bmatrix} (a^2+b^2)^{\frac{1}{2}} e^{i\left(\tan^{-1}\left(\frac{b}{a}\right)\right)} \\ (c^2+d^2)^{\frac{1}{2}} e^{i\left(\tan^{-1}\left(\frac{d}{c}\right)\right)} \end{bmatrix} \tag{3-31},$$

where

$$a = \left\{ \left(\tfrac{1}{\sqrt{2}}\cos\tfrac{\phi}{2}\right) - \left(\sqrt{2}\xi\sin\tfrac{\phi}{2}\right) \right\} \tag{3-32a},$$

$$b = \left\{ \tfrac{1}{\sqrt{2}}\cos\tfrac{\phi}{2} \right\} \tag{3-32b},$$

$$c = \left\{ \tfrac{1}{\sqrt{2}}\sin\tfrac{\phi}{2} \right\} \tag{3-32c},$$

$$d = \left\{ \left(\tfrac{1}{\sqrt{2}}\sin\tfrac{\phi}{2}\right) + \left(\sqrt{2}\xi\cos\tfrac{\phi}{2}\right) \right\} \tag{3-32d}.$$

Eq. (3-31) indicates that the effect of the misalignment gives rise to a rotating elliptical polarisation. The ellipticity expression of the beam calculated from (Eq. 3-27) is found to be

$$ellipticity = \tan\left[\tfrac{1}{2}\sin^{-1}\left\{(\sin 2A')|\sin\varsigma'|\right\}\right] \tag{3-33},$$

where

$$A' = \left| \tan^{-1}\left(\frac{c^2+d^2}{a^2+b^2}\right)^{\frac{1}{2}} \right| \tag{3-34a},$$

$$\varsigma' = \left(\tan^{-1}\left(\frac{c}{d}\right) - \tan^{-1}\left(\frac{b}{a}\right) \right) \tag{3-34b}.$$

It is noted that for a particular phase modulation (e.g. $\phi = 0$ or π) the corresponding ellipticity calculated from Eq. (3-33) is found to be equal to ξ. This is shown in Fig. 3-12 where the value of orientational misalignment is chosen to be 0.5° ($\approx 9 \times 10^{-3}$ rad), a degree of precision met in practice, which is measured from the +x plane toward the +y plane. This figure also illustrates that, at this particular modulation phase, the largest ellipticity of the output beam is obtained.

Again, the analysis was considered on the basis of a perfectly aligned linear input beam. With an introduction of a small misalignment at the input as well as the QWP, the electric vector of the input is given by Eq. (3-29). By following the procedures for determining the time-varying ellipticity in the misalignment case above, the trend of the ellipticity can be found (Fig. 3-13). It can be clearly observed that under this additional input misalignment a larger change in the ellipticity than was seen before is introduced. This suggests a higher degree of system error would occur.
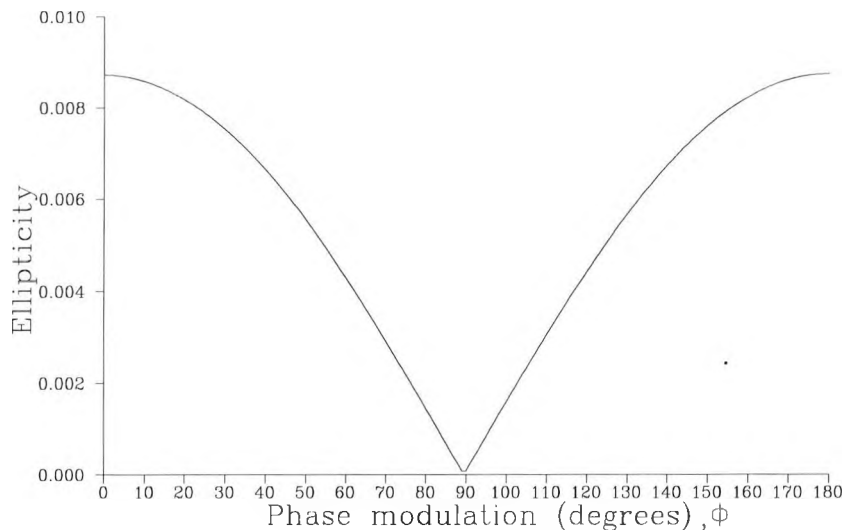
Figure 3-12 Illustration of an ellipticity evolution when a QWP used in the optical fibre polarisation modulation system is misaligned by 0.5° from the reference direction.

Comparing the scales of the two illustrations, Figs. 3-9 and 3-12, of the ellipticity obtained from the two error sources considered, it can be seen that the imperfections of the QWP tend to introduce larger errors in the output beam than the QWP misalignment does. In other words, the material imperfection is most responsible for the occurrence of the output ellipticity.

Certainly, with the previous improvements to the fibre and the modulation method and employing a higher quality QWP, the performance of the optical fibre system should be further improved on what was obtained earlier.

To investigate this experimentally, the system was tested using a high quality quartz QWP ($\gamma = \pi / 250$). Again, the "straight through" arrangement under longitudinal modulation was employed. A polariser with its transmission axis at 45° to the reference signal was placed in the detection arm. Intensities I_p and I_s were recorded and the ratio I_s / I_p were calculated.
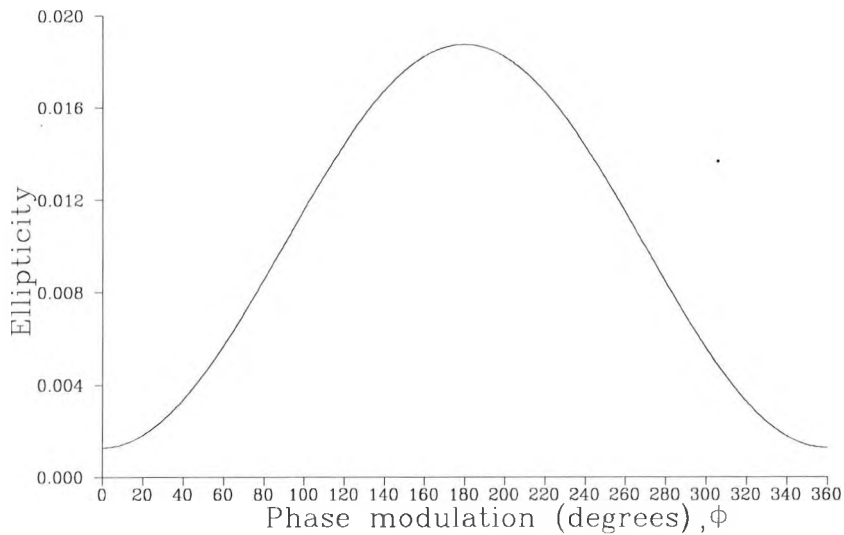
Figure 3-13 Illustration of an ellipticity evolution when the input beam is misaligned by 0.5° from a reference direction and a QWP used in the system is misaligned by 0.5° from the reference direction.

Modified Polarisation Modulation (polished end faces + longitudinal modulation)	Clockwise rotation	Counterclockwise rotation
with a mica QWP ($\gamma = \pi/25$)	1.083	1.020
with a quartz QWP ($\gamma = \pi/250$)	0.999	1.008

Table 3-4 The comparison of the average of the ratio I_s / I_p of the fringes situated on each side of a turning point from a longitudinal polarisation modulation with different quality QWPs.

Table 3-4 shows the comparison of the optical fibre systems with a standard quality mica QWP (i.e. retardance error, $\gamma = \pi / 25$) and a high quality quartz QWP (i.e. $\gamma = \pi / 250$) at the output end in terms of the average ratio I_s / I_p for two different direction of rotations; i.e. clockwise and counterclockwise.

Clearly, the table indicates that a significant improvement can be obtained when using the high quality QWP. This can be seen as the ratio I_s / I_p comes closer to unity for both directions of rotation.

It is also worth mentioning that some environmental effects, usually seen as relevant to the overall performance of an optical fibre based system, were not found significantly to perturb the output beam. Good illustrations of the errors involved are seen in temperature and pressure effects (Jones, 1985). Theoretically, the internal birefringence of the Bow-Tie HiBi fibre is a function of the environmental temperature (Chiang *et al*, 1990); hence, the temperature change will cause fluctuations of the output polarisation azimuth and thus reduce the stability and resolution of the system. However, this was of little consequence in the arrangement used, as the referencing scheme employed allows the tracking of the drifting of the output signal due to the effect.

In the same manner, although the birefringence is also pressure-dependent (Tatam *et al*, 1986), the factor again did not affect the system.

Lastly, a consideration which is worth noting here is the fibre polarisation-holding ability. The effect is an important criterion of HiBi fibres, indicating how well they hold polarisation or, equivalently, the average rate at which the perturbations couple power out of the desired eigenmode into the orthogonal mode (Rashleigh *et al*, 1982a). Typical Bow-Tie HiBi fibres have polarisation-holding parameters, h, of $h \leq 10^{-5}$ m^{-1} which indicates that the unexcited polarisation mode is suppressed, on average, by more than -30 dB after 100 m of fibre (Rashleigh and Marrone, 1982b). This polarisation holding ability can still be maintained as long as the fibre used is kept lying straight. In practice, all conditions supporting the polarisation-holding

ability were met; for instance, a short length (1 m) of fibre is used, and care is taken in the positioning of the fibre during the experiment.

3-5 Conclusions

The optical fibre polarisation modulation technique necessary for incorporation in a novel polarimetric measurement system has been modified to improve its performance. The reduction of the light reflections at the end faces of the fibre and power coupling between the two eigenmodes has been successfully achieved. A series of investigations has been carried out and, as a result, an improvement in the performance of the polarisation modulation technique has been observed. This was achieved by polishing the end faces of the fibre at an angle, modulating the fibre either by the use of heating or longitudinal stretching and using a high quality QWP. It is also worth mentioning at this stage that different modulation methods can offer dissimilar modulating frequencies and, thus, give rise to various measurement speeds which are suitable for different applications. For instance, in a sensing application whereby rapid changes of medium properties often occur, an optical method such as ellipsometry (discussed in detail in the next Chapter) equipped with a high frequency modulation method could provide high measurement speeds to enable detection of such changes.

In addition to the performance-related aspects of the optical fibre configuration, some potential factors such as temperature, pressure and polarisation-holding ability were considered but reasonably dismissed because their possible detrimental effects on the system could be minimised by taking some simple precautions.

Having optimised the HiBi fibre scheme, work described in the next Chapter uses this optical fibre polarisation modulation system in the ellipsometric measurement of a range of optical materials.

CHAPTER 4
ELLIPSOMETRIC MEASUREMENTS USING A HIBI FIBRE POLARISATION MODULATION SCHEME

4-0 Introduction

The HiBi fibre polarisation modulation technique used to generate a rotating plane polarised beam has now been thoroughly studied and optimised, as described in the last Chapter. Achievements thus far may be summarised as: (1) by reducing some potential sources of depolarisation (i.e. replacing a number of discrete optical components with a piece of fibre), the degree of polarisation becomes acceptable for polarimetric applications (i.e. DOP > 99%), (2) with the optical fibre configuration chosen, limitations normally introduced by the mechanical-base arrangement such as low measuring speed, precise engineering for discrete and bulky components can be avoided, and (3) the significant reduction of the observed asymmetric output (i.e. the percentage of asymmetry between the different orientational direction of linear light is found to be reduced from 10-20% down to 1-5%). As a result, the system performance is now significantly improved from its original state. To illustrate the potential of the present configuration, its application was demonstrated by characterising some materials via an ellipsometric system.

Generally, ellipsometry is known as an optical technique for the characterisation of interfaces and films, and it is based on the transformation of polarisation of an incident beam by various optical interactions such as reflection, transmission or scattering. One particular example, the reflection ellipsometer, uses the fact that the reflection of polarised light from an optically smooth surface is accompanied by a change in phase and intensity of the composite components giving, in general, an elliptically polarised beam. Frequently, to ease the mathematical

analysis, the input polarisation state is chosen to be linear or circular. These parameters allow the optical properties of the material under study to be evaluated (Yoshino and Kurosawa, 1984).

One of the most useful optical characteristics obtained by this method is the complex index of refraction (also called the complex refractive index). This parameter is important because it is used to classify an optical sample of interest. For example, if an optical medium is dielectric and non-absorbing, the refractive index, n, a real constant will be measured, whereas, when there is absorption (as there always is in the case of metals) the refractive index becomes a complex quantity $N = n\text{-}ik$, so that two constants are involved. In this case n is the *refractive index* and k the *absorption coefficient* of the medium (Hecht, 1974). The definition of the complex index is quite analogous to that for the ordinary real index. For example, the progress of a plane wave in the medium can be written $\bar{E} = E_o \exp\left[i\omega\left(t - \left(\frac{N}{c}\right)\bar{x}\right)\right]$. When N is real, c/N is merely the velocity of the wave in the medium. It is clear that when N is a complex quantity, the amplitude of the wave decreases with distance, which corresponds to the absorption present.

4-1 Function of Ellipsometric Instrumentation

The motivation for the development of ellipsometric measurement is the determination of some aspect (physical, optical, electrical, etc.) of the state of a specimen in the optical system. To obtain such a measurement, the following procedures (Hague, 1980) in the configuration of the device are required:

Firstly, it is essential to employ an incident beam with known properties of the state of polarisation and its orientation. This provides a knowledge of the initial conditions before the interaction between the beam and a medium under study occurs. Therefore, any effect from the sample on the incident beam can be clearly found and, in principle, correctly quantified.

Ellipsometry, as a technique, employs an appropriate interaction to gain access to the system under study. In the case of optical interfaces, in this study, either

transmission or reflection can be used. The criterion for choosing which interaction mainly depends on the properties of the measured system itself. For instance, if the system is not transparent enough to make the transmitted wave accessible for measurement, the use of the reflected wave would be preferable. Also, in the case of a thin film coated on a substrate (considered in the next Chapter), the use of the reflection could avoid complicating the mathematical treatment due to propagation through the substrate used.

Then, in order to obtain information relating to the sample, it is necessary to measure the emerging polarisation state after the selected interaction. This step is important because only the development and use of a proper arrangement for data acquisition will allow the full capability of the polarisation modulation approach proposed to be exploited.

Polarisation State Generator
(Rotating Polarisation
Production unit)

Polarisation State Detector

Sample
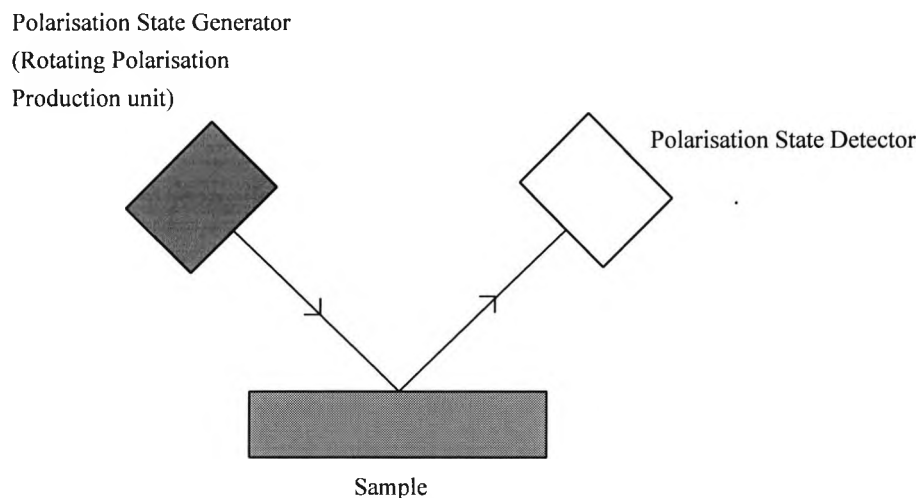
Figure 4-1 The essential arrangement of the reflection ellipsometer

Following the previous procedure, the information gained may then be used to determine the required characteristics such as the refractive index, the absorption coefficient or the thickness of the optical medium, via some manipulation, based on an appropriate theoretical analysis (Azzam and Bashara, 1977).

This can be achieved by implementing the HiBi fibre polarisation modulation technique, presented here. The approach does not only produce a linear state of known orientations but also permits its speedy and continuous controllability.

Fig. 4-1 shows, in a simple schematic diagram, the selected configuration which will be utilised throughout the following investigations.

With the degree of the absorption varying according to the sample type, it is clear that the transmitted-beam method is very inaccessible for measurement, especially in the case of the metal plate. Hence, these considerations favour the application of the reflection approach.

4-2 Reflection: Theoretical Background
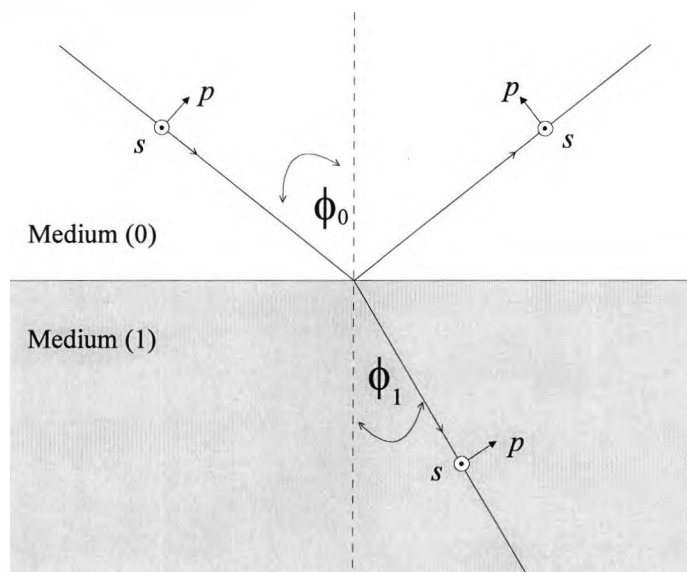
Figure 4-2 Oblique reflection and transmission of a plane wave at the planar interface between two semi-infinite media 0 and 1.

ϕ_0 and ϕ_1 are the angles of incidence and refraction, respectively.

p and s are axes parallel and perpendicular to the plane of incidence.

With reference to Fig. 4-2, the oblique reflection of an optical plane wave at the planar interface between two semi-infinite homogeneous optically isotropic media 0 and 1 with complex indices of refraction N_0 and N_1, respectively may be considered. The wave incident from medium 0 gives rise to a reflected wave in the same medium and a transmitted wave in medium 1. The angle of incidence, ϕ_0, and

the angle of transmission, ϕ_1, are both measured from the direction of the normal to the interface. The propagation of the electromagnetic fields inside media 0 and 1 obey Maxwell's equations.

This leads to certain requirements which must be met by the fields in order to be continuous at the interface. These are referred to as the boundary conditions (BC). Specifically, one of these is that the component of the electric field which is at a tangent to the interface must be continuous across it (Klein, 1970). This particular BC results in (1) the angle of incidence must equal the angle of reflection and (2) the angle of incidence ϕ_0 and transmission ϕ_1 must be related by $N_0 \sin\phi_0 = N_1 \sin\phi_1$, which is familiar as Snell's law.

Furthermore, the same BC may then be applied to the corresponding magnetic components. Consequently, application of the BC and solving the resulting equations leads to the Fresnel's laws of refraction (Fowles, 1975). The laws state the relationship between the incident, reflected, and transmitted waves in terms of two composite polarised components. One component, designated p, is in the plane of incidence. The other, designated s, is normal to the plane of incidence.

In general, if a polarised beam is reflected by an optical medium, the phases of the p and s components are shifted, as well as their amplitudes altered. $\left(\vec{E}_{ip}, \vec{E}_{is}\right)$ and $\left(\vec{E}_{rp}, \vec{E}_{rs}\right)$ may be used to represent the complex amplitudes of the components of the electric field vectors of the incident and reflected waves, respectively.

$$\frac{\vec{E}_{rp}}{\vec{E}_{ip}} = r_p = \frac{N_1 \cos\phi_0 - N_0 \cos\phi_1}{N_1 \cos\phi_0 + N_0 \cos\phi_1} \qquad (4\text{-}1),$$

and

$$\frac{\vec{E}_{rs}}{\vec{E}_{is}} = r_s = \frac{N_0 \cos\phi_0 - N_1 \cos\phi_1}{N_0 \cos\phi_0 + N_1 \cos\phi_1} \qquad (4\text{-}2),$$

which are the Fresnel complex amplitude reflection coefficients for the p (r_p) and s (r_s) polarisations. It is worth noting that Eqs. (4-1) and (4-2) explicitly contain the

complex refractive indices. Knowledge of ϕ_0, r_p and r_p will then allow the determination of these indices.

If media 0 and 1 are transparent, so that N_0 and N_1 are both real numbers, then the system analysis becomes simple. However if one of the media, normally medium 1, is absorbing, the corresponding index then becomes a complex quantity and the investigation is inevitably more complicated.

In order to examine the effect of reflection on the amplitude and phase of the wave separately, the complex Fresnel coefficients may be rewritten as

$$r_p = |r_p| e^{i\delta_{rp}} \qquad\qquad (4\text{-}3),$$

and

$$r_s = |r_s| e^{i\delta_{rs}} \qquad\qquad (4\text{-}4).$$

$|r_p|$ gives the ratio of the amplitude of the reflected to that of the incident electric vector when the beam is polarised parallel to the plane of incidence, with there being a similar meaning for $|r_s|$. δ_{rp} represents the phase shift upon reflection experienced by the electric vibration parallel to the plane of incidence, with a similar meaning to δ_{rs}.

The ratio of the complex p and s reflection coefficients, ρ, is customarily related to the measurable, real ellipsometric parameters, ψ and Δ, by the relation

$$\rho = \frac{r_p}{r_s} \equiv \tan\psi \cdot e^{i\Delta} \qquad\qquad (4\text{-}5).$$

From Eqs. (4-3) and (4-4), it is readily seen that

$$\tan\psi = \frac{|r_p|}{|r_s|} \qquad\qquad (4\text{-}8),$$

$$\Delta = \delta_{rp} - \delta_{rs} \qquad\qquad (4\text{-}9).$$

Thus ψ and Δ determine the differential changes in amplitude and phase, respectively, experienced upon reflection by the component vibrations of the electric vector parallel and perpendicular to plane of incidence.

Substituting r_p and r_s in Eq. (4-5), using their values from Eqs. (4-3) and (4-4), and making use of Snell's law, the equation can be solved for $\dot{N_1} / N_0$ in terms of ρ and ϕ_0 to give

$$\frac{N_1}{N_0} = \sin\phi_0 \left[1 + \left(\frac{1-\rho}{1+\rho} \right)^2 \tan^2 \phi_0 \right]^{\frac{1}{2}}$$

(4-10),

Eq. (4-10) shows that the complex index of refraction of medium 1 can be determined if the index of refraction of medium 0 (the medium of incidence) is known and the ellipsometric ratio, ρ, is measured at one specific angle of incidence, ϕ_0.

It is interesting to know that if the complex index of refraction of medium 1 is given by $N_1 = n_1 - ik_1$, the real term is found to be (the details are discussed in Appendix B),

$$n_1 = N_0 \sin\phi_0 \left(a^2 + b^2 \right)^{\frac{1}{4}} \cos\kappa$$

(4-11),

and the imaginary part can be expressed as

$$k_1 = N_0 \sin\phi_0 \left(a^2 + b^2 \right)^{\frac{1}{4}} \sin\kappa$$

(4-12),

where

$$a = 1 + \tan^2 \phi_0 \left\{ \frac{\left(1 - \tan^2 \psi \right)^2 - 4\tan^2 \psi \sin^2 \Delta}{\left(1 + \tan^2 \psi + 2\cos\Delta \tan\psi \right)^2} \right\}$$

(4-13),

$$b = \tan^2 \phi_0 \left\{ \frac{4\left(1 - \tan^2 \psi \right)\left(\tan\psi \sin\Delta \right)}{\left(1 + \tan^2 \psi + 2\cos\Delta \tan\psi \right)^2} \right\}$$

(4-14),

and

$$\kappa = \tfrac{1}{2} \left\{ \tan^{-1}\left(-\tfrac{b}{a} \right) \right\}$$

(4-15).

For the purpose of the measurement, it is necessary to know that amplitude reflection coefficients r_p and r_s are related to measurable quantities R_p and R_s known as reflectances by (Azzam and Bashara, 1977)

$$R_p = \left| r_p \right|^2$$

(4-16),

$$R_s = \left| r_s \right|^2$$

(4-17),

which give the fraction of the total intensity of an incident plane wave that appears in the reflected wave for p and s polarisations, respectively.

It can be concluded at this stage that the measurement of the effect of reflection on the state of polarisation of a polarised beam is sufficient to determine the complex index of refraction of a sample. This concept is the essence of a reflection ellipsometer.
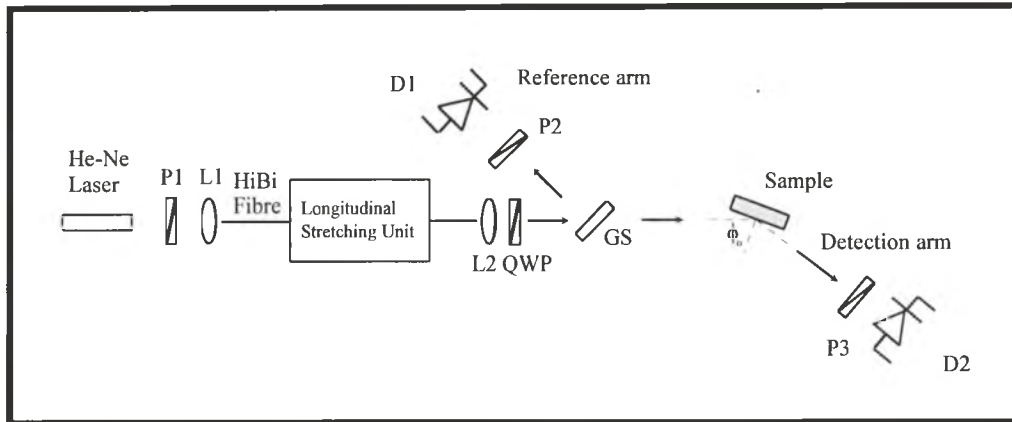
Figure 4-3 Illustration of a HiBi fibre polarisation modulation scheme for reflection ellipsometry.
Ps, Polarising Prisms; Ls, Lenses; QWP, Quarter-Wave Plate; GS, Glass Slide; Ds, Detectors.

The configuration of the ellipsometric system is shown in Fig. 4-3 utilising the HiBi fibre polarisation modulation technique. To analyse the process, the rotating plane polarised beam, $\bar{E}_1$, used to illuminate a sample is given by Eq. (2-17)

$$\bar{E}_1 = \begin{bmatrix} \cos\phi' \\ -\sin\phi' \end{bmatrix} E_o e^{i\varepsilon} \qquad (4\text{-}18),$$

where $\phi' = \frac{1}{2}(\phi^{(2)} - \frac{\pi}{2})$ and $\varepsilon = \omega_o t + \phi_s + \frac{\pi}{4} + \phi^{(2)}$.

This beam is then transformed by the Jones matrix of the sample, S, to yield the new Jones vector:

$$\bar{E}_2 = S\bar{E}_1$$
$$= \begin{bmatrix} r_p \cos\phi' \\ -r_s \sin\phi' \end{bmatrix} E_o e^{i\varepsilon} \qquad (4\text{-}19),$$

where the Jones matrix of the sample S can be written in the form (Singher, 1990),

$$S = \begin{bmatrix} r_p & 0 \\ 0 & r_s \end{bmatrix} \qquad (4\text{-}20),$$

where r_p and r_s are as given in Eqs. (4-3) and (4-4).

If this reflected electric field, $\bar{E}_2$, is detected by a detector, the corresponding intensity, I_2, is given by

$$I_2 = \left(\bar{E}_2 \cdot \bar{E}_2^*\right) = I_0\left(R_p \cos^2 \phi' + R_s \sin^2 \phi'\right) \qquad (4\text{-}21).$$

It can be seen that, with an appropriate phase modulation ϕ', Eq. (4-21) allows the determination of $|r_p|/|r_s|$ but certainly not the relative phase shift, Δ. Thus, the information for evaluating the sample index of refraction (cf. Eq. (4-10)) is not obtained. However, the problem of this inadequacy of information can be solved by considering the situation when both components of the incident wave are resolved into a common plane. Under this condition an interference term between the two eigenstates will be introduced and the phase information of the reflected beam will be maintained.

This circumstance can be accomplished by placing a polarising prism orientated at an arbitrary angle, θ, relative to the plane of incidence in front of the detector. Thus the electric vector transmitted by the polariser, $\bar{E}_{3,\,\theta}$, can be represented by the vector

$$\begin{aligned}
\bar{E}_{3,\,\theta} &= P_\theta \bar{E}_2 \\
&= \begin{bmatrix} r_p \cos\phi' \cos^2\theta - r_s \sin\phi' \cos\theta \sin\theta \\ r_p \cos\phi' \cos\theta \sin\theta - r_s \sin\phi' \sin^2\theta \end{bmatrix} E_o e^{i\varepsilon}
\end{aligned} \qquad (4\text{-}22).$$

To simplify the signal representation and provide the most practical solution of the problem, the polariser is oriented at an angle of 45° to the plane of incidence. The Eq. (4-22) becomes

$$\bar{E}_{3,\,45^o} = \begin{bmatrix} 1 \\ 1 \end{bmatrix}\left(r_p \cos\phi' - r_s \sin\phi'\right)\frac{E_o}{2} e^{i\varepsilon} \qquad (4\text{-}23).$$

This electric field is then detected by the photodetector in the system and its intensity, $I_{3,\,45^o}$, may be given by

$$I_{3,\,45^o} = \left(\bar{E}_{3,\,45^o} \cdot \bar{E}_{3,45^o}^*\right) = \frac{I_0}{2}\left(R_p \cos^2 \phi' + R_s \sin^2 \phi' - \sqrt{R_p R_s} \sin 2\phi' \cos\Delta\right) \qquad (4\text{-}24).$$

This suggests a practical solution for determining the ellipsometric parameters ψ and Δ and subsequently the sample index of refraction.

At the detection arm, when the light is modulated to be parallel to a plane of incidence (c.f. Eqs. (A-3) and (A-4)), the intensity at the detector is given by

$$I_{parallel} = (\vec{E}_{3,\,45^{\circ},\,\phi'=0}) \cdot (\vec{E}_{3,\,45^{\circ},\,\phi'=0})^{*} = \frac{I_0 R_p}{2} \qquad (4\text{-}25),$$

Similarly, when it becomes perpendicular to the plane of incidence, the intensity is found to be

$$I_{perpendicular} = (\vec{E}_{3,\,45^{\circ},\,\phi'=\frac{\pi}{2}}) \cdot (\vec{E}_{3,\,45^{\circ},\,\phi'=\frac{\pi}{2}})^{*} = \frac{I_0 R_s}{2} \qquad (4\text{-}26),$$

Other orientations of incident polarisation can also be identified but a great degree of simplification occurs when the azimuth is at 45° to the plane of incidence, where the intensity is then given by

$$I_{45^{\circ}} = (\vec{E}_{3,\,45^{\circ},\,\phi'=\frac{\pi}{4}}) \cdot (\vec{E}_{3,\,45^{\circ},\,\phi'=\frac{\pi}{4}})^{*} = \frac{I_0}{2}\left(\frac{R_p}{2} + \frac{R_s}{2} - \sqrt{R_p R_s}\cos\Delta\right) \qquad (4\text{-}27).$$

Clearly the ratio of Eqs. (4-25) to (4-26) would permit the determination of ψ and then substituting the two equations into Eq. (4-27), the relative phase shift Δ can be determined. Hence, ρ is obtained. Substitution of the parameter, ρ, into Eq. (4-10), allows the complex index of refraction of medium 1 (the medium under study) to be determined, provided that ϕ_0 and N_0 are given. It is obvious that the process of characterising the reflecting surface can be accomplished without mechanical movement of any optical components. This provides a major step forward in the use of this ellipsometric technique for real time applications.

It is worth pointing out at this stage that, in this experiment, data similar to Fig. 3-2 is detected. Therefore, a number of I_p, I_s and I_{45} can be collected from consecutive rotations of a polariser by using a reference signal. This allows determinations of I_p, I_s and I_{45} (subsequently ψ and Δ) in averaged forms. By doing this, the residual effect of direction of rotation should consequently be minimal (of course, a much smaller effect of rotation in different directions will be imposed on the

results due to the extensive improvements carried out on the polarisation modulation system).

4-3 Experimental Set-up Used in this Work

Since the experimental set-up of the rotating polarised beam production has already described in the previous Chapters, the following experimental arrangement mainly concerns the situation occurring following the use of the HiBi fibre polarisation modulation system. Fig. 4-3 illustrates that a reference signal was fractionally sampled from the main beam emitted from the polarisation modulation system (utilising longitudinal stretching). The reference signal scheme enables monitoring of the state of the rotating plane polarised beam input to the ellipsometer, as discussed in Sec. 4-2. The sampled beam was reflected by a microscope glass slide (at an angle of 3° to the plane of incidence) through a polarising prism onto a photodetector. This main beam was incident on a sample oriented at an appropriate angle of incidence, and was then reflected through a polarising prism with its transmission axis at 45° relative to the plane of incidence. After passing through the polariser, the reflected beam was detected by a photodetector. Finally the detected and reference signals were transferred to a computer for analysis.

The modulation technique used is that of longitudinal fibre stretching. In practice, the modulator was driven by a ramp signal whose amplitude was adjusted to be ≈ 1 Volt at a frequency of ≈ 30 Hz. Under these modulation conditions (and taking the strain coefficient of the differential modal retardance to be $\approx 6.5 \times 10^4$ rad.m^{-1}, [Tatam *et al,* 1987]) the length of the fibre stretching was found to be approximately 300 μm, i.e. $\approx 6\pi$ phase shift.

4-4 Experimental Conditions

To demonstrate the capability of the ellipsometric system, the optical medium studied involves two distinctive kinds of material: non-absorbing and absorbing. For a non-absorbing material, BK7 was used because its well-known optical properties

(especially the index of refraction) provided a very good calibration for the measuring system. In addition, the material is also recognised as an industry standard glass used in an enormous variety of optical applications.

In the case of the absorption, materials with different degrees of absorption were studied. Firstly, materials with low absorption at the wavelength used ($\lambda = 632.8$ nm) were employed. Some very suitable samples for this case are silicon (Si) and zinc selenide (ZnSe). Silicon is a material at the heart of semiconductor electronic technology, with high refractive index and low absorption coefficient. For ZnSe, one of its advantages that makes it one of the most popular materials for transmissive infrared optics in many applications is its low absorption in the red end of the visible spectrum (Melles Griot, 1992). This then allows the ubiquitous HeNe laser to be used as an inexpensive and convenient alignment tool for the infrared optical system. This advantage can be exploited here for examining the sensitivity of the proposed instrument in the low absorption region with the currently used wavelength. Therefore, such materials provide a very good investigation of the system sensitivity in terms of detecting the low absorption of such materials. In the second case, the sensitivity of the instrument in the case of high absorption was examined by using a copper plate as a sample under investigation.

With such a varying degree of the absorption, according to the sample type, it is clear that the transmitted beam is very inaccessible for use for measurement, especially in the case of the metal plate. Hence, these considerations confirm the more appropriate application of the reflection method in this study.

4-5 Experimental Results

4-5-1 Non-Absorbing Sample : air/BK7 Interface

In order to undertake a preliminary evaluation of the system designed, an evaluation of a standard optical wedge (of BK7) was undertaken. The wedge shape was used to separate the front and the back reflections from one another in order to avoid unwanted interference that could introduce errors to the measurement. Since the

BK7 wedge has no absorption at the wavelength used (λ = 632.8 nm), only the real part of the index of refraction is of concern in the investigation.

In the first set of measurements, the variation in the ellipsometric parameters involved (ψ and Δ) was obtained. This was done by recording the relevant values (r_p and r_s) at different angles of incidence. The incidence angle started at 10° and then increased by 10° steps up to 80°. The detection was straightforward, as described earlier in the Sec. 4-2. The relative ratio of R_p / R_s was obtained and, as a result, ψ and Δ were measured as a function of the angle of incidence. The result is shown in Fig. 4-4.

This illustrates a typical set of curves of ellipsometric parameters for glass materials. At the angle ϕ_B, known as *Brewster's angle* (marked in the figure) the *p*-polarised light wave incident on the interface entirely disappears (i.e. $R_p = 0$). This implies that the ellipsometric measurements at or near the Brewster angle are highly likely to introduce large errors as I_p (when $R_p \to 0$) becomes very small and comparable to the degree of background noise.
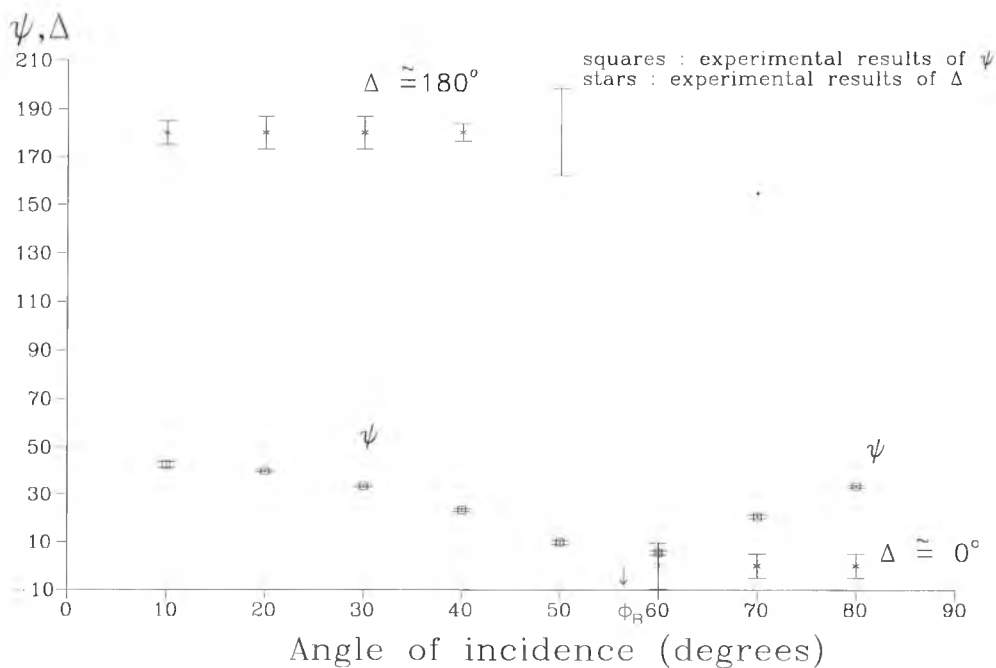
Figure 4-4 The ellipsometric parameters ψ and Δ as a function of the angle of incidence for the reflection at an air/BK7 interface : λ = 632.8 nm.
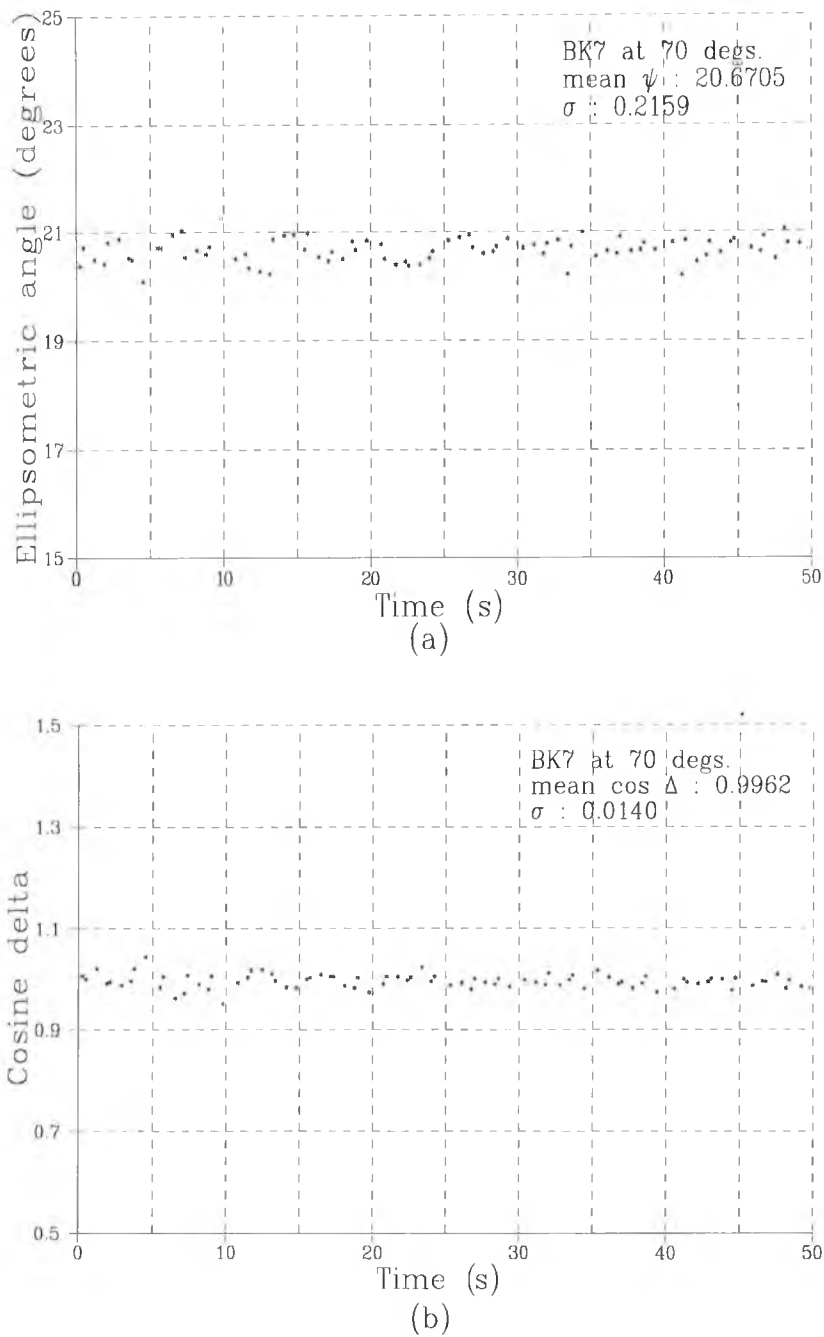
Figure 4-5 Experimental data on ψ (a) and cos Δ (b) taken from the air/BK7 interface during a 50 s period at $\lambda = 632.8$ nm, $N_{BK7} = 1.499$. The angle of incidence is 70°.

In addition, the figure also reveals that the sample causes a phase shift, Δ, of 180° when the incidence angle is less than the Brewster angle and 0° when the incidence angle is greater.

The second operation was the determination of the refractive index of the BK7. Because of the problem of operation near of the Brewster angle, the angle of incidence was chosen to be 70°. In addition, the ellipsometric parameters were recorded over a period of 50 s in order to examine the distribution of the ellipsometric parameters over a period of time (Fig. 4-5). The measured ψ was found to have a mean value of 20.67° and a standard deviation of 0.215° from the mean. The distribution over the operating period of ψ was within ±1 % around its mean (Fig. 4-5 (a)).

In the case of the phase shift, Δ, it is convenient to present this data as cosΔ, the absolute values of the cosine function of the phase shifts (c.f. Eq. (4-27)). The population mean of the cosine function of the phase shift should be unity because $\phi_0 > \phi_B$ and $\Delta = 0°$.

However, experimentally, the mean was found to be 0.996 with a standard deviation of 0.014 from the mean. The distribution over the operating period of cosΔ was within ±1 % of its mean (Fig. 4-5 (b)).

From all the information obtained at this stage, the refractive index of BK7 was calculated to be 1.49±0.01 in comparison with the value quoted of 1.519 (at $\lambda = 632.8$ nm) supplied by Comar Instruments.

It is noted that, as a result of a small drift in the measured cosΔ (≈ 0.996) from an ideal value (i.e. cos$\Delta = 1.00$), a smaller value of absorption coefficient, k, is generally expected. However, in principle, the coefficient is also a function of ψ and a range of other parameters shown in Eq. (4-12). By substituting all the information involved, the value of k was thus found to be 0.06±0.09.

4-5-2 Absorbing Samples

To examine the sensitivity of the instrument to absorption, two sets of absorbing samples with different degrees of absorption were used. The same experimental procedures as in the non-absorbing study were followed.

(a) Low Absorption : air/ZnSe Interface

Fig. 4-6 illustrates the experimental results obtained for ψ and Δ at different angles of incidence. The ψ curve which corresponds to the inverse tangent of the factor by which the amplitude ratio changes (c.f. Eq. (4-8)) implies the reflectance R_p for the p-polarisation exhibits a minimum value around an incidence angle of 70°. The angle is known as the *Pseudo-Brewster angle* (Hass and Thun, 1967). This also suggests that, the intensity I_p, as R_p approaches a minimum, may be comparable to the background noise and this can introduce errors. Thus, the angle of incidence used was chosen to be at 50°.
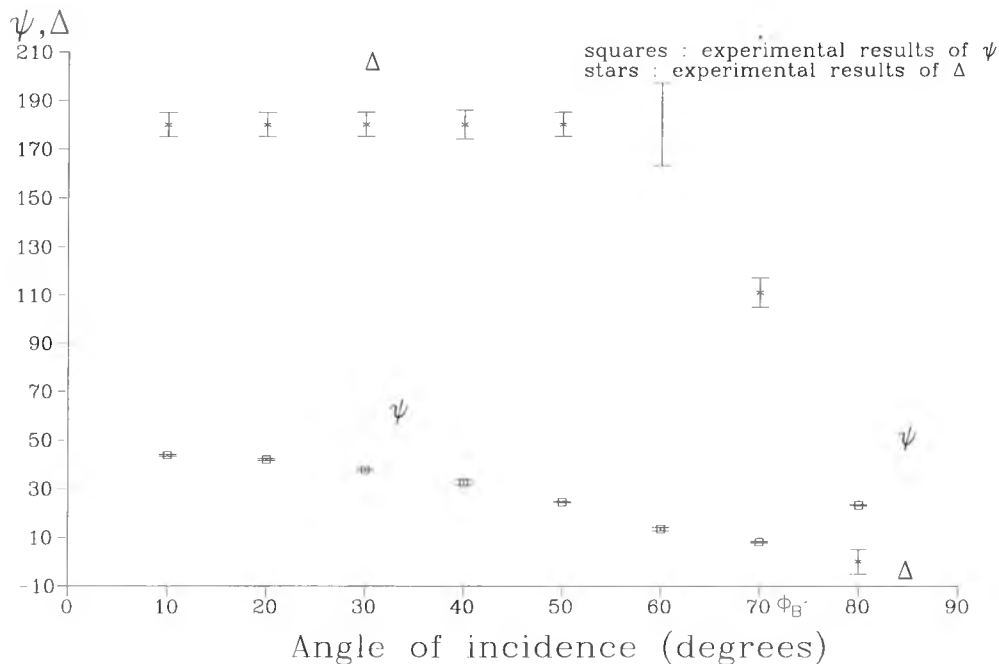
Figure 4-6 The ellipsometric parameters ψ and Δ as a function of the angle of incidence for the reflection at an air/Zinc Selenide interface : $\lambda = 632.8$ nm.

At this angle of incidence, the detection of ψ and $\cos\Delta$ was conducted for a period of 50 s. The mean value of ψ was calculated to be 27.20° and a standard deviation about the mean was 0.311°. The distribution over the chosen period of ψ was within ±1 % of its mean (Fig. 4-7 (a)). The $\cos\Delta$ was found to have a mean value of 0.96 and a standard deviation of 0.022 around the mean. In this case, the

distribution over the chosen period of cosΔ was found to be within ±2 % of its mean (Fig. 4-7 (b)).

$$ZnSe \ at \ 50 \ degs.$$
$$mean \ \psi = 27.2071$$
$$\sigma = 0.3113$$

(a)

$$ZnSe \ at \ 50 \ degs.$$
$$mean \ cos \ \Delta = 0.9614$$
$$\sigma = 0.0226$$

(b)
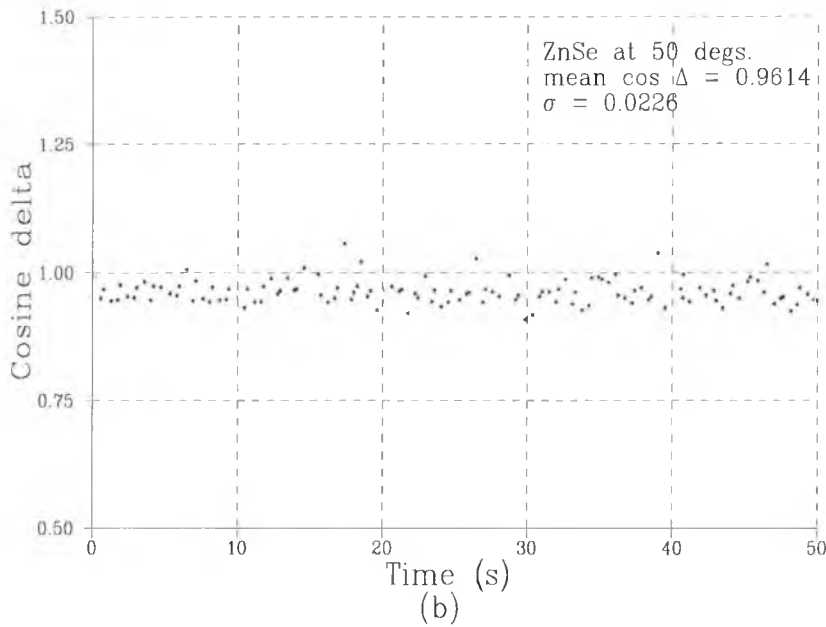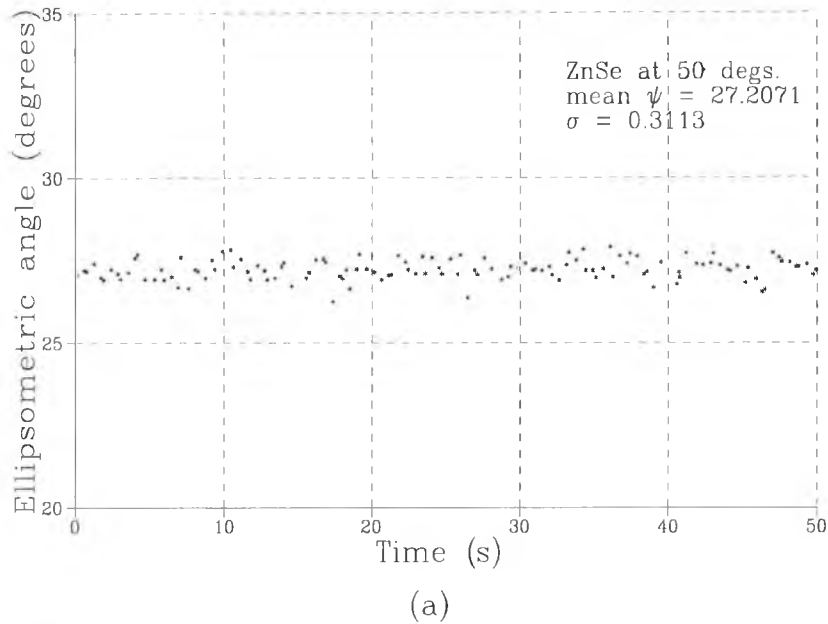
Figure 4-7 Experimental data on ψ (a) and cos Δ (b) taken from the air/Zinc Selenide interface during 50 s at λ = 632.8 nm, $N_{Zinc \ Selenide}$ = 2.53 -i0.89. The angle of incidence is 50°.

The index of refraction of ZnSe was calculated from Eqs. (4-11) and (4-12) to be 2.53(±0.30) -i0.89(±0.30). This shows a low magnitude of the complex part (low

absorption) at the wavelength used. Since the complex index of refraction of the ZnSe at $\lambda = 632.8$ nm was not available from other sources, a comparison can be made only in terms of the refractive index (real term). Pedinoff and Braunstein (1979) measured the refractive index of a ZnSe film on a KCl substrate by means of ellipsometry at the same wavelength as was used here. The refractive index they quoted is 2.45 which is comparable to the result obtained.

(b) Low absorption : air/Si Interface

Fig. 4-8 shows the experimental results of ψ and Δ at different angles of incidence for a sample of air/Si interface. As can be seen from the graph, a pseudo-Brewster angle is again found ($\approx 70^\circ$). This additionally implies that measurements at or close to this angle should be avoided because the value of I_p is comparable with the background noise. Therefore, the chosen angle of incidence was taken to be 50°.
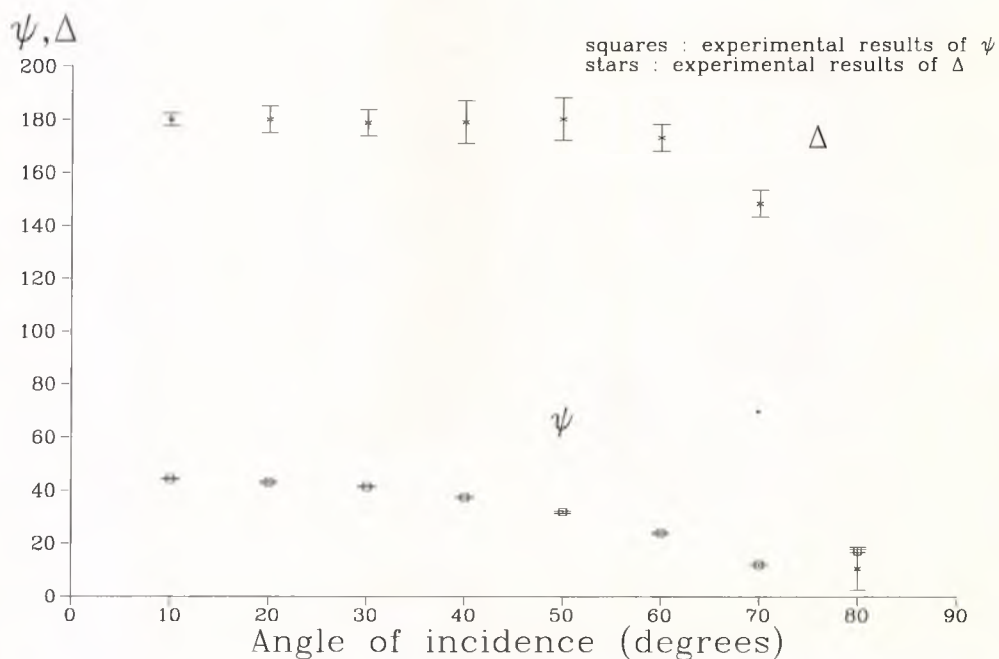
Figure 4-8 The ellipsometric parameters ψ and Δ as a function of the angle of incidence for the reflection at an air/Silicon interface : $\lambda = 632.8$ nm.

103

At this angle of incidence, the measurements of ψ and $\cos\Delta$ were again performed over a period of 50 s. The mean value of ψ was found to be 31.52° and a standard deviation around the mean was calculated to be 0.217°. The distribution of data detected over the chosen period of ψ was within ±0.7 % around the mean value (Fig. 4-9 (a)).
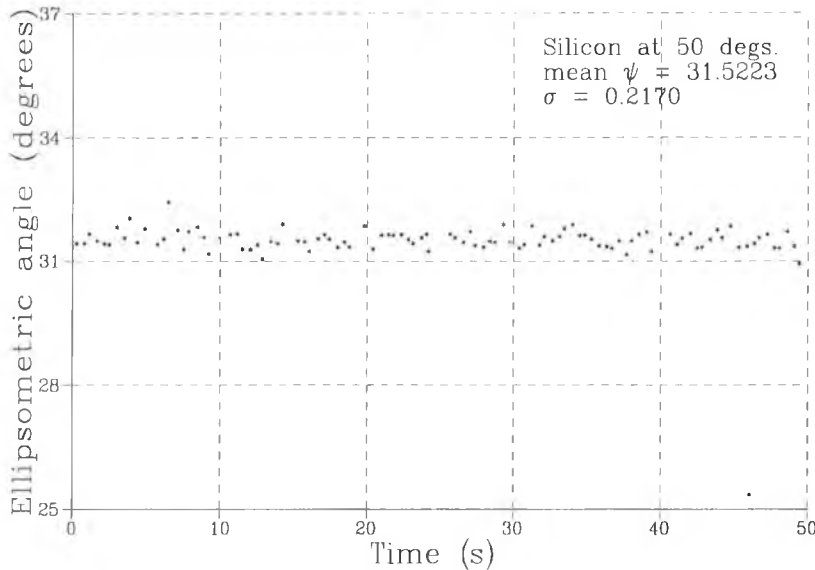
(a)
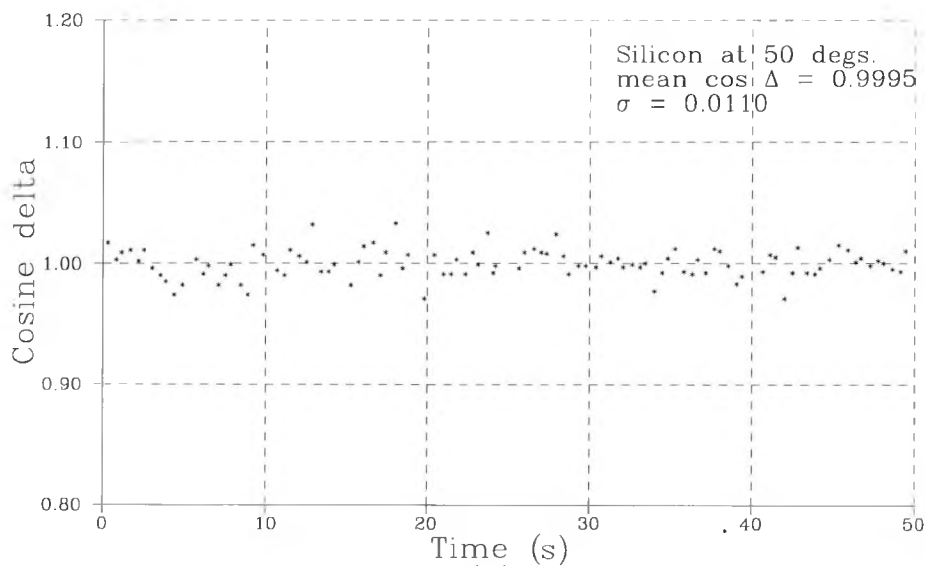
(b)

Figure 4-9 Experimental data on ψ (a) and $\cos\Delta$ (b) taken from the air/Silicon interface during 50 s at $\lambda = 632.8$ nm, $N_{Silicon} = 3.86 -i0.32$. The angle of incidence is 50°.

The mean of the cosΔ was calculated to be 0.999 and its standard deviation around the mean was 0.011. Again the distribution of cosΔ data collected was calculated and found to be within ± 1 % around its mean value (Fig. 4-9 (b)).

The index of refraction of the Si was calculated from Eqs. (4-11) and (4-12) to be 3.86(± 0.40) -i0.32(± 0.70) and compared to a typically quoted index of refraction of the material, 3.85 -i0.02, given by Zaghloul *et al* (1975). The value is obviously comparable for the real part (the refractive index); whereas, the complex part (the absorption coefficient) is rather different. It could be from the fact that such a small absorption coefficient, i.e. $k = 0.02$, partly implies a small phase shift which is very difficult to detect with the current data acquisition technique. In other words, the technique used is largely insensitive to a small phase change for a specific range phase near 0° or 180°. Nevertheless, an improvement can be obtained with a small modification to the present arrangement and this is discussed in the following section.

(c) Low absorption : Methods of Sensitivity Improvement

The sensitivity of the technique could be improved by adding an extra phase to the current phase shift between the two orthogonal components with a wave plate. One of the most suitable wave plates to be employed is a quarter-wave plate aligned parallel to the sample axes. A schematic of the modification is shown in Fig. 4-10.
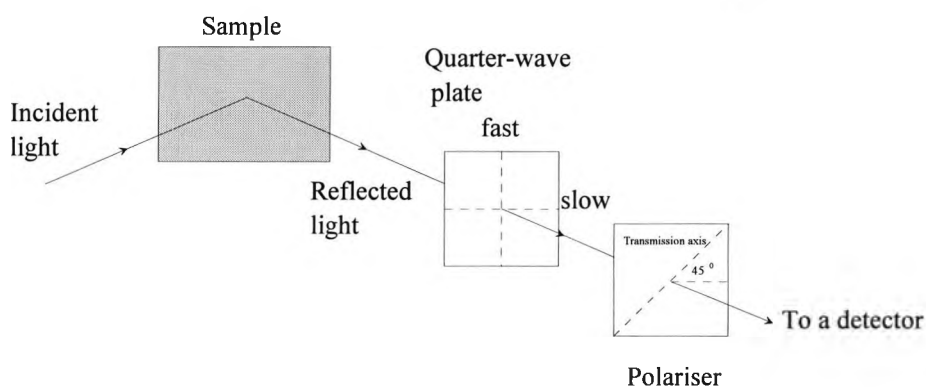
Figure 4-10 Illustration of an additional quarter-wave plate in the detection arm of the present polarisation modulated ellipsometer.

From Fig. 4-11, using this modification, an initial Δ (point A) would be shifted along the cosine curve (c.f. $\cos\Delta$ from Eq. (4-27)) to a position where a higher sensitivity, corresponding to a steeper slope on the curve, could be seen to where such a small alternating phase can be detected (point B).

Theoretically, the function of $\cos\Delta$ can be represented by a Taylor series (Spiegel, 1971) as

$$\cos\Delta = 1 - \frac{\Delta^2}{2!} + \frac{\Delta^4}{4!} - \dots \qquad (4\text{-}28).$$

If the sensitivity is defined as the change of $\cos\Delta$ relative to Δ, the value may be calculated to be

$$\frac{d\cos\Delta}{d\Delta} \approx -\Delta \qquad (4\text{-}29).$$

This means that the sensitivity of the system totally depends on the value of the phase shift. In other words, the smaller the value of $|\Delta|$ is, the less the sensitivity of the system.
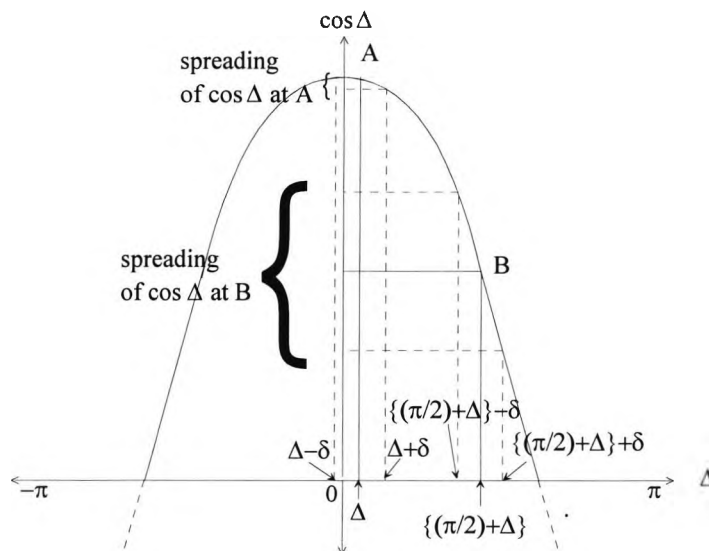
Figure 4-11 Illustrations of a shifted phase introduced by a quarter-wave plate along the cosΔ curve and spreading of data at relevant points.

However, if a quarter-wave plate is added to the detection arm, the function cosΔ then becomes $\cos\{(\pi/2)+\Delta\}$ or sinΔ. In this case, the series representing the function may be given by

$$\sin\Delta = \Delta - \frac{\Delta^3}{3!} + \frac{\Delta^5}{5!} + \dots \qquad (4\text{-}30).$$

Consequently, the sensitivity is found to be

$$\frac{d\sin\Delta}{d\Delta} \approx 1 - \Delta^2 \qquad (4\text{-}31).$$

This obviously shows that the sensitivity becomes much less dependent on the value of the phase shift ($\because \Delta \to 0$).

It is worth pointing out at this stage that, in practice, it is crucial to know exactly what phase value the additional quarter-wave plate introduces. An experiment to determine this can simply be performed using transmission ellipsometry (Azzam and Bashara, 1977).

The complex refractive index evaluations were carried out again with zinc selenide and silicon samples at the same angle of incidence of 50°. Before the experiments were performed, a calibration of the quarter-wave plate used had been made and the retardation of the plate was found to be 88.75°..In case of the air/Zinc Selenide interface, the ellipsometric parameter, ψ, was found to be 28.30° and a standard deviation around the mean was 0.356°. The spreading of the data around the mean value was within ±1.2 %. The mean value of cosΔ was calculated to be 0.237 and a standard deviation around the mean was 0.05, resulting in a spreading of ±21.1% around the mean. Again, using Eqs. (4-11) and (4-12), the refractive index of the ZnSe was calculated to be 2.81(±0.20) - i0.86(±0.50).

For Si, the mean value of ψ was calculated to be 31.915° and its standard deviation around the mean was 0.153°. This indicated a distribution of ±0.48 % around the mean. The averaged cosΔ was calculated to be 0.037 and a standard deviation around the mean found to be 0.011. The spreading of the data was

calculated to be within ±30.8 % around the mean. The Silicon index of refraction was determined to be 3.99(±0.10)-i0.13(±0.10).

From the results of the complex refractive indices obtained, particularly for the absorption coefficients, the work has clearly illustrated that the additional quarter-wave plate improved the ellipsometric performance. The improvement can be clearly seen, especially, in the study of Si, in that the newly measured absorption coefficient is smaller than the one obtained previously and approaches to the value quoted in the literature.

However, it is important to note that the accuracy of the system has to be sacrificed, especially, in case of measured cosΔ from both samples, as seen from the experiments. This can be explained by examination of Fig. 4-11. If the deviation in Δ is given by δ (arising from system error, e.g. misalignment of QWP), the resulting spread in cosΔ depends on the initial phase. For an initial phase near 0 rad (point A) the spread in cosΔ is small; whereas, for an initial phase near π/2 rad introduced by the inclusion of a QWP (point B) the resulting spread in cosΔ is large.

(d) High Absorption : air/Copper plate Interface

The performance of the ellipsometric system was also tested on a highly absorbing sample by investigating the characteristics of a copper plate. A point worth mentioning here is that the surface preparation of the metallic sample under test is as important as the measurement of the ellipsometric parameters. This is because a poor quality finish of a polished surface can give rise to diffuse reflections which do not obey the Fresnel's laws of reflection (Palais, 1988). A preparation process of the copper plate was carried out by polishing the copper surface with a chemical solution commercially available for metal polish. Immediately after that, the surface characterisation using the ellipsometry was performed in order to ensure specular reflections from the copper surface.
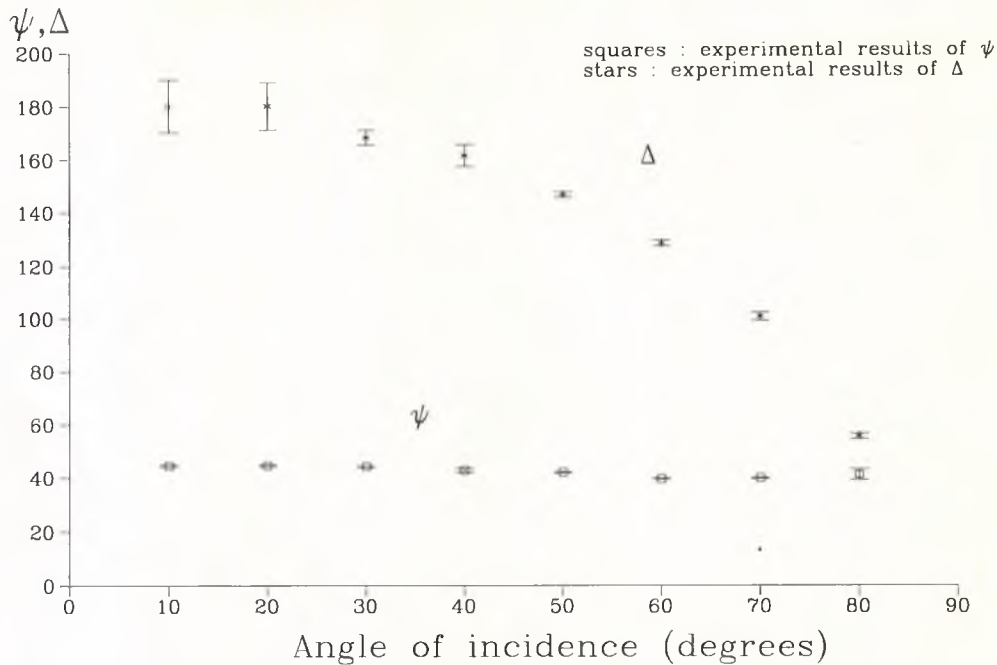
Figure 4-12 The ellipsometric parameters ψ and Δ as a function of the angle of incidence for the reflection at an air/Copper interface : λ = 632.8 nm.

The ellipsometric parameters ψ and Δ of the copper plate were measured at various angles of incidence (Fig. 4-12). Again the trends of the ellipsometric parameters obtained in the figures suggested that any angle of incidence could be selected for the refractive index measurement. This is because there is no angle where indicates a possibility of noise disturbance as found in previous samples.

Fig. 4-12 also reveals the curve of the phase shift, Δ, resulting from the highly absorbing material. This can be seen more clearly here than with the data obtained from the low absorbing samples.

The angle of incidence chosen for the measurement was 70°. The parameter ψ was measured to have a mean value of 41.51° and a standard deviation of 0.151° from the mean. The distribution of ψ over a period of 50 s was found to be within ±0.4 % around its mean (Fig. 4-13 (a)). The cosΔ was found to have a mean value of 0.16 and a standard deviation of 0.004 from the mean. The distribution of cosΔ over the certain period was within ± 0.03 % around its mean (Fig. 4-13 (b)).
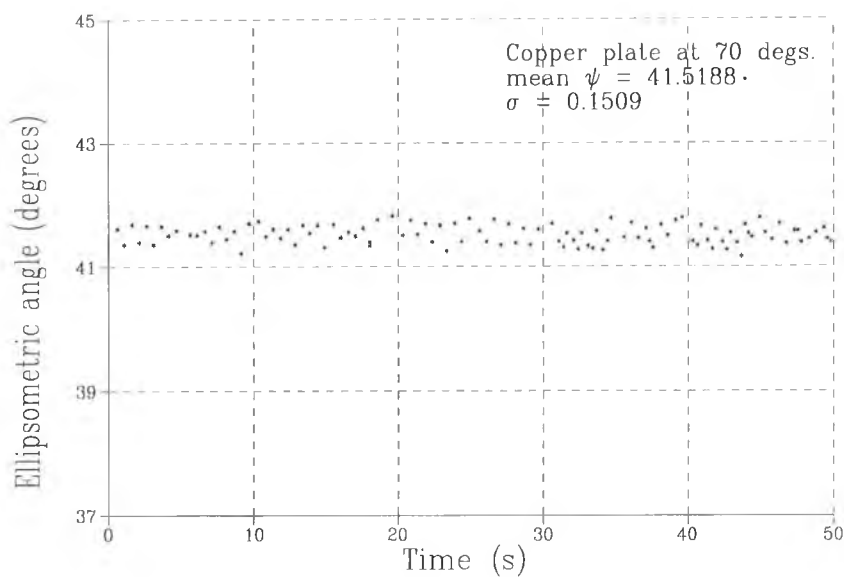
(a)
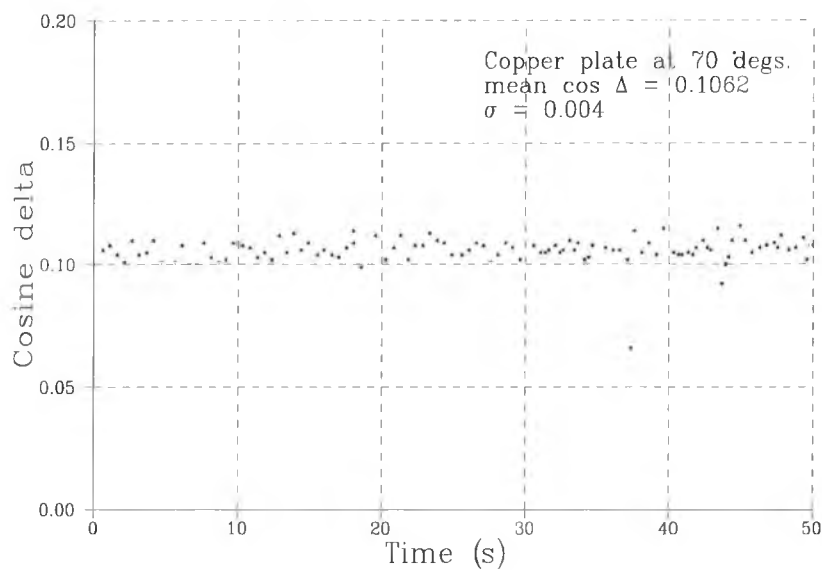
(b)

Figure 4-13 Experimental data on ψ (a) and $\cos \Delta$ (b) taken from the air/Copper plate interface during 50 s at λ = 632.8 nm, $N_{\text{Copper plate}}$ = 0.36 -i2.68. The angle of incidence is 70°.

The copper plate refractive index was calculated to be 0.36($\pm$0.02)-i2.68($\pm$ 0.02). A direct comparison between the copper refractive index measured here to the value from other sources is unable to do because the comparing index value is mostly

presented at different wavelengths, from the one used in this experiment, in the literature.

However, the value at the closet wavelength (λ = 650 nm) is given as 0.744 - i3.26 (Gray *et al*, 1957). Although the real terms of the index are rather different by comparison, imaginary parts from both sources certainly indicate high absorption property generally found in metallic samples.

4-6 Conclusions

The HiBi fibre polarisation modulation technique has been successfully applied to the ellipsometric measurement of different materials. The technique combining with the reflection from a sample under study and a fixed polarising prism orientated at an angle (45º) allows complete measurements of all the necessary ellipsometric information (ψ and Δ) to be taken and the required index of refraction to be evaluated, without any experimental adjustment during the operation.

Materials investigated under this novel ellipsometric approach were non-absorbing (BK7), low-absorbing (Si and ZnSe) and highly-absorbing (Cu). The experimental results showed that the instrument worked well in all cases. Nevertheless, an apparent difference in the absorption coefficient between the measured and typical values, in the case of low absorbing materials, causes a degree of concern about the sensitivity of the ellipsometer to that particular characteristic.

According to the results obtained and theory used, a small absorption coefficient corresponds to very small phase changes near 0º and 180º where the instrument is less sensitive. It has been demonstrated that an appropriate procedure to undertake is to improve this is by optically shifting these small phase changes away from that insensitive region. The process was simply accomplished by introducing a quarter-wave plate, with its optical axis parallel to the plane of incidence (into the detection arm) in front of the polarising prism. Physically the QWP will be placed in front of P3 of Fig. 4-3.

In addition, a test on the long term performance of the system was also conducted. The overall outcome from this examination showed that the concentration of measured data were within ± 2 % around a mean of the data.

For further applications, in the next Chapter, thin film materials will be investigated using this novel ellipsometric technique. This will reveal a prospect of the ellipsometric technique in thin film measurements and sensing applications.

CHAPTER 5
FIBRE OPTIC ELLIPSOMETRY FOR THIN FILM
MEASUREMENTS AND SENSOR APPLICATIONS

5-0 Introduction

A knowledge of the optical constants of dielectric materials in thin film form is necessary for predicting and understanding the performance of optical coatings incorporating these materials. A good practical use of this knowledge can be found in the design and fabrication technology of many optical components, which include optical filters, anti-reflection coatings and optical waveguides for integrated optics (Lukosz and Tienfenthaler, 1983).

It has been well known for many years that the determination of optical constants of thin films can be performed using the ellipsometric technique (Hall, 1969). Over this period of time, many different configurations of the technique have been proposed and implemented. No matter what arrangements are employed, they all have a common purpose of obtaining the two ellipsometric parameters, ψ and Δ, of the thin film under study. Unlike the previous case when the system under consideration was composed of two semi-infinite isotropic interfaces, this time the two parameters will be affected by the multiple reflections between ambient-film and film-substrate interfaces. From this point of view, the expressions for ψ and Δ are altered accordingly, but they can still be defined in terms of the Fresnel reflection coefficients for two principal component waves at the two interfaces and the optical thickness of the film. The full details of this are discussed in Appendix C.

An additional point being investigated here is the prospect of employing the ellipsometric system as a thin-film-based sensor. Normally, information measured by the system is simply related to fixed properties of the optical sample itself. However,

if the properties detected are known to be altered by some specific variables, such as the presence of a particular gas, the ellipsometric system can change its function to focus on sensing applications.

To demonstrate the capability of the proposed ellipsometric technique applied to thin film systems, a system of a single layer film (sol-gel) coated on a silicon (Si) substrate with different values of thickness was studied. The characterisation of the thin film systems was carried out in terms of the ellipsometric parameters (ψ and Δ). In addition, a comparison between experimental and reference results (obtained from a commercial instrument in conjunction with Appendix C) was also made for all samples used. Thus, the results obtained were then used to assess the suitability of the instrument to distinguish between different thin film thicknesses. Also, to show the potential of this fibre polarisation-modulated ellipsometer for application as a thin film sensor system, the device was used to monitor the change of the sol-gel thin film properties with time. Two particular environmental effects; heat and humidity, on the thin film characteristics were investigated.

5-1 Theoretical Background
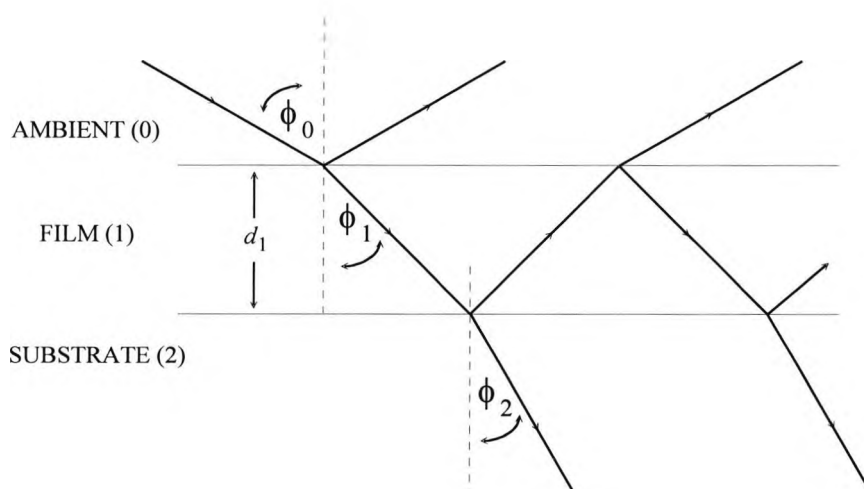
Figure 5-1 Oblique reflection and transmission of a plane wave by an ambient (0)-film(1)-substrate(2) system with parallel-plane boundaries.
d_1 is the film thickness. ϕ_0 is the angle of incidence in the ambient and
ϕ_1, ϕ_2 are the angles of transmission in the film and substrate, respectively.

The case of interest, showing light reflection by a substrate covered by a single film, is as shown in Fig. 5-1. The film of thickness d_1 has parallel plane boundaries and is sandwiched between semi-infinite ambient and substrate media. The ambient (medium 0), the film (medium 1) and substrate (medium 2) are all homogeneous and optically isotropic with refractive indices N_0, N_1 and N_2, respectively. Under normal circumstance, the medium of incidence and the film are transparent, (thus, N_0 and N_1 are real) while the substrate is absorbing and its complex index of refraction N_2 is given by n_2-ik_2, where n_2 and k_2 are an index of refraction and absorption coefficient of the substrate.

A plane wave incident on medium 1 (at an angle ϕ_0 in medium 0) will give rise to a resultant reflected wave in the same medium and to a resultant refracted wave (at the angle ϕ_2) in medium 2 (the substrate).

As can be seen from the figure, when the incident wave first meets the 0-1 interface, part of it is reflected in medium 0 and part is refracted in the film, as previously described in Sec. 4-2. Then, the refracted wave inside the film subsequently suffers multiple internal reflections at the 1-2 and 1-0 film boundary interfaces which are, in general, not perfectly reflecting. Thus, each time the multiply-reflected wave in the film strikes the 1-0 or the 1-2 interface, a component is refracted into the ambient or substrate medium, respectively. Here the main concern is the wave in the ambient medium.

If the Fresnel reflection coefficients at the 0-1 and 1-2 interfaces in the p and s directions are denoted r_{01p}, r_{12p}, r_{01s} and r_{12s}, respectively, the overall complex amplitude-reflection coefficients for light polarised in these two directions are given by (Azzam et al, 1975)

$$r_v = \frac{r_{01v} + r_{12v}e^{-i2\beta}}{1 + r_{01v}r_{12v}e^{-i2\beta}}$$

(5-1),

where v is taken to be p or s and β is the phase change that the multiply-reflected wave inside the film experiences as it transverses the film once from one boundary to the other (Hecht and Zajac, 1974).

In terms of the free space wavelength λ, the film thickness d_1, and the index of refraction N_1, the phase angle β (alternatively known as the film phase thickness) is given by

$$\beta = 2\pi\left(\frac{d_1}{\lambda}\right)\left(N_1^2 - N_0^2 \sin^2 \phi_0\right)^{\frac{1}{2}} \qquad (5\text{-}2).$$

The above expression is valid when the incident wave is linearly polarised either parallel (p) or perpendicular (s) to the plane of incidence.

However, the change in the polarisation state of polarised light reflected from a sample is still described in terms of the ellipsometric parameters ψ and Δ. With the same definitions for both ψ and Δ (Sec. 4-2), this time the two parameters of a given ambient-film-substrate are not only a function of the angle of incidence (as in the previous two isotropic interfaces system) but also the thickness of the thin film. Thus, for a chosen thin film system, a set of values of ψ and Δ found over a range of incidence angles will vary from one value of the film thickness to another. In addition, this also suggests that if there is any process that changes any of the optical variables in ψ and Δ, the ellipsometric technique may then be implemented as the basis of a sensing instrument.

Numerical methods are available to transform the ellipsometric parameters to values of thin film thickness and index of refraction (Kihara and Yokomori, 1992) but here, for simplicity, only the ellipsometric parameters are calculated and presented.

In order to obtain ψ and Δ from the system, similar procedures of R_p, R_s and Δ recovery as described in the system of two isotropic interfaces (Sec. 4-2) were performed. Once the experimental values of ψ and Δ have been found, they can be cross-checked with the corresponding reference ones (details discussed in Appendix C) provided that all the required parameters: N_0, N_1, N_2, d_1, ϕ_0 and λ are known.

5-2 Experiments

5-2-1 Procedures

Fig. 5-2 shows the, by now, familiar schematic diagram of the reflection ellipsometry. The rotating plane polarised beam generated by the HiBi fibre polarisation modulation system is incident on a thin film sample. The reflected beam then propagates through a polarising prism orientated at 45° to the plane of incidence and onto a photodetector. With the provision of a reference signal, the three required intensities, I_p, I_s and I_{45} can be found from the reflected signal allowing the determination of ellipsometric parameters ψ and Δ (c.f. Eqs (4-20), (4-21) and (4-22) - the same signal acquisition and processing).
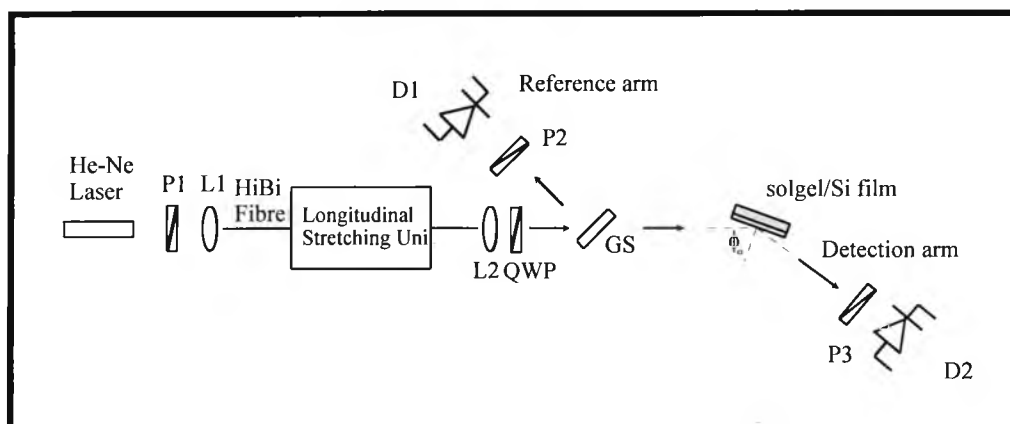
Figure 5-2 Illustration of a HiBi fibre polarisation modulation scheme for reflection ellipsometry.
Ps, Polarising Prisms; Ls, Lenses; QWP, Quarter-Wave Plate; GS, Glass Slide; Ds, Detectors.

Thus, the thin film can be characterised without mechanical movement of any optical components. Such a feature suggests the prospect of using the ellipsometric technique in real time applications, for instance a thin film growth monitoring device.

A suitable range of materials for initial studies were sol-gel thin films. Sol-gels are suitable for a number of applications such as anti-reflection coating and waveguides for integrated optics. In both cases, details of the refractive index and thickness of the thin film are important (Lukosz and Tienfenthaler, 1983).

5-2-2 Preparation of Thin Films

        The preparation process of the sol-gel thin film on a silicon substrate, using the dip-coating method, were performed by V Murphy and B D MacCraith, researchers at Dublin City University, Ireland. The solutions used are mixtures of SiO_2 and TiO_2 'Liquicoat' supplied by Merck. The procedures used by the researchers are as follows. Silicon substrates are withdrawn from the solution with constant velocity (typically, 60-100 mm/min). Dip coating is done at room temperature. The coated substrates are first dried at about 120°C for about 15 min to evaporate the more volatile components of the solution and subsequently are baked at a temperature of 500°C in flowing oxygen for 1 hour to obtain hard and resistant films. The refractive index of the film depends on the SiO_2:TiO_2 mixture ratio and the film thickness can be varied by changing the concentration of the mixtures or controlling the velocity of withdrawal of the substrate. Three similar films were produced and their refractive index and thickness recorded immediately after curing using a commercial Rudoff Auto El-III ellipsometer (again performed by the researchers at Dublin City University, Ireland).

5-2-3 Results and Discussions

        The samples were placed in the new fibre ellipsometer system for study. Results are presented for a range of angles of incidence from 10° to 80° in 10° steps.

        Fig. 5-3 illustrates ψ and Δ of the first sol-gel/Si film (A) as the angle of incidence is varied from 10° to 80°. The squares and stars indicate the measured values of the ellipsometric parameters ψ and Δ, respectively, and the solid curves represent the results of a theoretical calculation of the corresponding parameters assuming an ambient (air) index of 1.00, a sol-gel film index of 1.619, the original film thickness of 123.3 nm, the Si substrate index of 3.85 -i0.02 and λ = 623.8 nm. It should be noted that the numerical values of the thin film and substrate were derived from the commercial ellipsometer. These values were substituted into ψ and Δ expressions (Appendix C) to obtain theoretical results (i.e. values gained from a commercial ellipsometer).
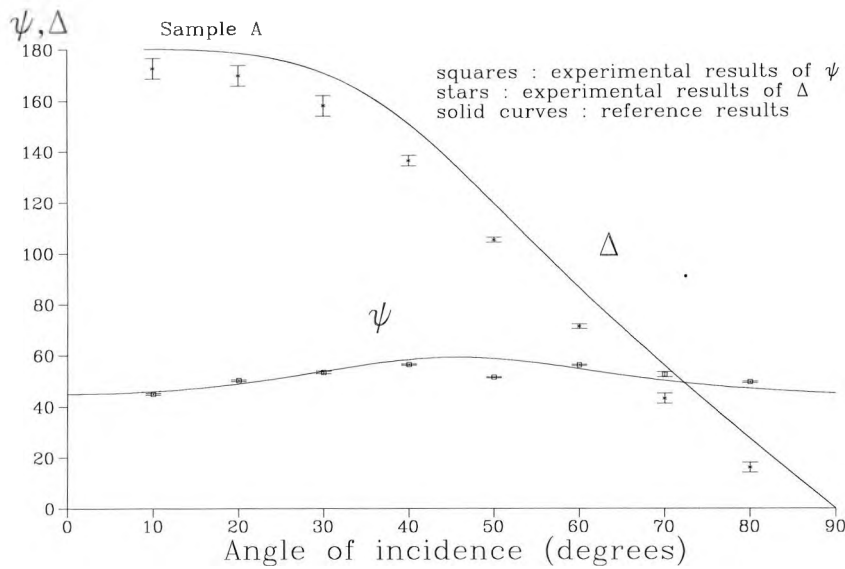
Figure 5-3 Illustration of ellipsometric parameters ψ and Δ as a function of angle of incidence for the air-solgel-Si system. Thin film thickness d_1 = 123.3 nm and refractive index n_1 = 1.619. ψ and Δ are in degrees. No errors are indicated on the reference curves, but it is noted that the typical accuracy of ψ and Δ from commercial apparatus is 0.01^o.

The figure reveals a relatively small scatter of the experimental points from the theory. This may arise since the properties of the film could have changed due to environmental effects such as temperature and humidity between the initial measurement of the thin film thickness and the measurements in this work. In addition, some systematic errors from optical elements used in the system, such as the imperfection of optical components, as well as noise (unavoidably obtained when detected signals are transformed from analogue to digital formats) are likely to contribute to the error in results observed (as analysed in Sec. 3-4-3).

It is worth pointing out at this point features of the behaviour of the Fresnel reflectances R_p and R_s. Clearly from Fig. 5-3, when the ellipsometric parameter ψ is less than 45° (seen here when angle of incidence is between 0° and 40°) R_p is less than R_s. But as the angle of incidence increases (from 40° onwards), ψ becomes larger than 45° and this corresponds to a situation when R_p is larger than R_s. This observation is in contrast to what is normally observed in the case of two semi-infinite isotropic interfaces (as presented in Chapter 4).

The data for the second sample (B) are shown in Fig. 5-4. All conditions of the system under investigation remained the same except the index of refraction and the thin film thickness. In this measurement, the index was given as 1.701 and the thickness was given to be 93.2 nm.
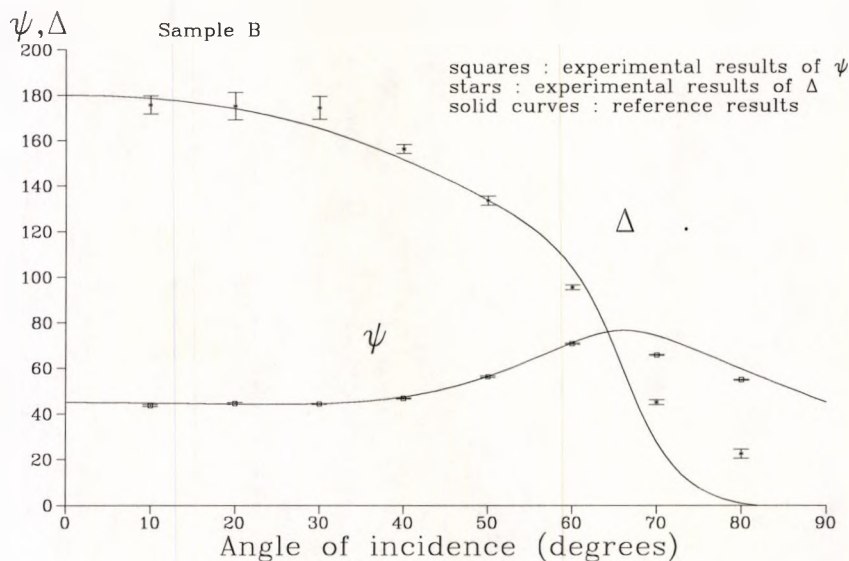
Figure 5-4 Illustration of ellipsometric parameters ψ and Δ as a function of angle of incidence for the air-solgel-Si system. Thin film thickness d_1 = 93.2 nm and refractive index n_1 = 1.701. ψ and Δ are in degrees. No errors are indicated on the reference curves, but it is noted that the typical accuracy of ψ and Δ from commercial apparatus is 0.01°.

In Fig. 5-4, the squares and stars represent experimental data of ψ and Δ, respectively, taken over the range of incidence angles. The solid curves show the theoretical values of the corresponding parameters, with the results also showing an agreement between experimental and theoretical results.

The data for the third sample (C) were obtained from a sol-gel thin film with a refractive index of 1.662 and a thickness of 147.1 nm. These are plotted in Fig. 5-5. Again, the squares and stars illustrate the experimental values of ψ and Δ, respectively, and the solid curves describe the theoretical values of the corresponding data. On this occasion the agreement between data and theory is very good. In this case, R_p is less than R_s for the complete range of incidence angles.
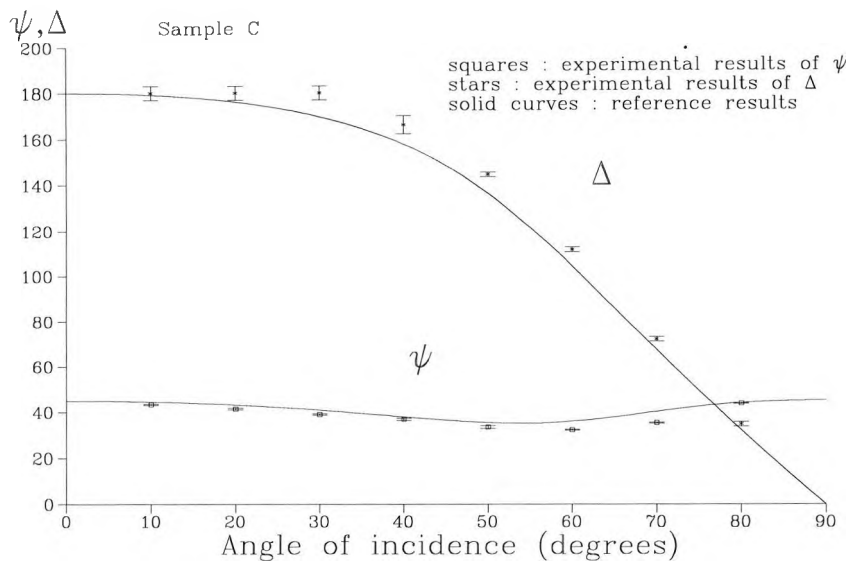
Figure 5-5 Illustration of ellipsometric parameters ψ and Δ as a function of angle of incidence for the air-solgel-Si system. Thin film thickness $d_1 = 147.1$ nm and refractive index $n_1 = 1.662$. ψ and Δ are in degrees. No errors are indicated on the reference curves, but it is noted that the typical accuracy of ψ and Δ from commercial apparatus is 0.01^o.

So far the polarisation modulated ellipsometer has been tested successfully on three different thicknesses of sol-gel thin film/Si substrates. However, there were still more studies to be performed as the history of the samples employed was not known, which may lead to an inconclusive interpretation in comparing results with theory because various effects such as temperature and humidity can affect the properties of the samples between the initial measurements of the thin film thickness (by the commercial ellipsometer at Dublin City University) and the measurements performed in the laboratory at the City University. This may explain some of the differences between experimental and theoretical results observed in Figs. 5-3, 5-4 and 5-5.

This speculation led to a simple experiment being carried out by leaving the sol-gel/Si film of the third sample exposed to the laboratory environment for a period of two weeks after taking the initial measurements of ψ and Δ. The measurement of the ellipsometric parameters was then repeated.
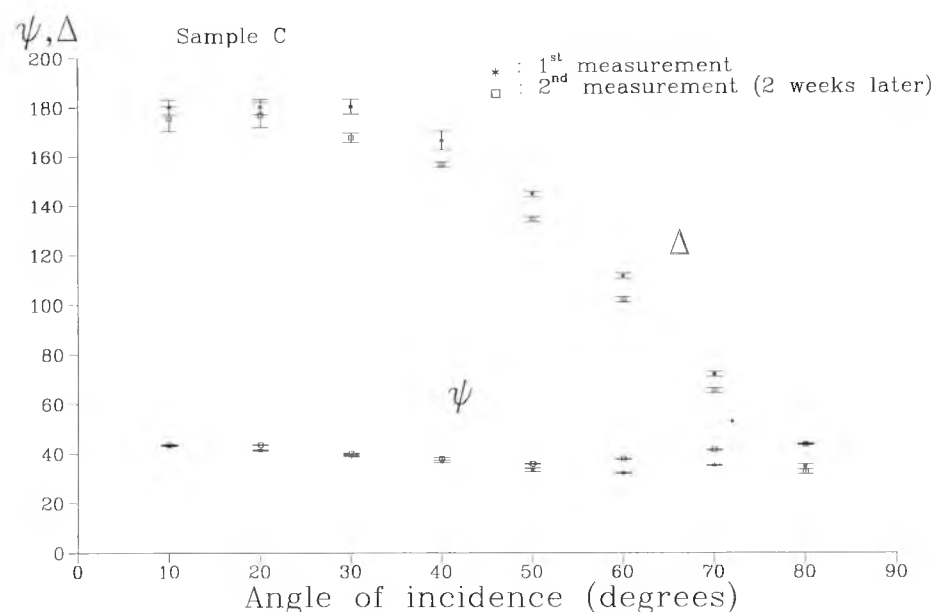
Figure 5-6 Comparison of ellipsometric parameters ψ and Δ as a function of angle of incidence for the air-solgel-Si system. Thin film thickness $d_1 = 147.1$ nm and refractive index $n_1 = 1.662$. ψ and Δ are in degrees.

Fig. 5-6 illustrates the two sets of data of both ψ and Δ of the sample, captured at an interval of two weeks. The stars indicate the first measurement of ψ and Δ and the squares show the results taken after two weeks. Clearly, a variation in the film characteristics over this period is reflected in these results, which certainly confirms the change in these properties of the samples with time, as expected.

For more performance studies of the system, eight more sol-gel thin film samples, again provided by Dublin City University, were characterised. This time, the sol-gel samples with eight different thicknesses were studied within a week of the samples being made in order to minimise the effects of environmental disturbances. In this set of samples, the mixture of SiO_2 and TiO_2 was controlled to give a SiO_2:TiO_2 ratio of 3:1 (the ratio was unknown for the first sample batch). This gave rise to similar refractive indices for all the samples under investigation. Nevertheless, the thickness was different for individual samples due to different coating speeds. Again, the commercial Rudoff Auto El-III ellipsometer was used to determine thickness and index of refraction, immediately after the films were produced. Even though the same

coating speed was used to pull a set of two samples, they do not have the same thicknesses. Variations of the bath surface, air currents and the swinging of the substrate while performing the dipping process can give rise to the thickness differences from one sample to the other (Phillips and Dodds, 1981).
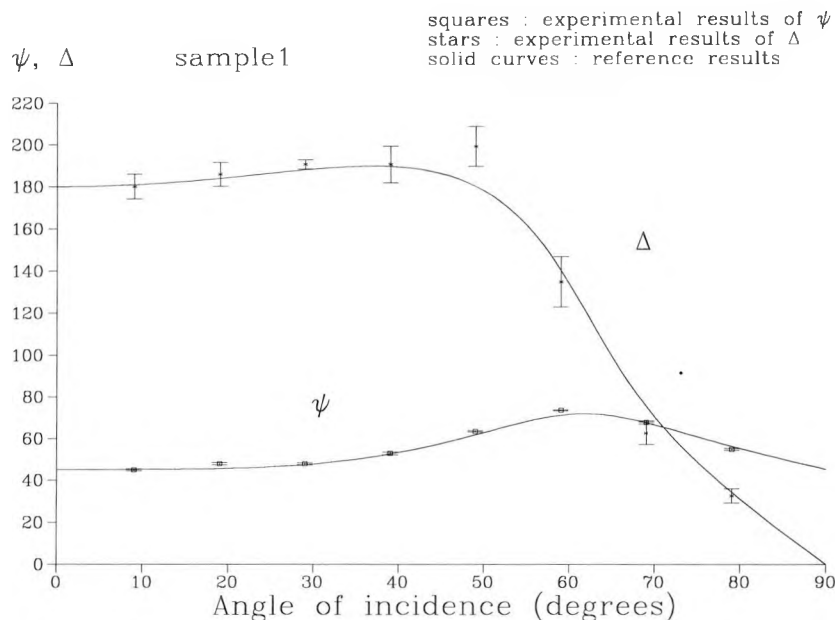
Figure 5-7 Illustration of ellipsometric parameters ψ and Δ as a function of angle of incidence for the air-solgel-Si system. Thin film thickness $d_1 = 119.6$ nm and refractive index $n_1 = 1.521$. ψ and Δ are in degrees. No errors are indicated on the reference curves, but it is noted that the typical accuracy of ψ and Δ from commercial apparatus is 0.01^o.

In Fig. 5-7, the results (ψ and Δ) obtained from the first sol-gel thin film sample with a refractive index of 1.521 and a thickness of 119.6 nm (an approximate coating speed of 0.49 mm/s) are shown. The squares and stars indicate the experimental values of ψ and Δ, respectively, and the solid curves show the theoretical results.

Next, experimental and theoretical ellipsometric parameters (ψ and Δ) of the second thin film sample with a refractive index of 1.520 and a thickness of 118.2 nm (with an approximate coating speed of 0.49 mm/s) are plotted in Fig. 5-8.
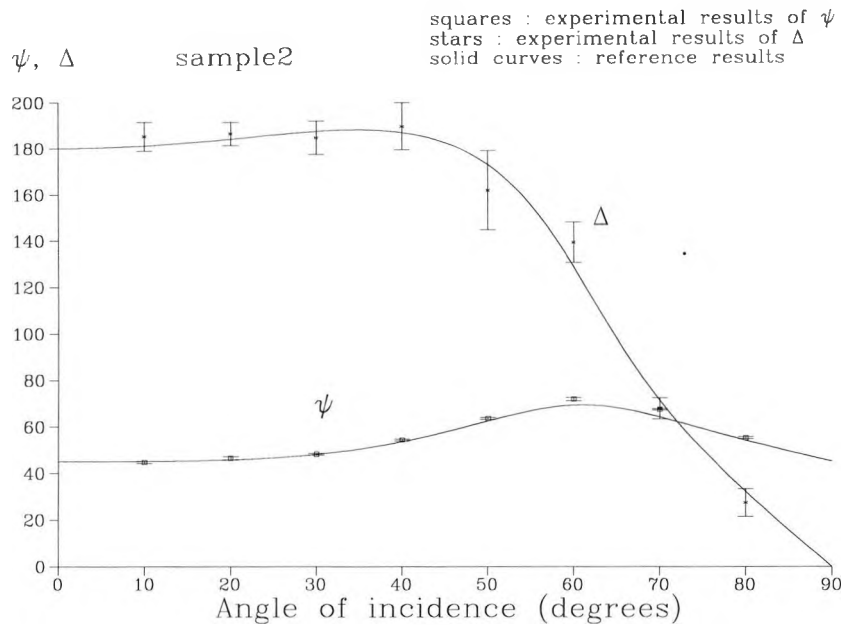
Figure 5-8 Illustration of ellipsometric parameters ψ and Δ as a function of angle of incidence for the air-solgel-Si system. Thin film thickness $d_1 = 118.2$ nm and refractive index $n_1 = 1.520$. ψ and Δ are in degrees. No errors are indicated on the reference curves, but it is noted that the typical accuracy of ψ and Δ from commercial apparatus is 0.01^o.

Note that the data trends from both figures (Figs. 5-7 and 5-8) are similar due to the small differences of thicknesses and refractive indices between the two samples.

The next two samples (samples 3 and 4) have the same index of refraction of 1.519. Sample 3 has a thickness of 142.8 nm and its ellipsometric parameters ψ and Δ (from experiment and theory) are shown in Fig. 5-9. The other sample (sample 4) has a slight different thickness (144.5 nm) and was also characterised in terms of ψ and Δ as shown in Fig. 5-10. These two samples were coated at an approximate speed of 0.798 mm/s.

As the coating speed increases, the thickness of the sol-gel thin film becomes thicker (the thickness is linearly related to the square root of the coating rate [Yodas, 1982]).

ψ, Δ sample3

squares : experimental results of ψ
stars : experimental results of Δ
solid curves : reference results
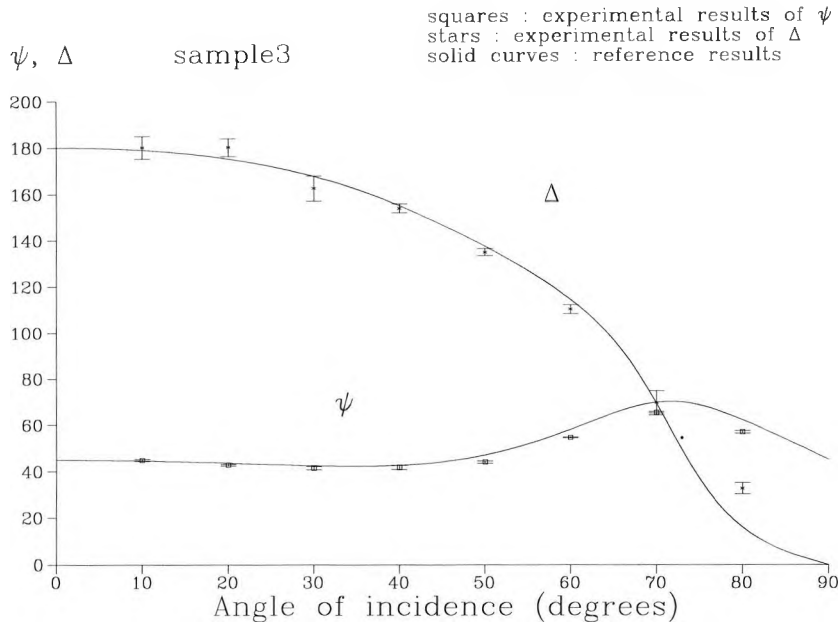
Figure 5-9 Illustration of ellipsometric parameters ψ and Δ as a function of angle of incidence for the air-solgel-Si system. Thin film thickness d_1 = 142.8 nm and refractive index n_1 = 1.519. ψ and Δ are in degrees. No errors are indicated on the reference curves, but it is noted that the typical accuracy of ψ and Δ from commercial apparatus is 0.01°.

ψ, Δ sample4

squares : experimental results of ψ
stars : experimental results of Δ
solid curves : reference results
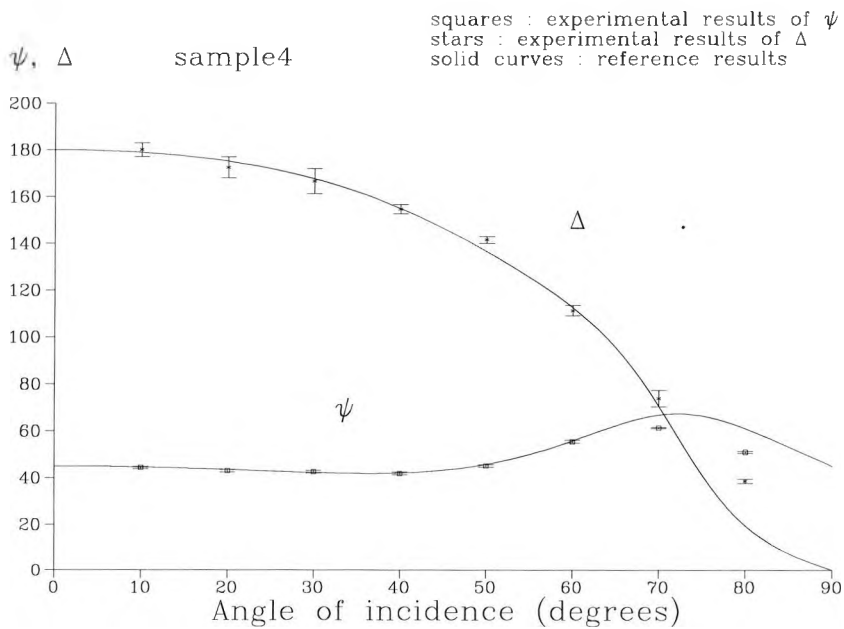
Figure 5-10 Illustration of ellipsometric parameters ψ and Δ as a function of angle of incidence for the air-solgel-Si system. Thin film thickness d_1 = 144.5 nm and refractive index n_1 = 1.519. ψ and Δ are in degrees. No errors are indicated on the reference curves, but it is noted that the typical accuracy of ψ and Δ from commercial apparatus is 0.01°.
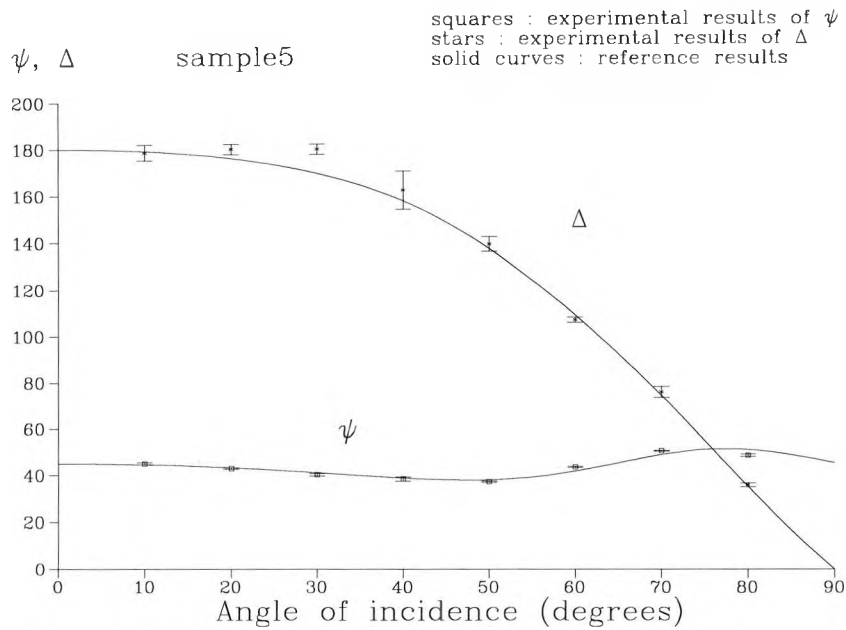
Figure 5-11 Illustration of ellipsometric parameters ψ and Δ as a function of angle of incidence for the air-solgel-Si system. Thin film thickness d_1 = 160.2 nm and refractive index n_1 = 1.571. ψ and Δ are in degrees. No errors are indicated on the reference curves, but it is noted that the typical accuracy of ψ and Δ from commercial apparatus is 0.01^o.
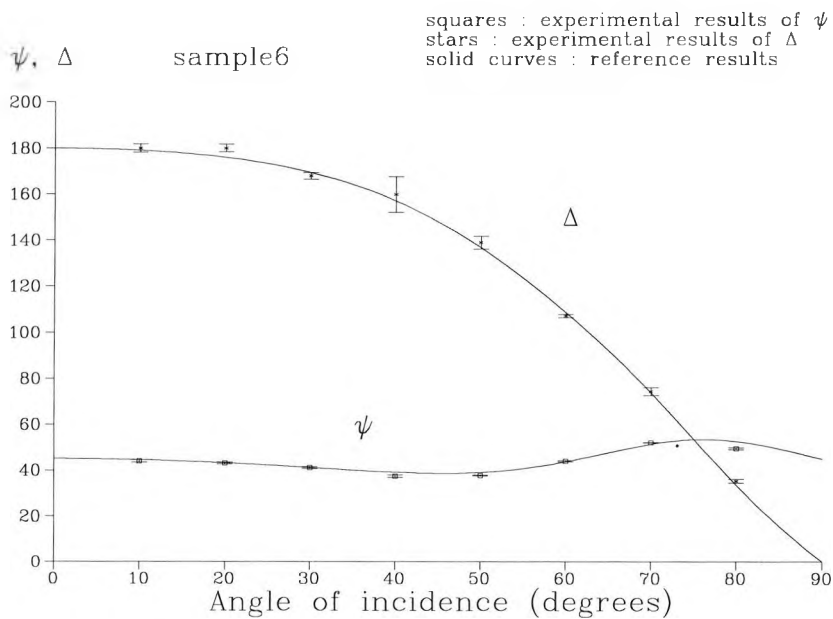
Figure 5-12 Illustration of ellipsometric parameters ψ and Δ as a function of angle of incidence for the air-solgel-Si system. Thin film thickness d_1 = 157.1 nm and refractive index n_1 = 1.517. ψ and Δ are in degrees. No errors are indicated on the reference curves, but it is noted that the typical accuracy of ψ and Δ from commercial apparatus is 0.01^o.

For the next two samples (samples 5 and 6), an approximate coating speed of 0.971 mm/s was applied. Sample 5 has a thickness of 160.2 nm and sample 6 has a thickness of 157.1 nm. Both of them have an index of refraction of 1.517.

The ellipsometric parameters ψ and Δ of the fifth sample are illustrated in Fig. 5-11 and the parameters of the sixth are shown in Fig. 5-12. The theoretical trend (solid curves) and experimental (squares, ψ, and stars, Δ) are indicated.
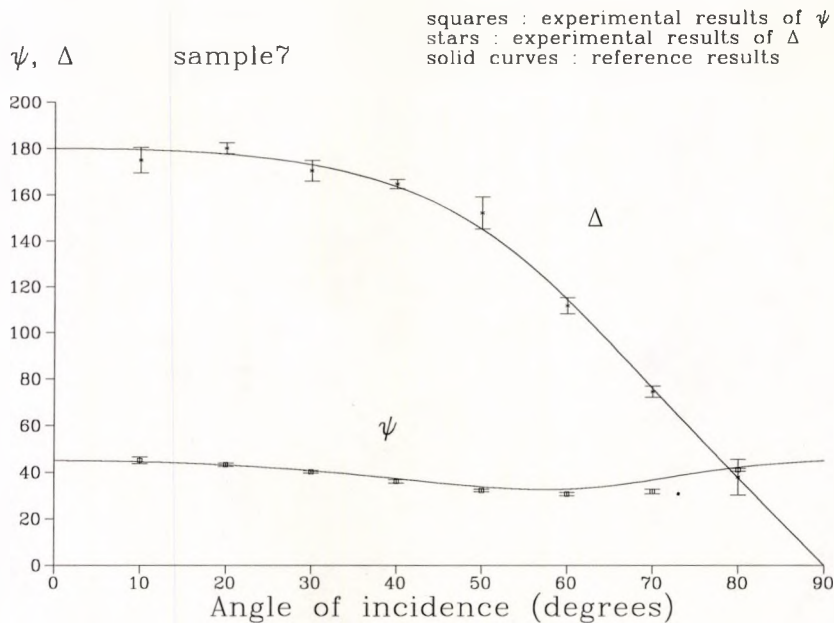
Figure 5-13 Illustration of ellipsometric parameters ψ and Δ as a function of angle of incidence for the air-solgel-Si system. Thin film thickness d_1 = 179.3 nm and refractive index n_1 = 1.515. ψ and Δ are in degrees. No errors are indicated on the reference curves, but it is noted that the typical accuracy of ψ and Δ from commercial apparatus is 0.01°.

For the final two sol-gel thin film samples (samples 7 and 8) with a similar refractive index of 1.515, an approximate coating speed of 1.235 mm/s was used. As a result, one of the samples (sample 7) has a thickness of 179.3. The characterisations of the sample 7 is presented in Fig. 5-13. The other sample (sample 8) has a thickness of 178.3 nm and has its characterisations illustrated in Fig. 5-14.

According to the results obtained from the newly produced sol-gel thin film samples, less scatter of the experimental results (when comparing to corresponded

theoretical results) was clearly observed. This could support the idea previously raised that there may be a change of sample properties with time. The new batch of samples were characterised within a week of their production and initial characterisations. In such a short period, minimal effect from the environment was expected.
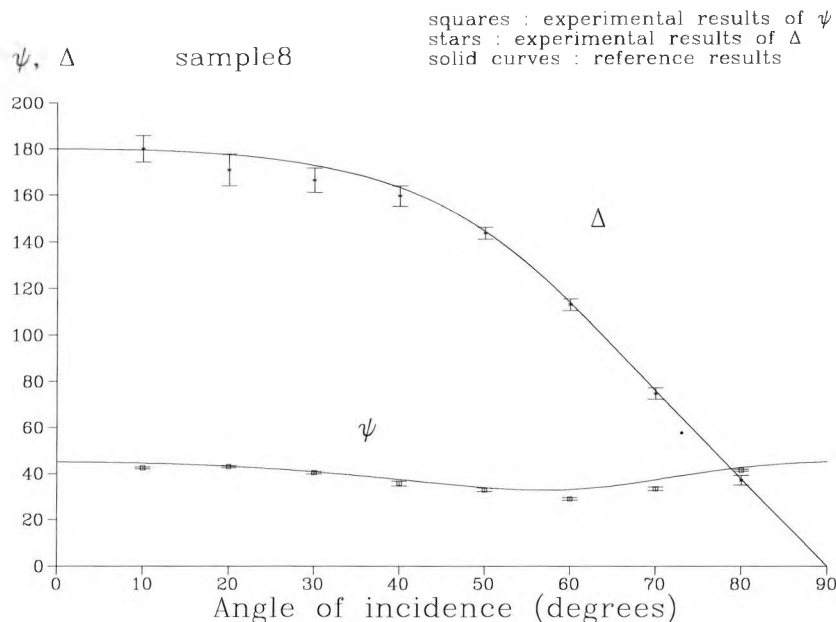
Figure 5-14 Illustration of ellipsometric parameters ψ and Δ as a function of angle of incidence for the air-solgel-Si system. Thin film thickness $d_1 = 178.3$ nm and refractive index $n_1 = 1.515$. ψ and Δ are in degrees. No errors are indicated on the reference curves, but it is noted that the typical accuracy of ψ and Δ from commercial apparatus is 0.01^o.

5-2-4 Sensing Applications

In this section, the prospect of the use of the polarisation modulated ellipsometer in sensing applications will be examined.

A further investigation of the device in relation to its sensing proficiency was prompted by the observation of the change in the sol-gel thin film characteristics (shown in Fig 5-6) as a particular sample had been left exposed to the laboratory environment for a period of time. However, the results did not provide evidence of clear behaviour of a particular effect; namely, of temperature and humidity on the

sample. Hence, in the next phase of the analysis, the humidity and temperature effects were examined explicitly on sol-gel samples from the second batch.

(a)

(b)
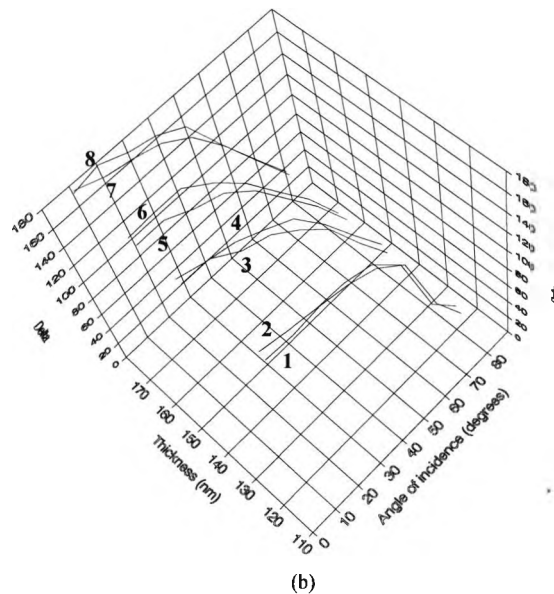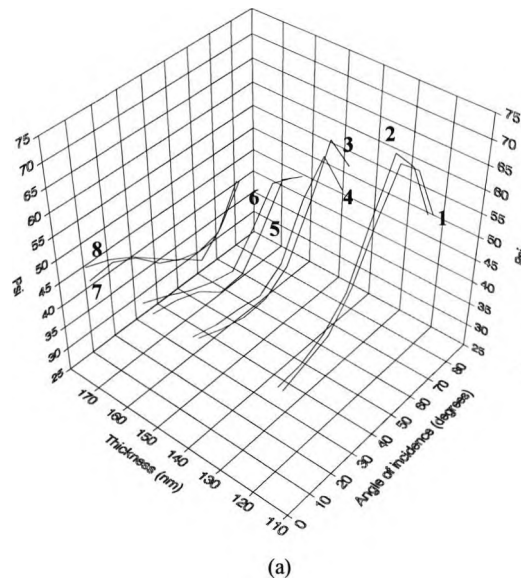
Figure 5-16 Illustrations of ellipsometric parameters ψ (a) and Δ (b) as functions of thickness and angle of incidence from all sol-gel thin film samples (new batch). Each curve has a number (1, 2, 3,..., or 8) indicating to which sample it belongs. Notice that, from 50° to 70° of angle of incidence in (a) and (b), as the thickness of a sol-gel thin film is changed, both ψ and Δ significantly alter.

The incidence angle used in subsequent experiments was chosen in the expectation of the influence of particular environmental effects; humidity or temperature, which may cause a change in a thin film thickness. As shown in Fig. 5-15, a range of incidence angles between 50°-70° is seen to be appropriate and offered the prospect of a sensitive response to the effects in terms of both ψ and Δ. This is indicated as the steep change of ψ (Fig. 5-15 (a)) and Δ (Fig. 5-15 (b)), as the thickness is changed.

First of all, the humidity effect on sol-gel samples was tested. This was carried out by placing a beaker of boiling water in close vicinity to a thin film sample under investigation. Precautions had been taken to avoid a significant temperature change and condensation around the sample since the phenomenon could mislead the sensor and the result be misinterpreted. The temperature was continuously monitored and the density of water vapour that could lead to condensation was continuously examined. Samples 4 and 7 were used. Fig. 5-16 indicates changes of ψ (a) and Δ (b) of the fourth sample during a 50 s period of investigation, at an incidence angle of 60°.

As these results represent the time evolution of ψ and Δ, no averaging was carried out as was the case in the previous results. The observed variation in the measured values is partly accounted for due to measurements corresponding to different directions of rotation.

To made a comparison, the sample was not exposed to the humid environment in the first 10 s. On exposure, alterations can be clearly seen in both ψ and Δ. The temperature of the humid atmosphere was measured to be approximately 35 °C. The change (in ψ and Δ) was observed to be irreversible as time went by. A possible reaction that could be occurring is that water molecules from the vapour may enter into the pores of the thin films (Ritter, 1969). This reaction may then give rise to alterations in both the thickness and index of refraction of the samples. Consequently, a change in ψ and Δ was observed. For the other sample at an incidence angle of 70° (sample 7) (Fig. 5-17), no change can be discerned in ψ (a) and Δ (b). One possible

explanation at this stage is that only a specific thin film fabrication method can show a clear response to the humidity.
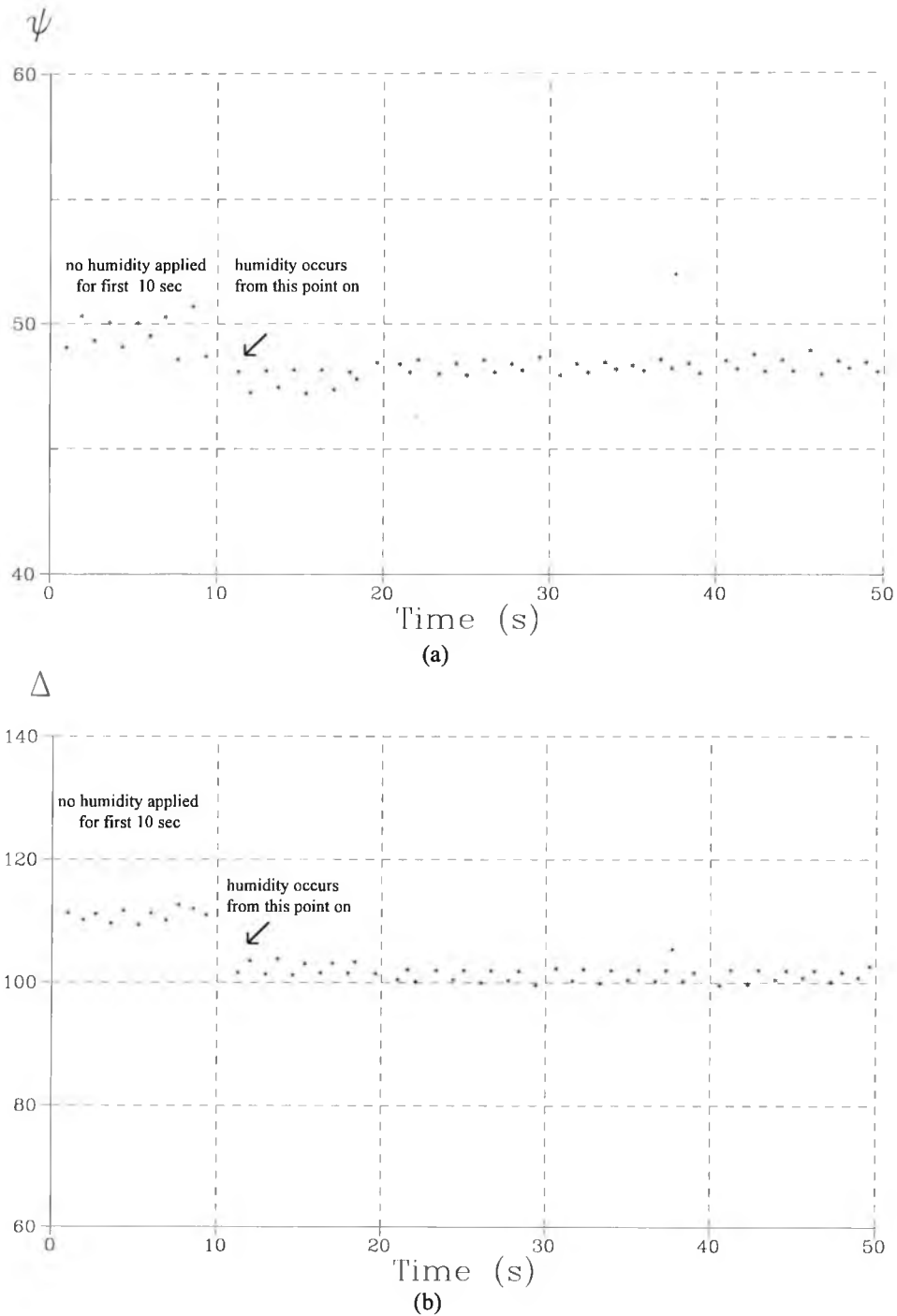
Figure 5-16 Illustrations of variation in ellipsometric parameters ψ (a) and Δ (b) as a function of humidity over a period of 50 s for sample 4. ψ and Δ are in degrees (an air-solgel-Si system at λ = 632.8 nm, the film refractive index = 1.519 and the film thickness d_1 = 144.5 nm). The angle of incidence is 60°.

(a)

(b)
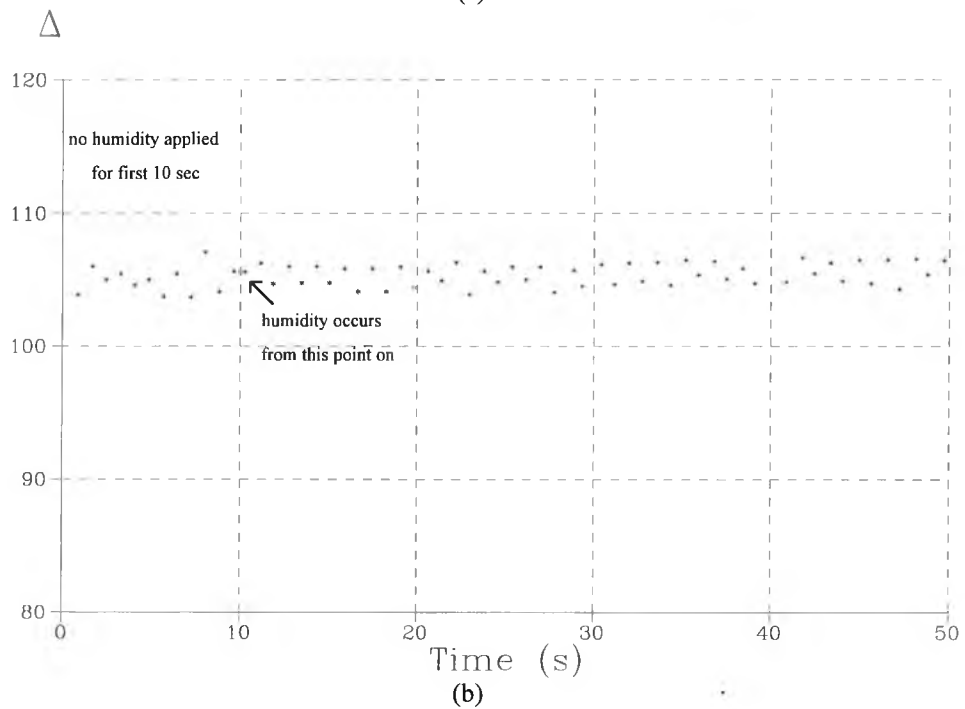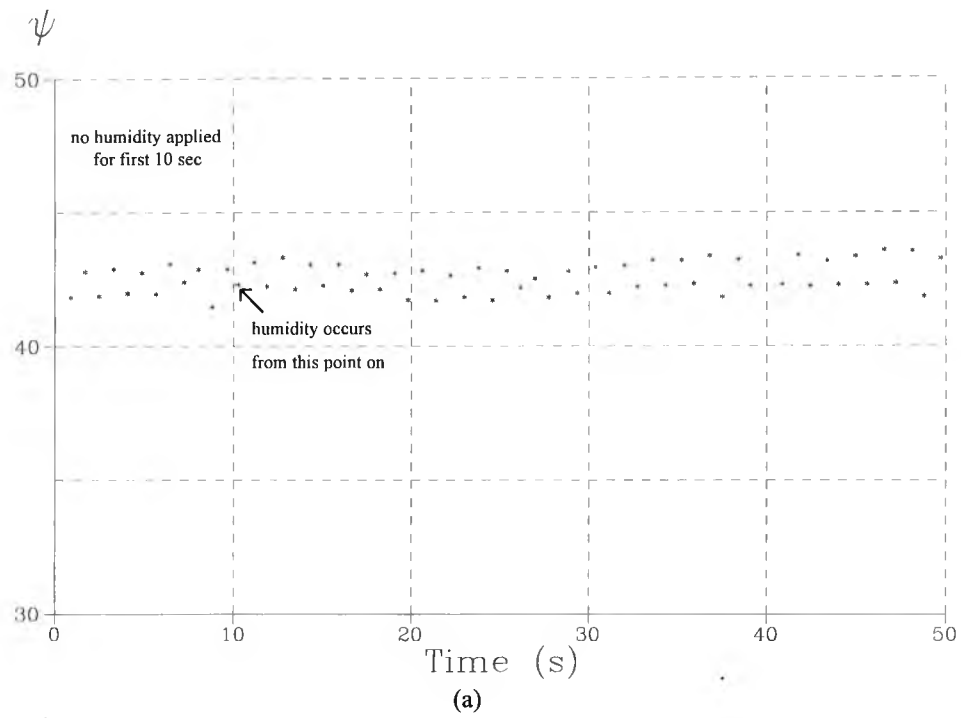
Figure 5-17 Illustrations of variation in ellipsometric parameters ψ (a) and Δ (b) as a function of humidity over a period of 50 s for sample 7. ψ and Δ are in degrees (an air-solgel-Si system at λ = 632.8 nm, the film refractive index = 1.515 and the film thickness d_1 = 179.3 nm). The angle of incidence is 60°.

ψ

no temperature
changes for first
5 sec

temperature sharply
increases

temperature maintains
at a maximum value
of 90C

Time (s)

(a)

Δ

no temperature
changes for first
5 sec

temperature sharply
increases

temperature maintains
at a maximum value of
90C

Time (s)
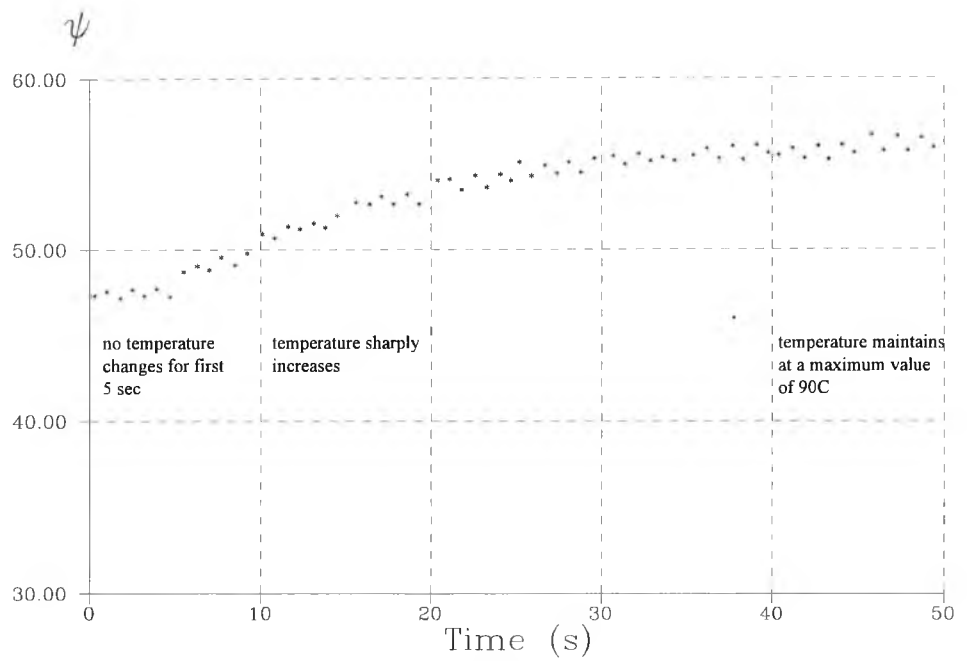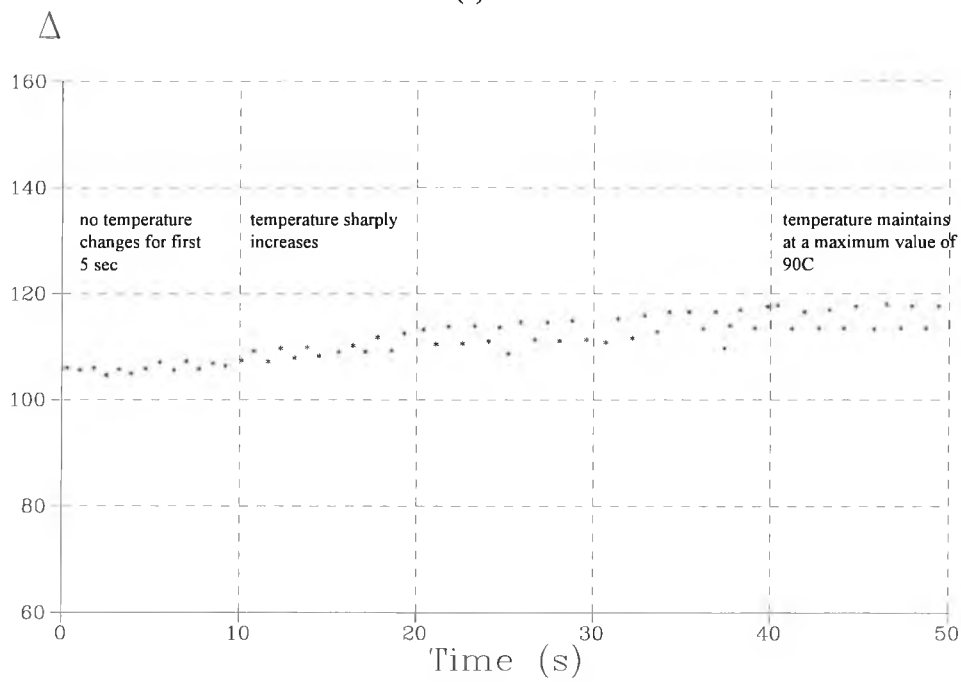
(b)

Figure 5-18 Illustrations of variation in ellipsometric parameters ψ (a) and Δ (b) as a function of temperature over a period of 50 s for sample 6. ψ and Δ are in degrees (an air-solgel-Si system at λ = 632.8 nm, the film refractive index = 1.517 and the film thickness d_1 = 157.1 nm). The angle of incidence is 60°.

(a)

(b)
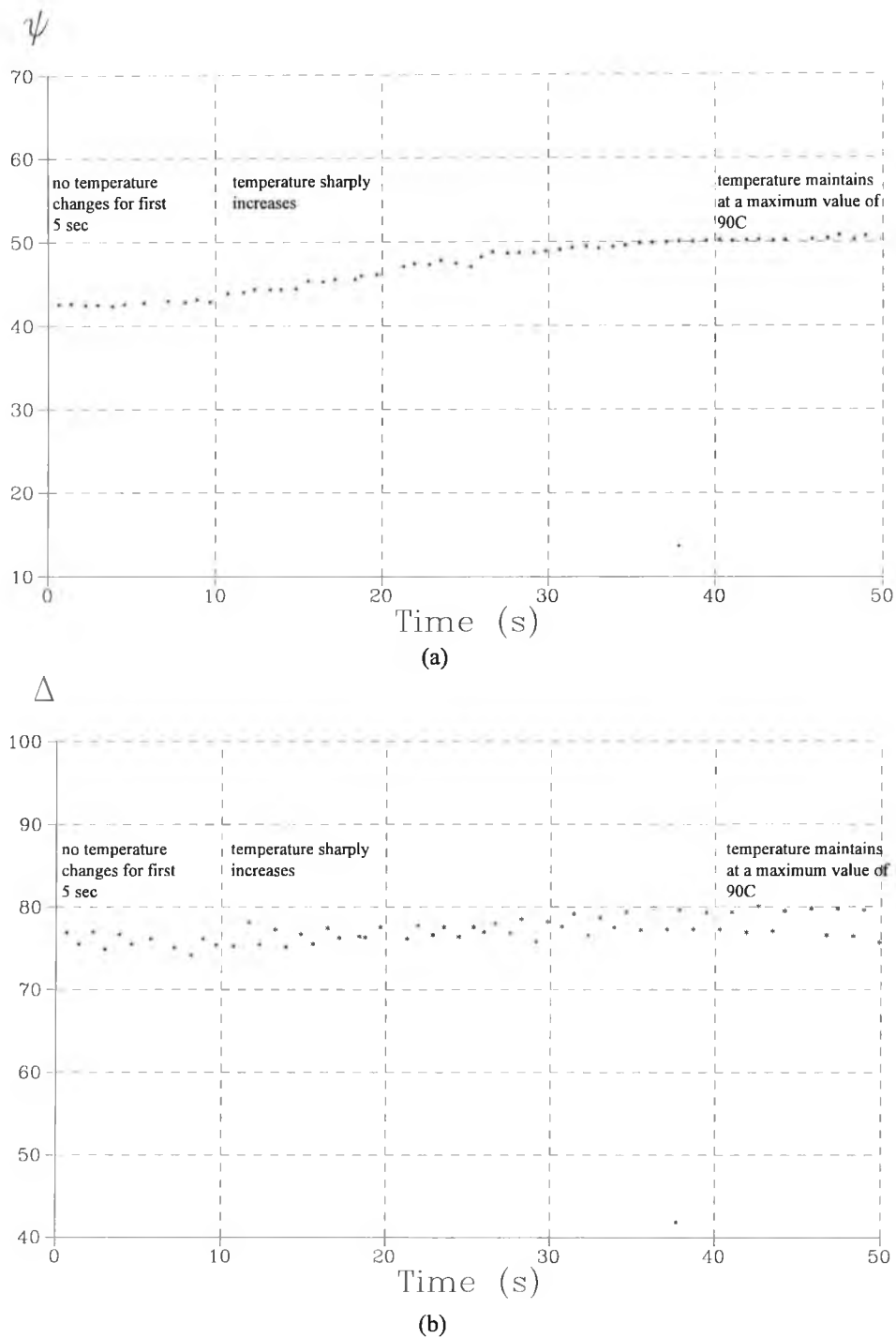
Figure 5-19 Illustrations of variation in ellipsometric parameters ψ (a) and Δ (b) as a function of temperature over a period of 50 s for sample 7. ψ and Δ are in degrees (an air-solgel-Si system at λ = 632.8 nm, the film refractive index = 1.515 and the film thickness d_1 = 179.3 nm). The angle of incidence is 70º.

Secondly, the effect of heat on the film was studied. A hot air blower was used to produce a rise in temperature at the sol-gel sample. The hot air blower was placed ≈ 15 cm from the sample. The heat generated by the blower could increase the sample temperature up to 90 $^{\circ}$C. The experiments were carried out with the sample 6 and 7 at an angle of incidence of 60° and 70°, respectively.

Fig. 5-18 shows changes of ellipsometric parameters ψ (a) and Δ (b) for sample 6 as the temperature increased over a time period of 50 s. The heat was applied after 5 s of the investigation (indicated in the figure). The graphs show clear increase with temperature during 5 to 30 s. After that the values of the ellipsometric parameters ψ and Δ remained constant as the temperature reached the maximum value at 90 $^{\circ}$C.

Similar trends can be seen from Fig. 5-19 showing ψ (a) and Δ (b) obtained from sample 7. From the experiments, the observed change is more significant in the case of ψ rather than Δ. This observation cannot readily be exploited in temperature measurement applications as the process is not reversible. In other words, such a high temperature in some ways altered the sample properties permanently.

From the results obtained in both experiments, the sol-gel thin film employed showed more susceptibly to temperature effects than humidity. However, the results still indicated no immediate application as a temperature sensor for this instrument, due to the irreversibility of the effect. However, it should be noted that the method used showed a real prospect for a sensing application as change could be detected.

Ultimately, the main application of such method in sensing will be in their use for optical chemical sensing. Temperature and humidity will have to be eliminated and the results shown indicate some problems may occur. Sol-gels have been used as media to contain chemically sensitive materials, e.g. pH and oxygen sensing dyes (Badini *et al*, 1989 and Ding *et al*, 1991). The changes that occur due to the effects of these chemicals could be sensed using the ellipsometer, but it could appear that a relatively constant temperature and humidity is necessary. This aspect is the subject of further study at City University on pH sensitivity materials.

5-3 Conclusions

A novel reflection ellipsometer employing the proposed HiBi fibre polarisation modulation technique has been further applied to the study of ambient-film-substrate systems. Firstly, the investigation concentrated on monitoring thin film systems of different thicknesses. The results obtained from each sample, presented in terms of ψ and Δ, were satisfactory in their agreement with results from a commercial ellipsometer and distinguishable. It is to be noted that, to the best of the author's knowledge, these results, characterising the thin films, are the first-ever obtained using an optical fibre-based ellipsometer.

As observed from the experiments, Δ was considered to be more sensitive to the film thickness because each sample was more recognisable by the distinctive trace of this parameter. However, this still implied that the ellipsometric technique possessed a good enough capability to characterise the thin film-substrate system.

Secondly, it should be noted that the differences between the experimental and reference results from the systems were slight. This suggests that some factors, such as the environmental effects imposed on the thin film, systematic errors from optical components involved and noise (e.g. when transforming the signals from analogue to digital forms), could contribute to the results obtained. The response of the system to its environmental effects formed the basis for the study of the potential of the ellipsometric scheme as a thin film based sensing device. Investigations of particular environmental effects; namely humidity and temperature, on sol-gel thin film samples were performed. Reactions between the humid atmospheric environment and chosen films were recorded in terms of ψ and Δ over a 50 s period. The results reveal that not all thin films exhibit sensitivity to humidity. One of the samples did show sensitivity suggesting the effect is highly dependent on the individual sample. This gives some hopes that chemically-sensitive thin films with no sensitivity to humidity could be produced routinely. A closer study of the differences in fabrication method is needed to ensure that these favourable conditions can be reproduced. The change of temperature was easily-detected using thin film samples during monitoring of the

optical characteristics ψ and Δ over a similar time period. Although the processes observed from both cases were irreversible, the overall results were still highly encouraging. This confirmed the prospect of employing the optical fibre polarisation modulated ellipsometer as a sensing device, if appropriate samples are available and clearly indicated further work is needed to optimise the sensitivities required and minimise those which are undesirable.

In addition, this polarisation modulated ellipsometer allows a simple modification of the system operating speed by means of using a suitably fast modulation method such as a longitudinal PZT stretching. This then can increase the monitoring speed of the system to match any quick change of the sol-gel thin film properties in a reaction, such as would be obtained for rapid chemical sensing purposes.

In conclusion, the prospects for the application of the new ellipsometric technique in thin film characterisation and sensor applications, utilising chemical sensitive thin films designed to be chemically sensitive (e.g. solgel-substrate coating for gas sensors [MacCraith, 1993]), appears a realistic proposal, albeit one which requires considerable further work on samples and their characterisations.

In the next Chapter, an overall conclusion of this study will be discussed. Also further work in this research theme will be suggested.

CHAPTER 6
CONCLUSION

<u>6-0 Summary</u>

All the objectives set at the beginning of the study were successfully achieved. The results obtained were satisfactory and provide encouragement for further applications of the technique in a practical measurement system. The following describes the summary of this research.

(i) Linear polarisation modulation techniques were investigated. The historical evolution and development were presented in two categories according to the light propagation medium, these two groups being free-space and optical fibre polarisation modulation systems. Following detailed consideration, two promising configurations; free-space and optical fibre polarisation modulation, were chosen as being expected to offer potentially the best performance. One of the notable features was the employment of a simple and non-mechanical modulation method which allowed a potentially high operating speed. A detailed study was carried out both theoretically and experimentally, on each of the arrangements.

For the theoretical point of view, Jones vectors were used to analyse the proposed schemes and predict what could be derived from the polarisation modulation systems. However, when the system investigation turned to the practical aspects, an alternative description, using Stokes vectors, was used. This was because of their convenience for simple direct measurement and easy transformation to describe the output polarisation state. The practical performances of both techniques were characterised in terms of the output degree of polarisation (DOP) and ellipticity.

(ii) For the theoretical study using Jones vectors, both modulation technique were demonstrated to offer similar potential in generating controllable linear polarisation states. Nevertheless, the experimental analysis obtained from the Stokes parameter measurements showed otherwise. The measured degree of polarisation and ellipticity (used as criteria of system quality) of the output beam revealed that the optical fibre scheme had better performance and was, therefore, most appropriate for polarisation-sensitive applications such as ellipsometry. Furthermore, the fibre optic scheme also appeared to be the better choice in terms of simplicity and ease of alignment over the free space one.

(iii) Further analyses on the chosen scheme were carried out so as to improve the quality of the system output, in terms of the rotating plane polarised light. Quantitative investigations into the performance of the fibre based system were extensively performed. Important performance-relating aspects; namely, the properties of the HiBi fibre used, the modulation method employed and optical components involved, were thoroughly examined and then appropriately improved. As a result, a higher quality output beam from the polarisation modulation system was satisfactorily obtained. The asymmetry effect: the difference between the intensity ratio, between the different orientational direction of linear polarisation is found to significantly reduced from 10-20% to 1-2%.

The improvements included

- using the HiBi fibre with end faces polished at an angle to reduce interference to the main beam from back reflections usually introduced by plane cut end faces,

- utilising a longitudinal fibre stretching method to modulate the light in order to avoid mode coupling inside the fibre which occurs when the fibre is wrapped around a cylindrical PZT, and,

- employing a high quality quartz quarter-wave plate (i.e. the retardation tolerance of $\lambda/500$) at the output end of the polarisation modulation system to reduce the output ellipticity.

The overall achievements of the optical fibre polarisation modulation technique for ellipsometric measurements are summarised in Table 6-1 against the system initial targets and commercial features.

Features	Commercial ellipsometers*	Proposed Spcifications	Achieved Specifications	Comments
1)period of measurement	1-10s	10^{-3}s	10^{-1}s	The measuring time may be decreased to 10^{-3}s with a high speed modulation technique such as PZT.
2)accuracy of ellipsometric parameters (ψ and Δ)	ψ: 0.002°-0.015° Δ: 0.004°-0.08°	ψ: 0.01° Δ: 0.01°	ψ: 0.02° Δ: 0.02°	This accuracy depends on a suitable angle of incidence chosen for characterising each material. The values quoted as 'achieved' are values indicated the average accuracy over all measurements carried out.

3)extinction ratio	10^{-8}-10^{-6}	10^{-4}	10^{-2}	This can be further decreased if optical fibre and polariser extinction ratios, QWP specifications and mount precision are higher.
4)mount precision	0.01^{o}	0.1^{o}	0.5^{o}	This is a limit from mounts employed in this study. It can be improved.
5)mechanical movement	main feature	none	none	A significant achievement obtained from the optical fibre based configuration.
6)software and D/A converter resolution	specially written for specific ellipso-meters and no mention of the resolution used	turbo-Pascal based programme and 8-bit resolution converter	turbo-Pascal based programme and 8-bit resol-ution converter	The execution time may be improved upon by further consider-ation of programme design and pro-gramming language. Error in conversion would be reduced if a higher bit resol-ution converter is used.

Table 6-1 Summary of specifications achieved in this study comparing to the commercial features and performance target expected

*Data represents typical values achievable using either the ELX-1 Precision Ellipsometer (LOT-Oriel Ltd., UK) or Variable Angle Spectroscope Ellipsometer (JA Woollam Co., USA).

(iv) The HiBi fibre polarisation modulation technique was then successfully applied to ellipsometric measurements. At the first stage, the implementation of the technique was performed on two semi-infinite isotropic media which were interfaces between air/BK7, Si, ZnSe or Cu. Several types of media were used to assess the sensitivity to absorption characteristic of the ellipsometric system. The results obtained were presented in terms of ellipsometric parameters ψ and Δ. In addition, the index of refraction corresponding to each sample was calculated from the parameters measured. The experimental results showed that the instrument worked well for the chosen systems studied. However, in the case of low-absorbing materials (Si and ZnSe), the introduction of a wave plate has been shown necessary for improved sensitivity.

The measurements were also conducted over a long time period. The ellipsometry performance was monitored and determined through the ellipsometric measurements of the same samples. The final result (as discussed in Sec. 4-5) from this examination showed that the measured data were within 2% of the mean value of the ellipsometric data.

(v) A further application of the HiBi fibre polarisation modulated ellipsometer was performed. In this investigation, an ambient-thin film-substrate system which was composed of a sol-gel thin film coated on a Si substrate was studied. The samples with different thicknesses were characterised in terms of the customary ellipsometric parameters ψ and Δ. The results were satisfactorily obtained, and clearly distinguishable data from each thin film thickness value was observed. This obviously indicated that this particular ellipsometric technique was capable of studying optical thin film systems. The differential of results between different thicknesses indicated that with

this value of refractive index and thickness changes of 5 nm could be monitored. It is to be noted that, to the best of the author's knowledge, these results, characterising the thin films, are the first-ever obtained using an optical fibre-based ellipsometer. Furthermore, a particular study on the prospect of the ellipsometer working as a thin film based sensing instrument was carried out. This was examined by monitoring the change of the thin film properties with environmental effects, i.e. temperature and humidity, over a period of 50 s. As expected, the ellipsometric scheme demonstrated its extended utility as a sensing device, providing promising results (measured in terms of the ellipsometric parameters) on the occurrence of changing properties of a sol-gel film. As a result, the application range of the ellipsometric system becomes even broader and highlights the need for further work in this area.

6-1 Suggestions for Further Work

Although, the current HiBi fibre polarisation modulated ellipsometer has showed promising performance, there are still some system features which can be modified for even better performance. These are suggested as follows.

(i) It is a fact that the measurement speed can be controlled via the modulation frequency and tailored for individual applications. This suggests that if a high speed operation, such as in the case of thin film growth monitoring or chemical reaction detections, is required, the modification can simply be done by replacing the low operating frequency fibre stretcher with a high frequency piezoelectric transducer. Typically, the replacement could bring the frequency of modulation up to the region of kHz or greater. In other words, a complete characterisation of the monitored surface can be obtained in a repetitive time slot of 10^{-3} s or less. Such an advantage is unlikely to be achieved in a mechanically-based ellipsometer.

(ii) In this study, a polished angle to be used at the end faces of the fibre was proposed to be greater than 5°. However, this may not provide an optimum operation for the polarisation modulation system. Therefore, it might be interesting to apply waveguide theory to optimise the polished angle for the HiBi fibre to gain the optimum system performance.

(iii) The adjustment of polarising elements involved in the polarisation modulation technique is not accurate, as found in this study (Sec. 3-4-3-1), and any error introduced in this way can inevitably affect the subsequent ellipsometric measurements. However, the degree of the error can be alleviated if a high-precision method of azimuthal alignments is applied. Such a method proposed has been recently by Monin *et al* (1994) could be implemented. The arrangement involves a nulling method and does not require any phase compensator (neither quarter-wave plate nor Babinet-Solei), which often introduces important errors in ellipsometry.

(iv) Although, the proposed HiBi fibre polarisation modulated ellipsometer offers considerable advantages over the conventional devices in terms of size, cost-effectiveness and speed, the system proposed here is still a hybrid arrangement made up of optical fibres and some conventional components such as objective lenses and a quarter-wave plate. The system could be even more attractive if it really can be arranged as an all-fibre system. It is understandable that the all-fibre structure would provide substantial advantages of mechanical stability and miniaturisation to the ellipsometry. There are some modifications that can be achieved with the current optical fibre technology. For instance, direct coupling from a light source to HiBi fibre may be successfully performed by using pigtail style power source couplers commercially available from OZ optics Ltd. Since the pigtails normally only allow the power to couple into one eigenmode, this piece of fibre has to be spliced with the other piece of HiBi fibre at an orientation of 45° relative to each other in order to satisfy the coupling

condition required in this study. In addition, at the output end of the ellipsometer, the quarter-wave plate could be substituted by a piece of HiBi fibre with a constant phase bias of $\pi/2$ as proposed by Tatam *et al* (1987). However, to reduce thermal effects that could impose a drift in phase, a specially designed elliptical core polarisation maintaining fibre studied by Wong and Poole (1993) would be a good selection.

(v) Finally, the results from the sensing tests, under environmental factors, i.e. temperature and humidity, by the novel ellipsometer using sol-gel thin films as sensing materials indicated highly dependent sensitivity of the instrument on the individual sol-gel sample. This means that appropriate care must be taken if the ellipsometer is to be implemented in particular sensing applications, such as chemical sensing. This is because the inconsistency of temperature and humidity may give rise to an inaccuracy of the instrument. Therefore, a closer study on sensing materials in terms of their fabrications, characteristics and responses to undesired factors, is needed to ensure that only the specific sensitivity required is exclusively obtained. When this stage of study is satisfactorily completed, an interesting aspect of the system - the ellipsometer incorporating chemically sensitive materials - should be tested with specific substances such as a particular gas or a family of gases. In this way, such a sensing status of the ellipsometric system can be additionally confirmed.

APPENDIX A
SIGNAL PROCESSING TECHNIQUES

In this Appendix, signal processing techniques are discussed as they are one of the most important procedures repeatedly employed wherever data acquisition, e.g. I_s, I_p and I_{45}, is required in this study. In general, the signal processing starts from the conversion of the incident light into electrically analogue signals by photodetectors (at both reference and detection arms). The signals then are transformed into digital form by an analogue-to-digital (A/D) converter, in order to be analysed by an on-line computer.

It is true that the signal at the detection arm provides all the desired information for analyses of interest such as an investigation of an output beam quality shown in Chapter 2. However, the information required, such as the index of refraction and the absorption coefficient of an optical sample, is entirely polarisation orientation-related, as the intensities parallel (I_p) and perpendicular (I_s) to a reference direction are required. In order to identify accurately, the orientation of the output beam under study, a reference signal has to be provided to define the polarisation direction. The importance of this has been shown when the system was used in several specific applications (Chapters 4 and 5).

As the light beam used in this configuration is a rotating polarised beam in which its azimuth depends upon the modulation signal, the use of the provided reference signal, defined by an orientation of the transmission axis of the reference polariser, allows the orientation of the rotating polarised beam to be identified. If the rotating polarisation is parallel to the transmission axis of the reference polariser, a maximum intensity is obtained i.e. a peak represents parallel polarisation (I_p); whereas a minimum intensity (a trough) corresponds to perpendicular polarisation (I_s).

To analyse the process, at the reference arm, the rotating plane polarised beam, given by Eq. (2-17), is reflected from a glass slide and propagates through a prealigned polariser parallel to the reference direction. Suppose, the reference direction is parallel to the incidence plane of the glass slide. The reflected electric field, $\bar{E}_{parallel}^{ref}$, is given by

$$\bar{E}_{parallel}^{ref} = \begin{bmatrix} r_p^{ref} \cos\phi' \\ 0 \end{bmatrix} E_0 e^{i\varepsilon} \qquad (A\text{-}1)$$

where r_p^{ref} is the Fresnel reflection coefficient of p-polarisation of the glass slide, $\phi' = \frac{1}{2}\left(\phi^{(2)} - \frac{\pi}{2}\right)$ and $\varepsilon = \omega_0 t + \phi_s + \frac{\pi}{4} + \phi^{(2)}$.

The corresponding intensity detected by a photodetector is found to be

$$I_{parallel}^{ref} = I_0 R_p^{ref} \cos^2\phi' = \frac{I_0 R_p^{ref}}{2}\left(1 + \cos 2\phi'\right) \qquad (A\text{-}2)$$

where R_p^{ref} is the reflectivity.

For a particular modulated phase of interest, $\phi' = 0^o$ (the parallel polarisation state), the intensity becomes

$$I_{parallel}^{ref} = I_0 R_p^{ref} \qquad (A\text{-}3)$$

This value obviously corresponds to peaks of the sinusoidal intensity (Eq. (A-2)) at the reference arm.

In addition, the perpendicular polarisation state can be found when $\phi' = 90^o$ and the intensity is given by

$$I_{perpendicular}^{ref} = 0 \qquad (A\text{-}4)$$

The value is found to be at the troughs of the reference intensity (Eq. (A-2)). Therefore, the two orientations, both parallel and perpendicular, of a beam under investigation can be identified from the reference signal.

Fig. A-1 shows typical reference and detected signals obtained from the experimental set-up. It can be seen that peaks and troughs of the reference signal (dashed line) can be used as an indicator to pinpoint parallel and perpendicular

orientations of the detected signal (solid line). This condition is obtained without any adjustment of the analyser after it is initially aligned.

Nevertheless, the above procedure would be useless if cumbersome readings of analogue signal were employed. By handling the above process in a digital form incorporating an on-line computer, a speedier reading and interpretation can be achieved. Because the signals (reference and detected) have to be converted from analogue to digital formats, an A/D converter (Thurlby DSA 524, Digital Storage Adapter) is required. The converter had 8-bit resolution, 20MS/s sampling rate and 5MHz bandwidth. It should be noted that the error from the conversion can be reduced if the converter has the resolution higher than 8 bit. The digital format then influences the method of signal processing presented later. The transformed reference and detected signals are read by an on-line computer. With a suitable programme running on the computer, the input data are then processed, analysed and, finally, the required parameters, e.g. I_p and I_s are determined.
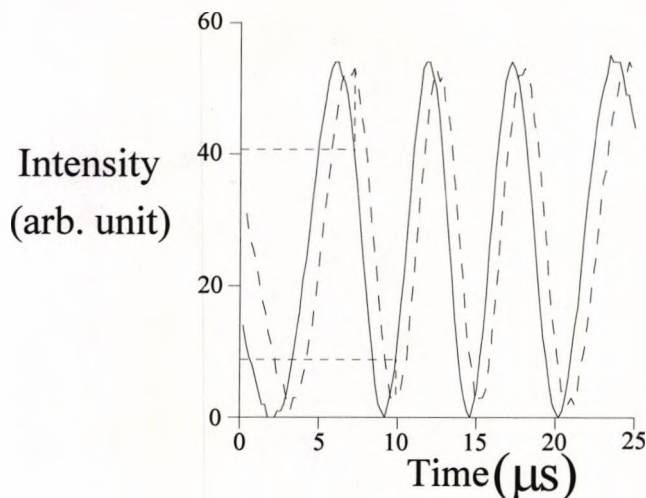
Figure A-1 Output signals from the polarisation modulation unit; solid line - a direct signal
from the polarisation modulation unit, dashed line - a reference signal in
which the peaks correspond to parallel direction and troughs correspond to
perpendicular direction relative to a polarising prism at a reference arm.

The signal processing details are given as follows:

(1) Both reference and detected signals are read into a memory of the computer for analysis.

(2) To improve the smoothness of the data, a simple processing average was made over three points. This required, at each data point, that the average of the value of intensity at that data point, the previous data point and the next data point be calculated and stored. If $I_r[i]$ is defined as a reference intensity at an index i, an averaged intensity over n points may be written

as $\frac{1}{n}\left(\sum_{j=i}^{n} I_r[j]\right)$. For convenience, n is chosen to be an odd number, i.e. n

$= 3$ in this program; therefore, the average then can simply be designated as an averaged reference intensity $I_r'[i']$ where $i' = \frac{1}{2}\left[(2 \times i) + (n-1)\right]$.

(3) In the signal, it is not known if a peak or a trough would be first encountered. The program therefore expects to deal with a peak at the beginning. In order to check for the occurence of a peak, the following procedures were applied.

First of all, an average of the sum over three consecutive points of the

reference, $\frac{1}{3}\left(\sum_{j=i'-1}^{i'+1} I_r'[j]\right)$, is calculated (provided that $I_r'[i'-1]$ is not less

than the first intensity point on the averaged reference curve). Secondly, the average of the sum over three consecutive points separated from the

first group by 9 points, $\frac{1}{3}\left(\sum_{j=(i'+9)-1}^{(i'+9)+1} I_r'[j]\right)$, is determined (provided that

$I_r'[(i'+9)+1]$ is not greater than the last intensity point on the reference curve).

Then, if the second average value is less than the first average, a peak is considered to have been found. If not, the program steps through the data applying the same arguments at each data point until the condition is satisfied. After that $I_r'[i']$ and $I_r'[i'+9]$ are recorded for a further analysis.

(4) The knowledge of an intensity, $I_r'[i']$, obtained can be related to a corresponding time, $t_r[i']$ and vice versa. Therefore, an average of the

sum of the corresponding times, $\frac{1}{2}\left(t_r[i'] + t_r[i'+9]\right)$, of the two intensities, $I_r'[i']$ and $I_r'[i'+9]$, would provide an estimate of the point in time representing the position of the peak and a parallel state of polarisation. However, due to the discrete nature of the data points (in time), this average does not provide an accurate estimate of the peak position. This is only accurate when the intensity calculated at the data points on either side of the peak are equal. This can be achieved by means of interpolation. Specifically, a curve fitting method is required to provide a continuous smooth variation of intensities on each side of the peak.

To generate the best curve fitting, a group of co-ordinates on each side of the peak are chosen. Firstly, on the side of $\left(t_r[i'], I_r'[i']\right)$, seven existing pairs of times and intensities; $\left(t_r[i'-3], I_r'[i'-3]\right), \ldots, \left(t_r[i'], I_r'[i']\right),$ $\ldots, \left(t_r[i'+3], I_r'[i'+3]\right)$ are selected. Secondly, a curve represented by a quadratic equation is fitted to these co-ordinates. Similarly, on the side of $\left(t_r[i'+9], I_r'[i'+9]\right)$, a second quadratic equation is also calculated.

(5) In practice, there must be a fixed point on one side of the peak. In this analysis, a temporal point on the side of $\left(t_r[i'+9], I_r'[i'+9]\right)$ is chosen. The value selected is then substituted into the corresponding quadratic equation and, as a result, an interpolated intensity, $I_{r,fixed}'$ is calculated.

In addition, a time value on the other side is chosen and then substituted into the corresponding quadratic equation to produce a value of intensity I_r'. The intensity found is compared to the fixed one, and the difference is obtained. If the difference is less than a chosen criterion, i.e. $\left|I_{r,fixed}' - I_r'\right| < 0.0001$, both intensities are considered to be approximately equal and their corresponding temporal elements are suitable to be used in the determination of the time coincident with a parallel polarisation state.

(6) Although the time indicating the parallel polarisation state is determined, the parallel intensity (I_p) in the detected signal can still not be identified

properly. It is because of the discrete form of the data and, consequently, it is unlikely that the time value will match one of the discrete time points of the detected signal. Therefore, a curve fit to the detected signal is required and again a quadratic equation was used. Consequently, a more accurate determination of I_p can be achieved.

(7) Similar procedures as described in the case of $.I_p$ are applied to the determination of I_s. It is clear that conditions previously used have to be suitably modified for the case of I_s determination.

(8) Furthermore, in some application such as surface characterisations by an ellipsometer, discussed in the Chapters 4 and 5, the knowledge of phase is very important. In order to obtain this, an evaluation of the intensity orientated between p and s polarisation states is needed. As a result of the times provided by I_p and I_s previously, it would be convenient to concentrate on a specific orientation of 45° relative to the principal directions.

The average time between the times corresponding to p and s polarisation states would provide a point in time coincident to the 45° polarisation state. However, this time is unlikely to match an existing intensity in the detected signal due to the discrete data form. Hence, a quadratic curve fitting for the detected signal around the time is needed. Then, the calculated time substituted in the quadratic equation can give a more precise value for the intensity of I_{45} in the detected signal.

An important point worth mentioning here is that the higher the sampling points per cycle (a signal range completely of I_p, I_s and I_{45}), the better the establishment of the fitting curve and the more precise the interpolated data. It should be noted that, from the experiment, a number of sampling points per cycle which offers the most satisfactory results is 50 and this corresponds to a time base (on the DSA) of 500 ms/div.

APPENDIX B
A COMPLEX INDEX OF REFRACTION

One of common characteristics of an optical samples is its complex index of refraction. The parameter is normally used to described how an electromagnetic wave incident on a material interacts and behaves. For example, under the illumination of HeNe laser (λ = 632.8 nm), some dielectric materials, such as glasses, have only a real term of the refractive index. This implies that the materials are transparent to the wavelength and there is no absorption. However, other dielectric materials, like zinc selenide and silicon, show a small absorption properties at this wavelength through a small magnitude of their absorption coefficient. And in a completely different class, metals, such as copper and aluminium, heavy absorption of this wavelength can be detected as the absorption coefficient is relatively large. Therefore, the materials appear to be opaque.

In this Appendix, a summary of the determination of the complex index of refraction are presented. It is noted that the resultant expression of the index is valid only for a system of planar interface between two semi-infinite homogeneous and isotropic media.

As mentioned in Sec. 4-2, the complex index of refraction of the medium 1 can be determined through an expression given by Eq. (4-10),

$$\frac{N_1}{N_0} = \sin \phi_0 \left[1 + \left(\frac{1-\rho}{1+\rho} \right)^2 \tan^2 \phi_0 \right]^{\frac{1}{2}}$$

Since $\quad \rho \equiv \tan \psi \cdot e^{i\Delta}$ (Eq. 4-5), the above expression then can be rewritten as

152

$$N_1 = N_0 \sin\phi_0 \left[1 + \left(\frac{1 - \tan\psi \cdot e^{i\Delta}}{1 + \tan\psi \cdot e^{i\Delta}} \right)^2 \tan^2\phi_0 \right]^{\frac{1}{2}} \qquad \text{(B-1).}$$

This equation obviously implies the existence of real and imaginary parts of the complex index of refraction. If N_1 is given by $n_1 - i k_1$, explicit forms for each terms can be shown as follows.

$$n_1 - i k_1 = N_0 \sin\phi_0 \left[1 + \tan^2\phi_0 \left\{ \frac{\left(1 - \tan^2\psi\right)^2 - 4\tan^2\psi \sin^2\Delta}{\left(1 + \tan^2\psi + 2\cos\Delta \tan\psi\right)^2} \right\} - i \tan^2\phi_0 \left\{ \frac{4\left(1 - \tan^2\psi\right)\left(\tan\psi \sin\Delta\right)}{\left(1 + \tan^2\psi + 2\cos\Delta \tan\psi\right)^2} \right\} \right]^{\frac{1}{2}}$$

$$\text{(B-2).}$$

Given
$$a = 1 + \tan^2\phi_0 \left\{ \frac{\left(1 - \tan^2\psi\right)^2 - 4\tan^2\psi \sin^2\Delta}{\left(1 + \tan^2\psi + 2\cos\Delta \tan\psi\right)^2} \right\} \qquad \text{(B-3),}$$

$$b = \tan^2\phi_0 \left\{ \frac{4\left(1 - \tan^2\psi\right)\left(\tan\psi \sin\Delta\right)}{\left(1 + \tan^2\psi + 2\cos\Delta \tan\psi\right)^2} \right\} \qquad \text{(B-4),}$$

and
$$\kappa = \frac{1}{2} \left\{ \tan^{-1}\left(-\frac{b}{a} \right) \right\} \qquad \text{(B-5).}$$

Eq. (B-2) can then be rewritten as

$$n_1 - i k_1 = N_0 \sin\phi_0 \left[a - ib \right]^{\frac{1}{2}}$$
$$= N_0 \sin\phi_0 \left(a^2 + b^2 \right)^{\frac{1}{4}} \left(\cos\kappa + i \sin\kappa \right) \qquad \text{(B-6).}$$

Finally, equating real terms and imaginary terms on both sides, expression of n_1 and k_1 as functions of N_0, ϕ_0, ψ and Δ are given by

$$n_1 \left(refractive\ index \right) = N_0 \sin\phi_0 \left(a^2 + b^2 \right)^{\frac{1}{4}} \cos\kappa \qquad \text{(B-7),}$$

and
$$k_1 \left(absorption\ coefficient \right) = N_0 \sin\phi_0 \left(a^2 + b^2 \right)^{\frac{1}{4}} \sin\kappa \qquad \text{(B-8).}$$

APPENDIX C
SINGLE LAYER FILM

Generally, the expression of ellipsometric parameters ψ and Δ are valid for an individual optical structure. For example, simple forms of the ψ and Δ shown in Chapter 4 can be used only in a system consisting of the planar interface between two semi-infinite media. Therefore, in a different structure under investigation, a single layer film on a substrate, the expressions of both parameters have to be modified according to system conditions added. In this Appendix, the theoretical derivations of ψ and Δ corresponding to the system are demonstrated and an expression to determine the values if relevant optical information are known is also derived.

The general system of the ambient-film-substrate is shown in Fig. 5-1. A laser beam of wavelength λ is incident at an angle ϕ_0 on the sample which is made of homogeneous and optically isotropic material. This transparent film of index N_1 and thickness d_1 is supported by an absorbing substrate of complex index $N_2 = n_2 - ik_2$.
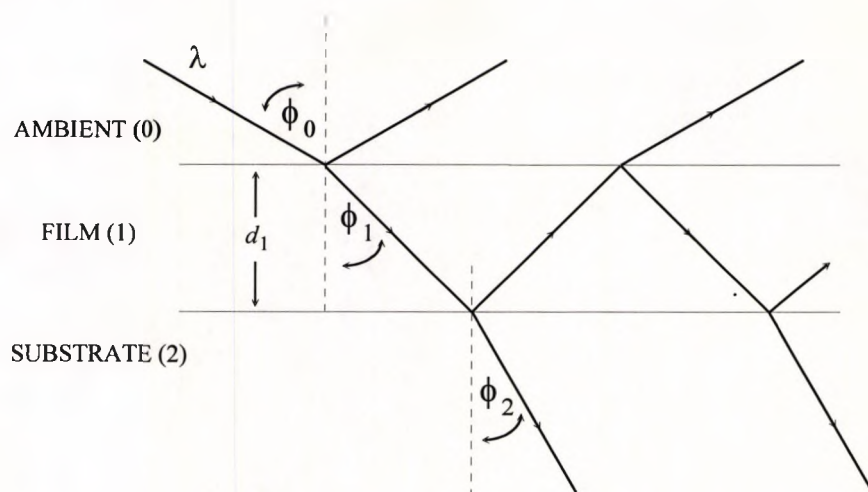
The amplitude reflectances r_p and r_s are given by Eq. (5-1)

$$r_v = \frac{r_{01v} + r_{12v}e^{-i2\beta}}{1 + r_{01v}r_{12v}e^{-i2\beta}}$$

where $v = p$ or s denoted as p or s polarisation. Here r_{01p} and r_{01s} are the Fresnel reflection coefficients at the interface between the incident medium of index N_0 and the film, and r_{12p} and r_{12s} are also the Fresnel reflection coefficients at the interface between the film and substrate.

The phase change that results from the double transversal of the film, 2β is given by Eq. (5-2)

$$2\beta = 4\pi\left(\frac{d_1}{\lambda}\right)\left(N_1^2 - N_0^2 \sin^2 \phi_0\right)^{\frac{1}{2}}$$

The Fresnel reflection coefficients at 0-1 and 1-2 interfaces that appears in Eq. (5-1) are given by

$$r_{01p} = \frac{N_1 \cos\phi_0 - N_0 \cos\phi_1}{N_1 \cos\phi_0 + N_0 \cos\phi_1} \qquad \text{(C-1)},$$

$$r_{12p} = \frac{N_2 \cos\phi_1 - N_1 \cos\phi_2}{N_2 \cos\phi_1 + N_1 \cos\phi_2} \qquad \text{(C-2)},$$

$$r_{01s} = \frac{N_0 \cos\phi_0 - N_1 \cos\phi_1}{N_0 \cos\phi_0 + N_1 \cos\phi_1} \qquad \text{(C-3)},$$

$$r_{12s} = \frac{N_1 \cos\phi_1 - N_2 \cos\phi_2}{N_1 \cos\phi_1 + N_2 \cos\phi_2} \qquad \text{(C-4)},$$

where ϕ_2 and N_2 are complex values. The three angles ϕ_0, ϕ_1 and ϕ_2 between the directions of propagation of the plane waves in media 0, 1 and 2 respectively, and the normal to the film boundaries are inter-related by Snell's law

$$N_0 \sin\phi_0 = N_1 \sin\phi_1 = N_2 \sin\phi_2 \qquad \text{(C-5)}.$$

Since the film is transparent, r_{01p} and r_{01s} are real. On the other hand, r_{12p} and r_{12s} are generally complex; hence, they can be defined as follows:

$$r_{12p} = |r_{12p}|e^{i\phi_{12p}} \qquad \text{(C-6)},$$

$$r_{12s} = |r_{12s}|e^{i\phi_{12s}} \qquad \text{(C-7)},$$

where $\left|r_{12p}\right|$, $\left|r_{12s}\right|$ give the absolute ratio of the amplitude of the reflected wave parallel and perpendicular to the plane of incidence, respectively and ϕ_{12p}, ϕ_{12s} are the phase shift upon the reflection experienced by the reflected wave parallel and perpendicular to the plane of incidence, respectively.

On replacing $N_2 \cos\phi_2$ by $u_2 - iv_2$ to Eqs. (C-2) and (C-4), the amplitude and phase terms of Eqs. (C-6) and (C-7) become (Kihara and Yokomori, 1990),

$$\left|r_{12p}\right|^2 = \frac{\left[\left(n_2^2 - k_2^2\right)\cos\phi_1 - N_1 u_2\right]^2 + \left(2n_2 k_2 \cos\phi_1 + N_1 v_2\right)^2}{\left[\left(n_2^2 - k_2^2\right)\cos\phi_1 + N_1 u_2\right]^2 + \left(-2n_2 k_2 \cos\phi_1 + N_1 v_2\right)^2} \quad \text{(C-8)},$$

$$\left|r_{12s}\right|^2 = \frac{\left(N_1 \cos\phi_1 - u_1\right)^2 + v_2^2}{\left(N_1 \cos\phi_1 + u_1\right)^2 + v_2^2} \quad \text{(C-9)},$$

$$\tan\phi_{12p} = \frac{-2N_1 \cos\phi_1\left[2n_2 k_2 u_2 + \left(n_2^2 - k_2^2\right)v_2\right]}{\left(n_2^2 + k_2^2\right)^2 \cos^2\phi_1 - N_1^2\left(u_2^2 + v_2^2\right)} \quad \text{(C-10)},$$

and
$$\tan\phi_{12s} = \frac{2v_2 N_1 \cos\phi_1}{u_2^2 + v_2^2 - N_1^2 \cos^2\phi_1} \quad \text{(C-11)},$$

where u_2 and v_2 written in terms of ϕ_0, N_0 and N_1 are given by

$$2u_2^2 = \left(n_2^2 - k_2^2\right) - N_0^2 \sin^2\phi_0 + \left[\left(n_2^2 - k_2^2 - N_0^2 \sin^2\phi_0\right)^2 + 4n_2^2 k_2^2\right]^{\frac{1}{2}} \quad \text{(C-12)},$$

and
$$2v_2^2 = -\left(n_2^2 - k_2^2\right) + N_0^2 \sin^2\phi_0 + \left[\left(n_2^2 - k_2^2 - N_0^2 \sin^2\phi_0\right)^2 + 4n_2^2 k_2^2\right]^{\frac{1}{2}} \quad \text{(C-13)}.$$

Now, substituting Eqs. (C-6) and (C-7) into Eq. (5-1), the overall complex amplitude-reflection coefficients for light polarised in p and s directions may be written as

$$r_v = \frac{r_{01v} + \left|r_{12v}\right| e^{i(\phi_{12v} - 2\beta)}}{1 + r_{01v}\left|r_{12v}\right| e^{i(\phi_{12v} - 2\beta)}} \qquad , v = p, s \quad \text{(C-14)}.$$

In order to examine the change of amplitude and phase separately, as a plane wave is obliquely reflected from a film-covered substrate, the overall complex-amplitude reflection (r_p, r_s) are written in terms of their absolute values and angles,

$$r_p = |r_p| e^{i\delta_{rp}}$$ (C-15),

$$r_s = |r_s| e^{i\delta_{rs}}$$ (C-16),

where $|r_p|$ and δ_{rp} represents the amplitude attenuation and phase shift respectively, as p-polarised light is reflected by the film-covered substrate, with similar meaning for $|r_s|$ and δ_{rs} in the case of s-polarisation.

From Eqs. (C-1) - (C-4), the difference of the Fresnel reflection coefficients for the p and s polarisations are evident. Therefore, the overall reflection coefficients of an ambient-film-substrate systems for these two polarisations (r_p, r_s) are also different.   According to the practical point of view in this thin film investigation, it is clear that the elementary requirement for characterising the thin film system is the ellipsometric parameters ψ and Δ.

The ellipsometric angle ψ is given by

$$\psi = \tan^{-1}\left(\frac{r_p}{r_s}\right) = \tan^{-1}\left(\frac{R_p}{R_s}\right)^{\frac{1}{2}}$$ (C-17),

where

the reflectances $$R_v = \frac{r_{01v}^2 + |r_{12v}|^2 + 2r_{01v}|r_{12v}|\cos(\phi_{12v} - 2\beta)}{1 + r_{01v}^2|r_{12v}|^2 + 2r_{01v}|r_{12v}|\cos(\phi_{12v} - 2\beta)}$$, $v = p, s$ (C-18),

and the phase shift Δ can be written as

$$\Delta = \delta_{rp} - \delta_{rs}$$ (C-19),

where the phase shifts $$\delta_{rv} = \tan^{-1}\left(\frac{B_v C_v - A_v D_v}{A_v C_v + B_v D_v}\right)$$, $v = p, s$ (C-20),

where $$A_v = r_{01v} + |r_{12v}|\cos\left[\phi_{12v} - 4\pi\left(\frac{d_1}{\lambda}\right)\left(N_1^2 - N_0^2 \sin^2 \phi_0\right)^{\frac{1}{4}}\right]$$ (C-21),

$$B_v = |r_{12v}|\sin\left[\phi_{12v} - 4\pi\left(\frac{d_1}{\lambda}\right)\left(N_1^2 - N_0^2 \sin^2 \phi_0\right)^{\frac{1}{4}}\right]$$ (C-22),

$$C_v = 1 + r_{01v}|r_{12v}|\cos\left[\phi_{01v} + \phi_{12v} - 4\pi\left(\frac{d_1}{\lambda}\right)\left(N_1^2 - N_0^2 \sin^2 \phi_0\right)^{\frac{1}{4}}\right]$$ (C-23),

$$D_v = r_{01v}|r_{12v}|\sin\left[\phi_{01v} + \phi_{12v} - 4\pi\left(\frac{d_1}{\lambda}\right)\left(N_1^2 - N_0^2 \sin^2\phi_0\right)^{\frac{1}{4}}\right] \quad (C\text{-}24).$$

It can be seen that Eqs. (C-17) and (C-19) provide a mean to determine ψ and Δ as reference values provided that N_0, N_1, N_2, ϕ_0 and d_1 are known.

APPENDIX D
LIST OF PUBLICATIONS BY THE AUTHOR RELEVANT TO THE THESIS

1. CHITAREE, R., WEIR, K., PALMER, A. W. and GRATTAN, K. T. V. (1992) in Polarisation Modulation In Free Space and Fibre Optics, Conference on Applied Optics and Optoelectronics, 14-17 September 1992, Leeds, UK, Proceeding published by Institute of Physics : p 220-222.

2. WEIR, K., CHITAREE, R., PALMER, A. W. and GRATTAN, K. T. V. (1993) in High Speed Sensing Using an Ellipsometer for Investigating of Thin Films and Surfaces, 16-23 May 1993, Honolulu, Hawaii, USA, Proceeding published by The Electrochemical Society, Inc., USA : p 236-243.

3. CHITAREE, R., WEIR, K., PALMER, A. W. and GRATTAN, K. T. V. (1993) in A HiBi Fibre Polarisation Modulation Scheme for Ellipsometric Measurements, Conference on Sensor VI Technology, Systems and Applications, 12-15 September 1993, Manchester, UK, Sensor VI : Technology, Systems & Applications, Ed : K T V Grattan and A T Augousti, Published by Institute of Physics Bristol : p 275-280.

4. CHITAREE, R., WEIR, K., PALMER, A. W. and GRATTAN, K. T. V. (1994) A Highly Birefringent Fibre Polarisation Modulation Scheme for Ellipsometry: System Analysis and Performance, <u>Measurement Science and Technology (5)</u> : p 1226-1232 (a copy of this paper is presented at the end of this Appendix).

5. CHITAREE, R., MURPHY, V., WEIR, K., PALMER, A. W., GRATTAN, K. T. V. and MACCRAITH, B. D. Ellipsometric Measurement for Thin Film Based Sensor System (in preparation for Sensors and Actuators).

6. CHITAREE, R., WEIR, K., PALMER, A. W. and GRATTAN, K. T. V. in A HiBi Fibre-Based Polarisation Modulated Ellipsometer: The System Improvement on An Optical Component Relating Aspect (in preparation for Sensors and Actuators).

A highly birefringent fibre polarization modulation scheme for ellipsometry: system analysis and performance

R Chitaree, K Weir, A W Palmer and K T V Grattan

Measurement and Instrumentation Centre, Department of Electrical, Electronic, and Information Engineering, City University, Northampton Square, London EC1V 0HB, UK

Abstract. An investigation of the polarization modulation performance of a highly birefringent fibre was carried out. The performance of the system and aspects such as the modulation method and the properties of the highly birefringent fibre were analysed in order to enhance performance. An important application of such a polarization modulation technique is in a novel ellipsometer, and the use of the fibre-based system to make ellipsometric measurements to determine the refractive index of a bulk sample is described.

1. Introduction

Optical constants such as refractive index, absorption index, optical thickness, and the birefringence of optical surfaces and thin films can be determined by a variety of optical techniques, including ellipsometry which uses the fact that the reflection of linearly or circularly polarized light from a material is accompanied by a change in the phase and intensity of the composite components giving, in general, elliptically polarized light. This allows the optical properties of the material under study to be evaluated [1] by monitoring the reflected polarized light for various, known, input polarization states. The traditional instrument involves fine mechanical engineering to control accurately the position and orientation of the optical components to enable the measurement process to characterize the reflecting material completely.

In this work, the use of a polarization modulation technique to simplify the instrument is proposed and discussed, the main feature of which is the generation of linearly polarized light of continuously varying azimuth. This permits continuous, rapid and real time investigation of the ellipsometric parameters, and thus the optical material, to be performed with no mechanical adjustment of the optical components required. Several approaches can be used to achieve this. The use of free-space bulk optical components and fibre optics has previously been described [2]. In addition, several such approaches have been investigated and their experimental performance [3] compared in terms of the degree of polarization (DOP) and ellipticity. The results have demonstrated that a higher quality output,

more applicable to ellipsometric measurements, was achieved using a fibre optic scheme. Such schemes have been applied to the measurement of refractive index of both non-absorbing and absorbing samples using ellipsometric techniques [4, 5]. Nevertheless, further improvement to the quality of the rotating polarized light, which is the essence of the technique, is still required over that previously reported [5] for the system to be practicable.

This work reports an extensive investigation into the optimization of such a fibre-based system, detailing important performance related aspects of the instrument developed which could influence the nature of the rotating polarized light. In particular, the effects of multiple reflections and the use of different modulation techniques for application in the ellipsometer were investigated.

2. Theoretical analysis

The technique relies upon the fact that the two orthogonal (left and right) circularly polarized light beams combine to produce a linear state whose azimuth is dependent on the phase difference between the circular states. In the scheme to be described, the light from a laser passes through an initial polarizer, a length of modulated highly birefringent fibre and a quarter wave plate oriented at 45° to the eigenaxes of the fibre. This situation is easily described by the use of Jones vector notation [6] and the result is described by Tatam *et al* [2]:
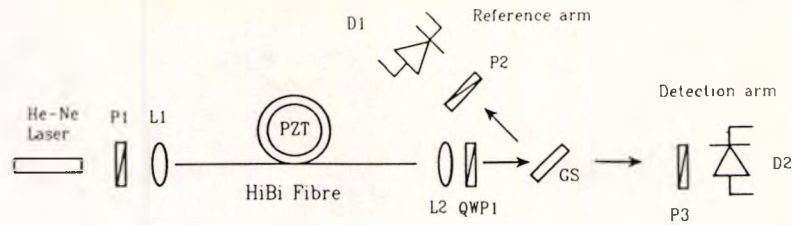
Figure 1. Illustration of a highly birefringent fibre polarization modulation arrangement. P, polarizing prism: L, lens: QWP, quarter wave plate; GS, glass slide; D, detector.

$$E_{\text{output}} = E_0 e^{i\zeta(t)} \begin{bmatrix} \cos\varphi(t) \\ \sin\varphi(t) \end{bmatrix} \qquad (1)$$

where

$$\zeta(t) = \frac{1}{2}(k_x + k_y)[L + \delta L(t)]$$

$$\varphi(t) = \frac{1}{2}(k_x - k_y)[L + \delta L(t)]$$

$$k_x = n_x \frac{2\pi}{\lambda_0}$$

$$k_y = n_y \frac{2\pi}{\lambda_0}$$

E_0 is an electric vector amplitude, n_x and n_y are indices of refraction along eigenaxes x and y of the fibre, λ_0 is the free space wavelength, L is the length of the highly birefringent fibre and $\delta L(t)$ is the fibre length extension due to the modulation unit (the modulation length). Clearly, there is a temperature and strain effect which will be reflected in k_x and k_y, but for the purposes of the operation of the instrument, k_x and k_y are assumed constant and all possible modulation effects are considered to be included implicitly in $\delta L(t)$. In the actual instrument, the referencing technique used means that details of the specific origin of the modulation are not required.

Equation (1) represents a linearly polarized wave in which the orientation of the polarization has been rotated through an angle $\varphi(t)$ proportional to the modulation caused by the highly birefringent fibre. Using an optical analyser, the intensity thus detected may be given by

$$I_{\text{analyser}} = \frac{I_0}{2}\{1 + \cos 2[\theta - \varphi(t)]\} \qquad (2)$$

showing that the output signal is a sinusoidal function of the orientation of the analyser θ and the modulation phase $\varphi(t)$.

In order to apply such a theoretical analysis to a particular ellipsometric measurement problem, the polarization modulation technique was examined experimentally to confirm the predicted operation, identify limitations imposed by the experimental arrangement and to maximize the system performance.

3. System performance

3.1. Basic configuration

The initial polarization modulation scheme employed was produced by winding a length (10 m) of highly birefringent fibre (York HB-600) around a cylindrical piezoelectric transducer (PZT), as shown schematically in figure 1 and described previously [5]. The PZT was driven sinusoidally to stretch the fibre and modulate its birefringence characteristic. Light from a HeNe laser ($\lambda = 632.8$ nm) was polarized at 45° to the eigenaxes of the fibre into which it was launched and the output was collimated via a further objective lens and passed through a quarter wave plate with its optical axis at 45° to the fibre axes. This transforms the output from each eigenmode into circularly polarized light of opposite handedness, these outputs then combining together to give a linear state. A reference signal was provided by reflecting a small fraction of the beam via a glass slide (at an incidence angle of 3°) through a polarizing prism onto a photodetector and the main beam was then analysed via a polarizer (oriented at 45° to that in the reference arm) and a photodiode. The photodetector circuits had a 3 dB bandwidth of 100 kHz. The evaluation procedures are summarized briefly and are illustrated by figure 2 which shows the peaks of the reference signal (dotted curve) which correspond to linearly polarized light with its azimuth parallel to the direction defined by the polarizing prism P2, whereas troughs of the reference signal correspond to a polarization direction perpendicular to the direction of the prism. By orientating the reference polarizing prism P2 in a known direction, the corresponding parallel 'h' and perpendicular 'v' intensities in the detected signal (full curve) may be identified.

3.2. Detailed analysis of the output signal

Figure 2 shows a typical output signal obtained from the polarization modulation unit when the output from the fibre is transmitted directly through polarizer P3 (angled at 45° relative to the orientation of the polarizer in the reference) onto the photodetector (figure 1). Since the polarized light thus produced is modulated by

1227

162
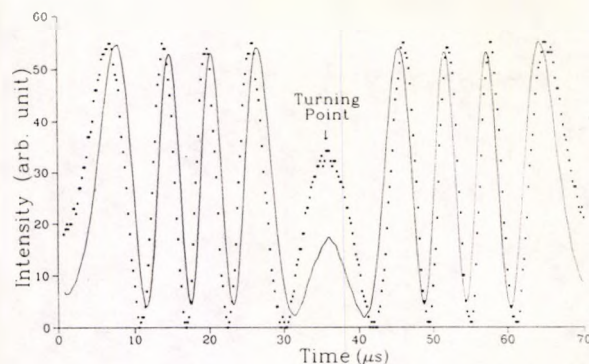
Figure 2. Illustration of typical output fringes obtained from the polarization modulation unit. Full curve, detected signal; dotted curve, reference signal.

driving the PZT sinusoidally (at a resonant frequency of 14 kHz), the linear output state rotates in one direction (say clockwise), and then vice versa (counter-clockwise) when the PZT is relaxed. Thus, as can be seen (figure 2), the group of fringes to the left of the turning point are a mirror image of the fringes on the right of the turning point (where the direction of rotation changes). Initial considerations suggest that both orientations of the rotating polarized light should result in the same output. However, by determining both the intensities parallel (I_h) and perpendicular (I_v) to the direction defined by the polarizing prism in the reference arm, it was found that the average (over several periods) of the ratio I_h/I_v of the fringes situated on one side of a turning point differed significantly from that found on the other side. This raised the question of differing performance depending on the direction of rotation. This observation is not predicted in the analysis, but it is important to note this observation as any inconsistency in this ratio will give rise to unreliable measurements. Therefore it is important that techniques to reduce this effect be examined. A closer analysis was made by monitoring the output of the polarization modulation system, as shown in figure 1, with the polarizer P3 removed from the detection arm. An ideal signal at the detector D2, would have constant amplitude but it was found that this signal, shown in figure 3(a), has intensity variations following the form of the reference observed at detector D1 in the reference arm (figure 3(b)). The peak-to-peak amplitude of the signal in figure 3(a) corresponds to 1% of the DC value.

3.3. Extended analysis

The purpose of this extended analysis was to describe the form of the detected signal as shown in figure 3. It is a requirement that the intensity is constant throughout the polarization modulation period as this is assumed in the application of the technique, but, as described above, this is not what was observed experimentally.

In practice the electric field in each eigenmode is not only composed of the main light flux but it also involves reflected components as the end faces of the fibre act as parallel mirrors. Hence the reflected light, which is
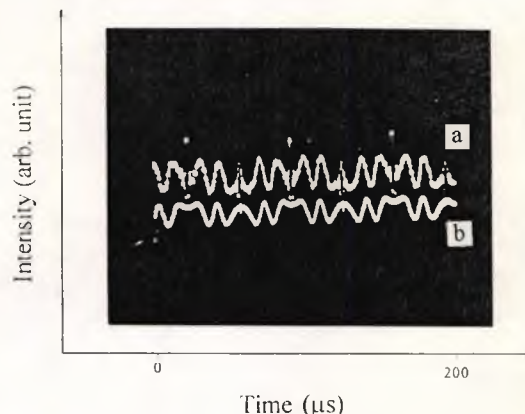
Figure 3. Signal (*a*) was detected at the output of the set-up of figure 1 (no polarizer P3) and signal (*b*) is the corresponding reference signal (different gain and offsets apply).

emitted from the fibre after being reflected by both end faces, backwards and forwards along the fibre for one of the eigenmodes (designated *x*), may be written in terms of the component of E_x (after propagating through the QWP), given by

$$E_x = \eta^2 E_0 e^{i\{\omega t - 3k_x[L + \delta L(t)] + \varepsilon_x\}} \begin{bmatrix} 1 \\ i \end{bmatrix} \qquad (3)$$

where η is the reflection coefficient at the fibre ends (assumed identical), $3k_x[L + \delta L(t)]$ is the phase of the reflected light for mode *x* and ε_x is an initial phase in eigenmode *x*. Similarly for the other eigenmode *y*, the electric field component is given by

$$E_y = \eta^2 E_0 e^{i\{\omega t - 3k_y[L + \delta L(t)] + \varepsilon_y - \pi/2\}} \begin{bmatrix} 1 \\ -i \end{bmatrix}. \qquad (4)$$

In addition, if the reflected light and the main light flux of both eigenmodes are detected simultaneously, the total intensity may then be given by

$$I_{total} = 2I_0[[2 + \eta^4 + \eta^2 + \eta^2 \cos\{2k_x[L + \delta L(t)]\} \\ + \eta^2 \cos\{2k_y[L + \delta L(t)]\}]]. \qquad (5)$$

If it is assumed that $\eta \approx \eta'$, the last two cosine terms in equation (5) can be written as

$$I' = 2\cos\{(k_x - k_y)[L + \delta L(t)]\}\cos\{(k_x + k_y)[L + \delta L(t)]\}. \qquad (6)$$

This indicates theoretically, the presence of a beat effect with a modulated amplitude of $\cos\{(k_x - k_y)[L + \delta L(t)]\}$.

The first factor of equation (6) is low frequency and the second is high frequency as can be seen in the following analysis. Analysis of the modulated amplitude factor may be made by writing it as a function of the phase shift between the two eigenmodes Δ_m to give

$$(k_x - k_y)[L + \delta L(t)] = \frac{n_x \Delta_m}{B} - \frac{n_y \Delta_m}{B} = \Delta_m \qquad (7)$$

where B is the modal birefringence of the fibre.
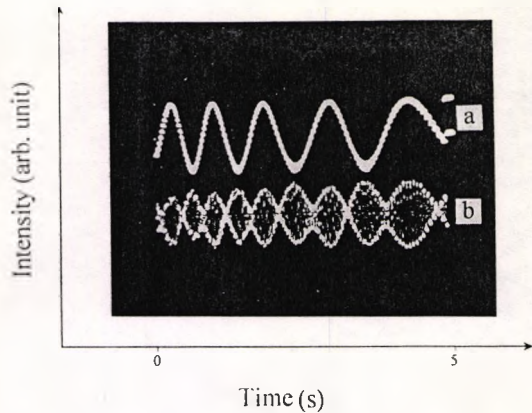
Figure 4. Illustration of the reference signal (*a*) and the beat pattern (*b*) due to the interference between the main light flux and the reflected light (different gain and offsets apply).

Equation (7) indicates how the shape of the envelope of the beat is similar to the modulation phase between the two eigenmodes. This is clearly illustrated in figure 4 which shows the output obtained (again from the arrangement of figure 1) where the modulation rate is greatly reduced (a low-frequency linear ramp was used, giving rise to a polarization rotation frequency of ≈ 1 Hz). Figure 4(*a*) is the reference signal and figure 4(*b*) is the signal with the polarizing prism P3 removed. The peak-to-peak amplitude of the signal of figure 4(*b*) corresponds to 6% of the DC value.

Additionally, the characteristic of the components inside the envelope may be investigated. Again, rewriting all factors in terms of the phase shift between the two eigenmodes Δ_m the phase of the high-frequency cosine factor (from equation (6)) may be given by

$$(k_x + k_y)[L + \delta L(t)] = \frac{n_x \Delta_m}{B} + \frac{n_y \Delta_m}{B} = \frac{\Delta_m}{B}(n_x + n_y). \tag{8}$$

As can be seen, this indicates a rapid phase change when compared to the modulation phase between the two eigenmodes, as a typical value of B for a highly birefringent fibre is of the order of 10^{-4}. A useful comparison of figures 3 and 4 can be made by considering the difference between the two modulation conditions in both frequency and form. In figure 3, the modulation was via the cylindrical PZT operating at a sinusoidal frequency of 14 kHz. In this case $\delta L(t)$ in equation (6) varies sinusoidally. Equation (6) may then be expanded as a Fourier series (whose terms are harmonics of the modulation frequency) with coefficients involving Bessel functions [7]. The actual detailed form of the power spectrum in such a situation depends on both the amplitude of modulation and the initial phase of the factors in equation (6). This situation was extensively modelled using a simple fast Fourier transform (FFT) computer algorithm. Removing the high-frequency components (above the cut-off frequency of the detector circuit) before performing the inverse Fourier transform was used to mimic the low pass

filtering effect of the detector. This confirmed the low-frequency content of equation (6) and the resultant, reconstructed time signal was *similar* in form to the reference signal (though of course reduced in amplitude relative to the original). The exact form of this reconstructed signal is sensitive to initial conditions of phase and modulation amplitude. This is in agreement with the signal shown in figure 3(*a*) which (for the particular initial phase and amplitude encountered experimentally) is observed to be similar to the reference signal, figure 3(*b*). In figure 4, thermal modulation corresponding to a linear ramp was used (resulting in a frequency of ≈ 1 Hz for the polarization rotation) and a simple, sinusoidal, high-frequency modulation and low-frequency envelope can be seen (figure 4(*b*)).

Clearly, these higher order reflections should be minimized to ensure optimum performance because, as well as giving rise to variations in intensity, changes in the output polarization may occur. When high-speed modulation is used, a sinusoidal modulation signal will normally be applied resulting in a complex frequency spectrum. Therefore, it is not an option merely to filter these high frequencies electronically.

3.4. System enhancement

In order to improve the output from the polarization modulation technique to be used in the ellipsometer, it is desirable that the amplitude of the reflected light which contributes to the amplitude of the beat frequency should be reduced as much as possible. Techniques to cut down the reflections at the end faces of the fibre included using index matching gel, anti-reflection (AR) coating of the fibre end face, the use of an immersion cell and an angled end face (not 90°) to deviate the reflected light. The polished angled end face was tested as the most practical approach to try in the laboratory. To achieve a low reflection factor, the angle of the end face was required to be greater than 5.8° [8] and this was achieved by hand polishing both end faces, not only to reduce their internal reflection but also to prevent power fluctuations due to light coupling back into the source.

The optical quality of the end face was checked by inspection and by coupling light from a HeNe laser ($\lambda = 632.8$ nm) into the fibre, then observing the far field output from the polished end for the situation with tilted end faces. In this case, a length of the fibre used in the experiment (see figure 1) was 1 m. The modal birefringence was modulated by heating a small part (≈ 50 mm) of the fibre with a hot air blower to achieve the polarization modulation. The results of this experiment were compared with those from the highly birefringent fibre with plane cut end faces. The same degree of polarization was achieved and the higher frequency components could still be observed, but the relative amplitude of the high-frequency components (the ratio of the high-frequency component amplitude to the total signal amplitude, under identical condition of modulation and detection) was reduced by a factor of five.

Table 1. The mean $\bar{x}$ and standard deviation σ of the intensities I_v, I_h, I_{45} for different polarization modulation techniques.

Modulation method (angled ends)	Clockwise			Counter clockwise		
	I_v	I_h	I_{45}	I_v	I_h	I_{45}
Cylindrical PZT $\bar{x}$	35.28	37.52	69.00	38.77	33.12	71.23
σ	2.26	2.70	0.82	0.78	0.53	0.39
Heating $\bar{x}$	32.63	33.34	64.50	32.57	33.09	65.90
σ	0.88	1.19	0.49	0.343	0.30	0.49
Stretching $\bar{x}$	26.51	28.63	62.90	28.12	28.77	61.67
σ	1.12	0.44	0.24	0.88	0.32	0.20

This clearly indicates that the performance of the highly birefringent fibre system can be improved considerably by polishing the end faces of the fibre at an angle, although some residual reflection factor apparently remains. In subsequent work, the end faces of the fibre were polished at an angle of 6° for improved performance.

3.5. Alternative methods of modulation

Mode coupling in a highly birefringent fibre, i.e. the coupling of optical energy from one mode to the other [9], can also affect the system by introducing inconsistent power levels into each eigenmode. This arises as the fibre undergoes variations in external force, and a study of different modulation techniques was made to investigate this. The distribution of intensities, particularly the intensity parallel I_h, perpendicular I_v, and at 45° to these directions, I_{45}, relative to the orientation defined by the reference signal, were studied.

The intrinsic birefringence in the York Bow-Tie highly birefringent fibre is caused by the difference in thermal expansion between the cladding and the stress applying regions inside the fibre, as it cools. If the fibre is stretched with a uniform axial strain, the stress applying regions and the cladding of the fibre are strained differently in the longitudinal direction, introducing a strain-induced birefringence, which will increase the value of the intrinsic birefringence, but will not affect its direction, potentially reducing the problem of the energy coupling. The case of thermal modulation (induced by heating a short length of the fibre) is similar to the modulation achieved by fibre stretching and the direction of the intrinsic birefringence is not affected because there is no external force that can cause the redirection of the birefringence. This results in an effective polarization modulation method, although the technique is not particularly practical for a measurement system due to the low bandwidth achievable. In the study a low-frequency linear ramp was used to assess this method of modulation. The resulting frequency of polarization rotation was $\approx$ 1 Hz.

A comparative investigation was made on the distribution of measured intensities I_v, I_h and I_{45} and the stable means and standard deviations were calculate from a large number of measurements. Clockwise and

Table 2. A comparison of the average of the ratio I_v/I_h of the fringes for different directions of polarization rotation and modulation techniques.

Modulation method (angled ends)	Average I_v/I_h	
	Clockwise	Counter-clockwise
Cylindrical PZT	1.100	0.855
Heating	1.021	1.016
Stretching	1.083	1.020

counter clockwise directions of rotation were considered separately. The experimental arrangement was as described previously except, of course, for the change of the modulation method. For the uniform stretching set-up, a section of 200 mm from a 1 m length of highly birefringent fibre was held under longitudinal strain with one end mounted at a fixed point and the other end attached firmly to a 30 Hz sinusoidal modulator.

Table 1 summarizes the distribution (mean, $\bar{x}$ and standard deviation, σ) of the intensities of interest, for the clockwise or counter clockwise. An important point to note from table 1 is that there is a larger spread (standard deviation) in the measured values when the modulation was performed via a cylindrical PZT. It is most likely that this is due to mode coupling within the fibre coiled around the cylindrical PZT modulator [9]. Loading on the fibre then introduces birefringence which does not have the same direction as the intrinsic birefringence.

Further, using the data of table 1, the averages of the ratio I_v/I_h, calculated for different directions of rotation, were compared as shown in table 2. These results indicate that the problem of the variation in values due to the direction of rotation is reduced when using heating or stretching as the means of modulation.

In summary, the results obtained from the thermal and longitudinal stretching modulation scheme showed not only less scatter in I_v, I_h and I_{45} around their mean values but also a reduction in the variation with direction of rotation. Thus, by careful choice of the method of modulation, and reduction in the reflected components, the system performance can be improved.

5
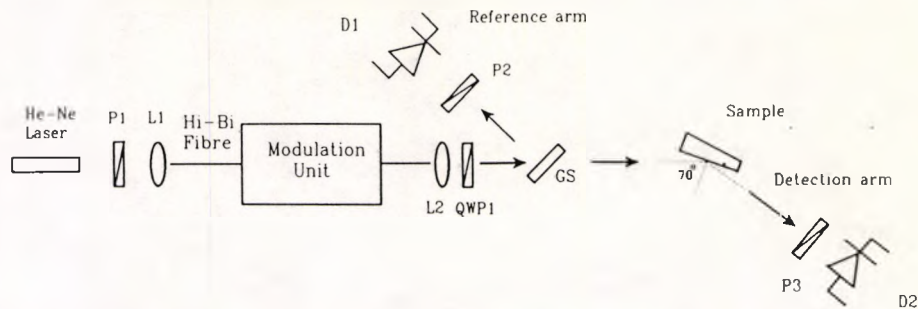
Figure 5. Schematic of the highly birefringent fibre polarization modulation scheme for ellipsometric measurement.

4. Experimental measurements using the ellipsometer

With these improvements, this modified polarization modulation technique can be integrated into a simplified ellipsometric measuring system. This was used to measure the refractive index of a sample, to illustrate the capabilities of the system.

In order to characterize a sample, it is customary to determine the ratio ρ of the complex Fresnel reflection coefficients for the p and s polarizations [1] where p is parallel and s perpendicular to the plane of incidence, i.e.

$$\rho = \tan \psi e^{\mathrm{i}\Delta}. \qquad (9)$$

The angle Δ is defined as the phase difference between the p and s components, and the angle ψ the inverse tangent of the factor by which the amplitude ratio changes.

Figure 5 illustrates the highly birefringent fibre polarization modulation scheme as used in the ellipsometer. By following the change in the polarization of the light passing through, the effect on the input beam can also be described in terms of the Jones matrices. In most practical situations, the final polarizer is orientated at an angle of 45° to the plane of incidence and I_f, the detected intensity, is simplified to:

$$I_f = \frac{I_0}{2}\left[\left(\frac{R_p + R_s}{2}\right) + \left(\frac{R_p - R_s}{2}\right)\cos[\varphi(t)] + \sqrt{R_p R_s}\,\sin[\varphi(t)]\cos\Delta\right] \qquad (10)$$

where $R_p(= r_p^2)$ is the reflection coefficient for the 'p' component and $R_s(= r_s^2)$ is the reflection coefficient for the 's' component.

Since the light used in this experiment is rotating polarized light in which its azimuth depends upon the modulation signal, the use of a reference signal allows the input orientation of the rotating polarized light to be identified. The transmission axis of the polarizer in the reference arm was orientated such that it was perpendicular to the plane of incidence at the sample and the two orientations, both parallel and perpendicular, can

then be identified from the reference signal. The peaks of the reference signal indicate the perpendicular states (s) while its troughs show the parallel states (p). The point in time half way between a peak and a consecutive trough corresponds to the 45° orientation. Thus the intensities corresponding to the input polarized states can be identified in the detected signal intensities (I_p, I_s, I_{45}).

Substitution of the corresponding intensities I_p, I_s, I_{45} and modulation angle $\varphi(t)$ in equation (10), then allows ψ and Δ to be determined, thus enabling the characterization of the reflecting surface without mechanical movement of any of the optical components being necessary, marking a major step forward in the use of ellipsometric techniques in real time applications.

By using Snell's law and expressions for the Fresnel complex amplitude reflections [1], the equation used to determine the complex refractive index characterizing a bulk sample is

$$\frac{N_1}{N_0} = \sin\phi_0\left[1 + \left(\frac{1-\rho}{1+\rho}\right)^2 \tan^2\phi_0\right]^{1/2} \qquad (11)$$

where ϕ_0 is the angle of incidence, N_0 is the complex refractive index of medium 0 (the incidence medium) and N_1 is the complex refractive index of medium 1 (the reflecting medium). Equation (11) shows that, from a measurement of ρ, the complex refractive index of medium 1 can be calculated if the values of the angle of incidence and N_0 are given. In order to undertake an evaluation of the system designed and described, a determination of the refractive index of a standard optical wedge (of BK7) was made. The wedge shape was used to separate the front and the back reflections from one another in order to avoid unwanted interference that could introduce errors to the measurement.

Table 3 shows the comparison of the output performance in terms of the mean and standard deviation of the measured refractive index and cosine of the ellipsometric phase difference Δ of the three different methods of polarization modulation over a large number of measurements (including results from a similar number of clockwise and counter-clockwise rotations). For a non-absorbing sample such as BK7, the phase difference Δ is 180° when the incidence angle is less

1231

166

R Chitaree *et al*

Table 3. Ellipsometric determination of the refractive index and cosine of the ellipsometric phases difference (of BK7) for different methods of polarization modulation.

Modulation method (angled ends)	Refractive index, n^{*}	$\cos(\Delta)$
Cylindrical PZT $\bar{x}$	1.530	0.979
σ	0.08	0.173
Heating $\bar{x}$	1.499	0.999
σ	0.039	0.129
Stretching $\bar{x}$	1.503	0.999
σ	0.034	0.148

* The quoted value for the refractive index of BK7 at a wavelength of 632.8 nm is 1.519.

than the Brewster angle ($< 56.3°$) and $0°$ when the incidence angle is greater. Absolute values of the cosine function of the phase difference concerned ($\cos \Delta$) are shown.

From table 3 it may be seen that the mean value of refractive index was lower when using the PZT. However, the spread (standard deviation) is the more important parameter as the mean value, for all means of modulation, may be affected by systematic errors arising from, for example, small misalignments. Thus the results in table 3 again illustrate that the two preferred ways of modulation considered for use in the ellipsometer, heating and stretching, produce better results, as measured by the standard deviation, than using the cylindrical PZT modulation. These results favour their use in actual measurement situations, using the ellipsometer design discussed. However, it is envisaged that the longitudinal stretching would be more practical in a measurement system due to the higher bandwidth that is available.

5. Conclusions and discussion

A series of invetigations has been carried out and, as a result, a considerable improvement in performance of the polarization modulation technique has been observed. The system has then been successfully applied to the ellipsometric measurement of a standard sample. This improvement was achieved by polishing the end faces of the fibre at an angle and modulating the fibre either by the use of heating or longitudinal stretching. The analysis was modified to include multiple reflection effects and the results obtained from the system showed an improvement in accuracy over previous similar systems, as potential error sources were reduced or eliminated.

Further development of the system to increase modulation frequency and investigate the application of the polarization modulation scheme to further, real time ellipsometric measurements over a range of materials, employed for various sensing purposes, is the subject of continuing work.

References

[1] Azzam R M A and Bashara N M 1977 *Ellipsometry and Polarised Light* (Amsterdam: North-Holland)
[2] Tatam R P, James J D C and Jackson D A 1986 Optical polarisation state control scheme using fibre optics or Bragg cells *J. Phys. E: Sci. Instrum.* **19** 711–7
[3] Chitaree R, Weir K, Palmer A W and Grattan K T V 1992 Polarisation modulation in free space and fibre optics *Proc. Conf. Applied Optics and Opto-Electronics (Leeds, UK) 14–17 September 1992* (Bristol: IOP Publishing) pp 220–2
[4] Yoshiko T and Kurosawa K 1984 All-fibre ellipsometry *Appl. Opt.* **23** 1100–2
[5] Chitaree R, Weir K, Palmer A W and Grattan K T V 1993 A HiBi fibre polarisation modulation scheme for ellipsometric measurements *Proc. Conf. Sensor VI Technology, Systems and Applications (Manchester, UK) 12–15 September 1993* ed K T V Grattan and A T Augousti (Bristol: Adam Hilger) pp 275–80
[6] Jones R C 1941 A new calculus for the treatment of optical system *J. Opt. Soc. Am.* **31** 488–93
[7] Jackson D A 1985 Monomode optical fibre interferometers for precision measurement *J. Phys. E: Sci. Instrum.* **18** 981–1001
[8] Ulrich R and Rashleigh S C 1980 Beam-to-fibre coupling with low standing wave ratio *Appl. Opt.* **19** 2453–6
[9] Rashleigh S C 1983 Origins and control of polarization effects in single-mode fibers *J. Lightwave Technol.* **1** 312–31

1232

REFERENCES

ARCHER, R. J. (1962) Determination of the Properties of Films on Silicon by the Method of Ellipsometry. Journal of the Optical Society of America (52) : p 970-977.

ASPNES, D. E. and STUDA, A. A. (1975) High Precision Scanning Ellipsometer. Applied Optics (14) : 220-228.

AZZAM, R. M. A. and BASHARA, N. M. (1977) Ellipsometry and Polarised Light. (Amsterdam: North Holland).

AZZAM, R. M. A., ZAGHLOUL, A. -R. M. and BASHARA, N. M. (1975) Ellipsometric function of a film-substrate system: Applications to the design of reflection-type optical devices and to ellipsometry. Journal of the Optical Society of America (65) : p 252-260.

BADINI, G. E., GRATTAN, K. T. V., PALMER, A. W. and TSEUNG, A. C. C. (1989) Development of pH Sensitive Substrates for Optical Sensors Applications. Proc. OFS '89. Proceedings in Physics(44). (Paris: Springer-Verlag) : p 436-442.

BORN, M and WOLF, E. (1989) Principles of Optics. 6th Ed. (Oxford: Press).

CHIANG, K. S., WONG, D., and CHU, P. L. (1990). Strain-Induced Birefringence in a Highly Birefringence Optical Fibre. Electronics Letters (26) : p 1344-1346.

COLLIN, R. W. (1990) Automatic Rotating Element Ellipsometers: Calibration, Operation, and Real-Time Applications. Review of Scientific Instruments Reviews (61) : p 2029-2062.

CONN, G. K. T. and EATON, G. K. (1954) On the Analysis of Elliptically Polarised Radiation. Journal of the Optical Society of America (44) : p 546-552.

CONNOR, F. C., (1973). Modulation. (London: The Pitman Press) : 27.

DING, J. Y., SHAHRIARI, M. R. and SIGEL, JUN., G. H. (1991) Fibre Optics pH Sensors Prepared by Sol-Gel Immobilisation Technique. <u>Electronics Letters (27)</u> : p 1561-1562.

FOWLES, G. R. (1975) Introduction to Modern Optics 2nd Ed. (London: Holt, Rinehart and Winston INC.).

GRAY, D. E. (1957) American Institute of Physics Handbook. (London: McGraw-Hill Book Company) : p 6-105.

HALL, A. C. (1969) A Century of Ellipsometry. <u>Surface Science (16)</u> : p 1-13.

HASS, G. and THUN, R. E., (1967) Physics of Thin film Vol. 4. (London: Academic Press) : p 81.

HAUGE, P. S. (1980) Recent Development in Instrumentation in Ellipsometry. <u>Surface Science (96)</u> : p 108-140.

HECHT, E. (1970). Note on an Operational Definition of the Stokes Parameters. <u>American Journal of Physics(38)</u> : 1156-1158.

HECHT, E. and ZAJAC, A. (1974). Optics. (London: Addison-Weisley Publishing Company).

HU, H. Z. (1983) Polarisation Heterodyne Interferometry Using a Simple Rotating Analyser. 1: Theory and Error Analysis. <u>Applied Optics (22)</u> : p 2052-2056.

JACKSON, D. A., KERSEY, A. D., LEIBADY, P. A. and JONES, J. D. C. (1986). High Frequency Non-Mechanical Optical Linear Polarisation State Rotator. <u>Journal of Physics E: Measurement Science and Technology (19)</u> : 146-148.

JAFFE, B., COOK, W. R. Jr and JAFFE, H. (1971). Piezoelectric Ceramics. (London: Academic Press) : p 37.

JASPERSON, S. N. and SCHNATTERLY, S. E. (1969) An Improved Method for High Reflectivity Ellipsometry Based on a New Polarisation Modulation Technique. <u>The Review of Scientific Instruments (40)</u> : p 761-767.

JELLISON, G. E. and MODINE, F. A. (1990) Two-Channel Polarisation Modulation Ellipsometer. <u>Applied Optics (29)</u> : p 959-974.

JENKINS, F. A. and WHITE, H. E. (1957) Fundamental of Optics. (London: Mc GRAWHILL).

JOHNSON, M. AND PANNELL, C. N. (1992) Remote State-Of-Polarisation Control in Polarisation-Maintaining Fibre. Optics Communications (90) : p 32-34.

JONES, B. E. (1985). Optical Fibre Sensor and Systems for Industry. Journal of Physics E: Measurement Science and Technology (18) : p 770

JONES, R. C. (1941). A New Calculus for the Treatment of Optical System. Journal of the Optical Society of America (31) : 488-493.

KIHARA, T. and YOKOMORI, K. (1990) Simultaneous measurement of refractive index and thickness of thin film by polarised reflectances. Applied Optics (29) : p 5069-5073.

KIHARA, T. and YOKOMORI, K. (1992) Simultaneous measurement of the refractive index and thickness of thin film by s-polarised reflectances. Applied Optics (31) : p 4482-4487.

KIM, Y. -T, COLLINS, R. W. and VEDAM, K. (1990) Fast Scanning Spectro Electo-Chemical Ellipsometry: in-situ Characterisation of Gold Oxide. Surface Science (233) : p 341-350.

KLEIN, M. V. (1970) Optics. (London: John Wiley & Son).

KUBOTA, M., OHARA, T., FURUYA, K. and SUEMATSU, Y. (1980) Control on Single-Mode Optical Fibres. Electronics Letters (16) : p 573.

LEFEVRE, H. C. (1980) Single-Mode Fibre Fractional Wave Devices and Polarisation Controllers. Electronics Letters (16) : p 778-780.

LIN, C., CHOU, C. and CHANG, K. (1990) Real Time Interferometric Ellipsometry with Optical Heterodyne and Phase-Lock Techniques. Applied Optics (29) : p 5159-5162.

LONGHURST, R. S. (1973). Geometrical and Physical Optics. (London: Longman).

LUKOSZ, W. and TIEFENTHALER, K. (1983) Embossing Technique for Fabricating Integrated Optical Components in Hard Inorganic Waveguiding Material. Optics Letters (8) : p 537-539.

MacCRAITH, B.D. (1993) Enhanced Evanescent Wave Sensors Based On Sol-Gel-Derived Porous Glass Coating. Sensors and Actuators B (11) : p 29-34.

MATSUMOTO, T. and KANO, H, (1986) Endless Rotatable Fractional-Wave Device for Single-Mode Fibre Optics. Electronics Letters (22) : p 78-79.

MELLES GRIOT. (1992) Optics Guide 5, Hampshire, UK.

MONIN, J., SAHSAH, H., SIBLINI,A. and BREVET-PHILIBERT, O.(1994) Azimuthal Alignments in Ellipsometry: A High-Precision Method Using A Polarisation Modulator. Applied Optics (33) : p 1213-1217.

MORITANI, A., OKUDA, Y., KUBO, H. and NAKAI, J. (1983) High Speed Retardation Modulation Ellipsometer, Applied Optics (22) : p 2422-2436.

NODA, J., OKAMOTO, K. and SASAKI, Y. (1986) Polarisation-Maintaining and Their Applications. Journal of Lightwave Technology (LT-4) : p 1071-1089.

NUSSBAUM, A. and PHILLIPS, R. (1976). Contemporary Optics for Scientists and Engineers. (New Jersy: Prentice-hall): p 360-361.

OKOSHI, T., CHENG, Y. H. and KIKUCHI, K. (1985a) New Polarisation-Control Scheme for Optical Heterodyne Receiver Using Two Faraday Rotators. Electronics Letters (21) : p 787-788.

OKOSHI, T., FUKAY, N. and KIKUCHI, K. (1985b) New Polarisation-State Control Device: Rotatable Fibre Cranks. Electronics Letters (21) : p 895-896.

OZ OPTICS LTD. (1991) Data Sheet : p 5. USA.

PALAIS, J. C. (1988). Fibre Optics Communications. 2nd Ed., (London: Prentice-Hall International).

PEDINOFF, M. E. and BRAUNSTEIN, M. (1979) Strain induced anisotropy in As_2S_3, As_2Se_3 and ZnSe film on KCl substrate via 10.6 μm & 0.632 μm ellipsometer measurement and 0.632 μm reflector measurement. Applied Optics (18) : p 201-210.

PHILLIPS, R. W. and DODDS, W. J. (1981) Optical interference coatings prepared from solution. Applied Optics (20) : p 40-47.

RASHLEIGH, S. C. (1983) Origin and Control of Polarisation Effect in Single-Mode Fibres. Journal of Lightwave Technology (LT-5) : p 312-331.

RASHLEIGH, S. C., BURNS, W. K., MOELLER, R. P. and ULRICH, R. (1982a). Polarisation-Holding in Birefringence Single-Mode Fibres. Optical Letters (7) : p 40-42.

RASHLEIGH, S. C. and MARRONE, M. J. (1982b). Polarisation-Holding in Coiled High-Birefringence Fibres. Electronics Letters 19 : p 850-851. ·

RITTER, E. (1969) in Physics of Thin films, HASS, G., FRANCOMBE, M. H. and HOFFMAN, R. W., Eds. (New York: Academic Press): p 14.

SCHURCLIFF, W. A. (1962). Polarisation Light Production and Use. (Massachusetts: Harvard U P).

SELBY, S. M. (1968). C R C Mathematical tables. 16th Ed. (Ohio: The Chemical Rubber Co).

SHAMIR, J. and KLEIN, A. (1986) Ellipsometry with Rotating Plane-Polarised Light. Applied Optics (25) : p 1476-1480.

SHIBATA, N., TSUBOKAWA, M., OHASHI, M. and SEIKAI, S. (1985) Bending Loss Measurement of LP_{11} Mode in Quasi-Single-Mode Operation Region. Electronics Letters (21) : p 1042-1043.

SINGHER, L., BRUNFELD, A. and SHAMIR, J. (1990) Ellipsometry with a Stabilised Zeeman Laser. Applied Optics (29) : p 2405-2408.

SPIEGEL, M. R. (1971) Advanced Mathematics for Engineers and Scientists, Schaum's Outline Series. (London: McGraw-Hill Book Company).

TAKASAKI, H. (1961a) Photoelectric Measurement of Polarised Light by Means of an ADP Polarisation Modulator, II Photoelectric Elliptic Polarimeter. Journal of Optical Society of American (51) : p 463.

TAKASAKI, H. (1961b) Photoelectric Measurement of Polarised Light by Means of an ADP Polarisation Modulation, I Photoelectric Polarimeter. Journal of the Optical Society of America (51) : p 462-463.

TAKASAKI, H. and YOSHINO, Y. (1969) Polarisation Interferometer. Applied Optics (8) : p 2344-2345.

TATAM, R. P., JONES, J. D. C. and JACKSON, D. A. (1986) Optical Polarisation Control Schemes Using Fibre Optics or Bragg Cells. Journal of Physics E: Science and Instrumentation (19) : p 711-717.

TATAM, R. P., PANNELL, C. N., JONES, J. D. C. and JACKSON, D. A. (1987) Full Polarisation State Control Utilising Linearly Birefringent Monomode Optical Fibre. Journal of Lightwave Technology (LT-5) : p 980-985.

TATAM, R. P., HILL, D. C., JONES, J. D. C. and JACKSON, D. A. (1988) All-Fibre Optic Polarisation State Azimuth Control: Application to Faraday Rotation. Journal of Lightwave Technology (LT-6) : p 1171-1175.

ULRICH, R. (1979) Polarisation Stabilisation on Single-Mode Fibre. Applied Physics Letters (35) : p 840-842.

ULRICH, R. and RASHLEIGH, S. C. (1980). Beam-to-fibre coupling with low standing wave ratio. Applied Optics (19) : p 2453-2456.

VARNHAM, M. P., PAYNE, D. N. and LOVE, J. D. (1984). Fundamental Limits to the transmission of Linearly Polarised Light by Birefringent Optical Fibre. Electronics Letters (20) : p 55-56.

WILLIAMSON, S. J. and CUMMING, H. Z. (1983) Light and Color in Nature and Art. (New York: John Wiley and Sons) : p 118.

WONG, D. and POOLE, S. (1993). Temperature Independent Birefringent Fibres. International Journal of Optoelectronics (8): p 179-186.

YODAS, B. E. (1982) Deposition and properties of optical oxide coating from polymerized solution. Applied Optics (21) : p 2960-2964.

YOSHINO, T. and KUROSAWA, K. (1984) All Fibre Ellipsometry. Applied Optics (23) : p 1100-1102.

ZAGHLOUL, A. -R. M., AZZAM, R. M. A. and BASHARA, N. M. (1975) Design of film-substrate single-reflection retarders. Journal of the Optical Society of America (65): p 1043- 1049.